Working Paper
86 - 5

The Physical Oceanography of Pamlico Sound

Leonard J. Pietrafesa
Gerald S. Janowitz
Tieh-Ying Chao
Robert H. Wiesberg
Farid Askari
and
Elizabeth Noble

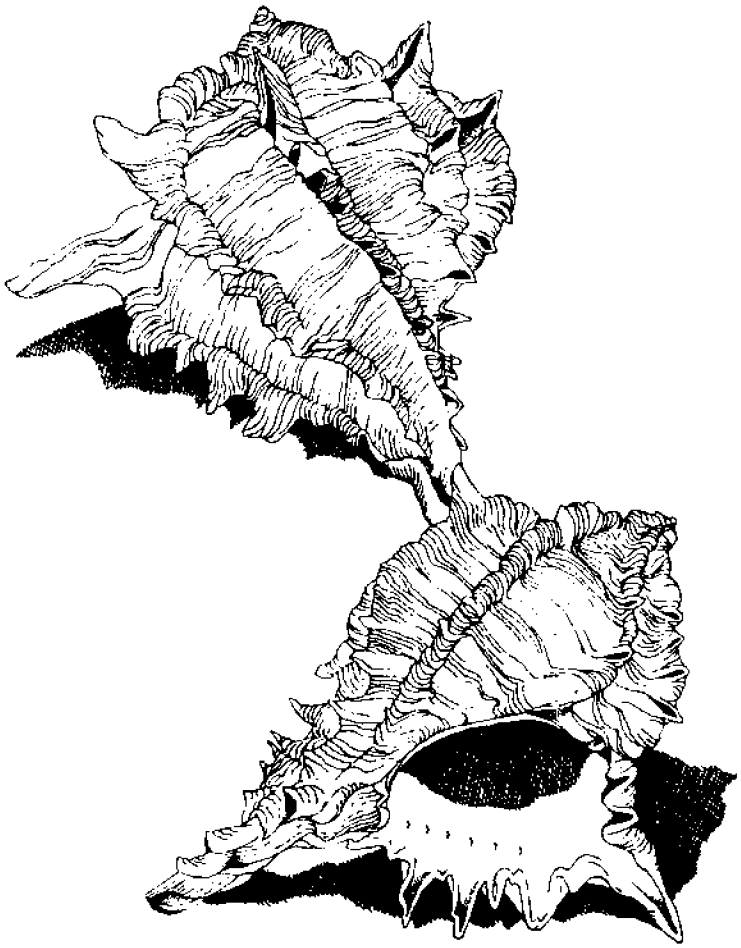

UNC Sea Grant College Program
Box 8605
North Carolina State University
Raleigh, N.C. 27695

The Physical Oceanography of Pamlico Sound

by

Leonard J. Pietrafesa
Gerald S. Janowitz
Tieh-Ying Chao
Robert H. Weisberg
Farid Askari
and
Elizabeth Noble

Department of Marine, Earth and Atmospheric Sciences
North Carolina State University
Raleigh, North Carolina 27695

This work was sponsored by the Office of Sea Grant, NOAA, U.S. Department of Commerce, under Grant No. NA86AA-D-SG046 and the North Carolina Department of Administration. The U.S. Government is authorized to produce and distribute reprints for governmental purposes notwithstanding any copyright that may appear hereon.

UNC Sea Grant Publication UNC-WP-86-5

November 1986

$4

Table of Contents

Forword and Acknowledgment of Support

This is Part I of a two-part report on the physical oceanography of Pamlico Sound and the peripheral nursery regions. Part I provides an overview of the present knowledge based on field and modeling studies of the sound proper, conducted principally at North Carolina State University. The sound field program at NCSU was conducted during 1978 and 1979. The modeling effort was also conducted at NCSU during 1979 and 1980. While the sound study was under way, an NCSU continental shelf program was also in place in the Carolina Capes coastal waters. This allowed for a coherent, coupled study. The sound study was funded by the University of North Carolina Sea Grant College Program, Office of Sea Grant, National Oceanographic and Atmospheric Administration, U.S. Department of Commerce under Grant No. NA81AA-D-0002; the U.S. Army Corps of Engineers; the North Carolina Department of Administration; and the Water Resources Research Institute. The complementary coastal study was funded by the U.S. Department of Energy under Contract No. DOE-AS09-EY00902 and Grant No. DE-FG09-85ER60376. Several reports, three peer-reviewed publications, seven talks at national conferences, and five graduate student theses (1 completed, 4 in progress) will have resulted, either totally or partially, from this Pamlico study. These studies have provided new insights into how fish are recruited from the Gulf Stream to the coast through barrier island inlets and across the sound to the nurseries.

Part II of the Pamlico Sound report will deal specifically with the nature and cause of salinity fluctuations within the nursery areas around Pamlico Sound. While Pamlico Sound is found to respond to the wind field and to the coastal ocean forcing, in that order, the nursery waters are found to respond to Pamlico Sound, the wind field and drainage, in that order.

While Part I and II of the Pamlico Sound story yield revealing insights into the fundamental physical oceanography, and hydrodynamic processes at work in the system, they also point to the need for a more inclusive coordinated field and modeling effort.

LIST OF FIGURES

LIST OF TABLES

1. INTRODUCTION

1. Setting

Pamlico Sound, North Carolina, a barrier island estuary, is the largest lagoonal estuary in the United States. It is 100 to 140 km long, 35 to 50 km wide, has a mean depth of 4.5 m and covers 4350 km^2. The Outer Banks, an island chain consisting of Hatteras, Ocracoke and Portsmouth islands, creates a barrier between the ocean and the sound. Oregon, Hatteras and Ocracoke inlets provide connections between sound and ocean waters. On the mainland side, the Trent-Neuse and Tar-Pungo-Pamlico river systems drain into Pamlico Sound. Freshwater sources are also present via Core Sound to the south, and from Albemarle Sound via connections to Pamlico Sound through the lesser sounds Roanoke and Croatan to the north. Shoaling regions within Pamlico Sound are found near the mouths of Roanoke, Croatan and Core sounds, the Neuse and Pamlico rivers and close to the Outer Banks inlets. Bluff Shoal, extending from Ocracoke due north to Bluff Point, roughly separates Pamlico Sound into two broad basins with the gently sloping bottom of the northern basin reaching a maximum depth of 7.3 m in its center. The southern basin bottoms at 7 m but is generally less deep than the northern basin. The entire estuarine system is depicted in Figure 1 and the sound bathymetry is shown in Figures 2 and 3.

2. Salinity

Roelofs and Bumpus (1953), Woods (1967), Williams et al (1973) and Schwartz and Chestnut (1973) have provided monthly summaries of the hydrography of Pamlico Sound with some insights into the hydrologic cycle from 1948 to 1966. From these data, Giese et al (1985) were able to prepare two snapshots of the average surface salinity (S) Pamlico Sound for the months of April and December; the former, the month of lowest S and the latter, the greatest. These snapshots are provided in Figures 4a,b.

Vertical stratification of S in Pamlico Sound has been reported to be between 0.1 and 1.0 parts per thousand (ppt) with the bottom waters more saline (Woods, 1967). Roelofs and Bumpus (1953) claim that the horizontally spatially averaged bottom minus surface S of the sound is 0.66 ppt. These authors attribute this scant differential to the effectiveness of the wind in mixing the water column vertically throughout the shallow sound. Undoubtly local topography can induce vertical motion locally, and the vertical orbital motion associated with the gravity wave field can also contribute to the breakup of any vertical structure. Alternately, Woods (1967) reported finding 6 ppt vertical differences in the southern basin during the spring, summer and fall of 1964. This was some four to seven weeks after a wet spring and reflected the phase lag in the drainage provided by the Neuse and Pamlico rivers. Pietrafesa et al (1986b) found that in upper Rose Bay (Figure 5), a juvenile fish nursery area, differences of 5 ppt over depths of two meters are not unusual. In fact, preliminary results from the recent studies of the sound nurseries (cf Gilliam et al, 1985) indicated that vertical S gradients in the rivers and bays are substantially greater than those in adjacent sound waters.

In the study of Rose Bay, conducted by Pietrafesa et al (1985) in the southwestern corner of Pamlico Sound, summer S ranges from 7 to 17 ppt; fall S

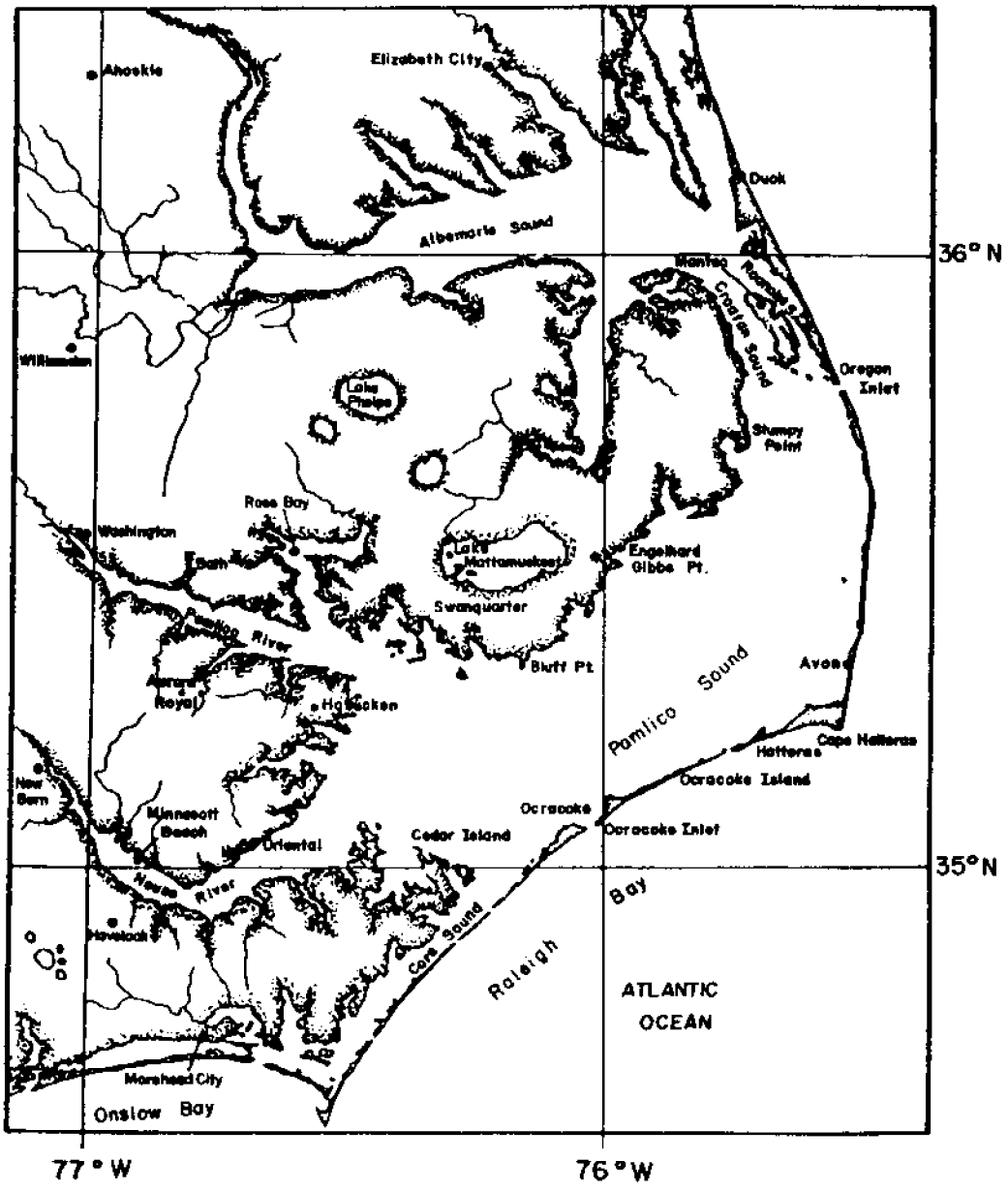

Figure 1. The geography of Pamlico Sound, North Carolina.

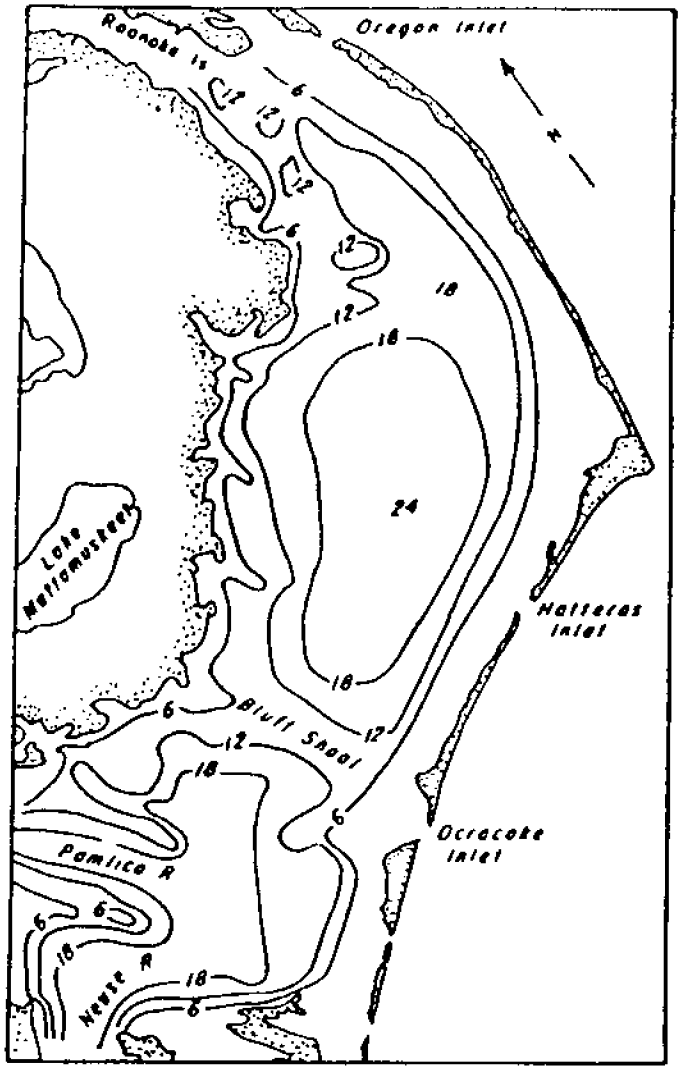

Figure 2. Bathymetry of Pamlico Sound.

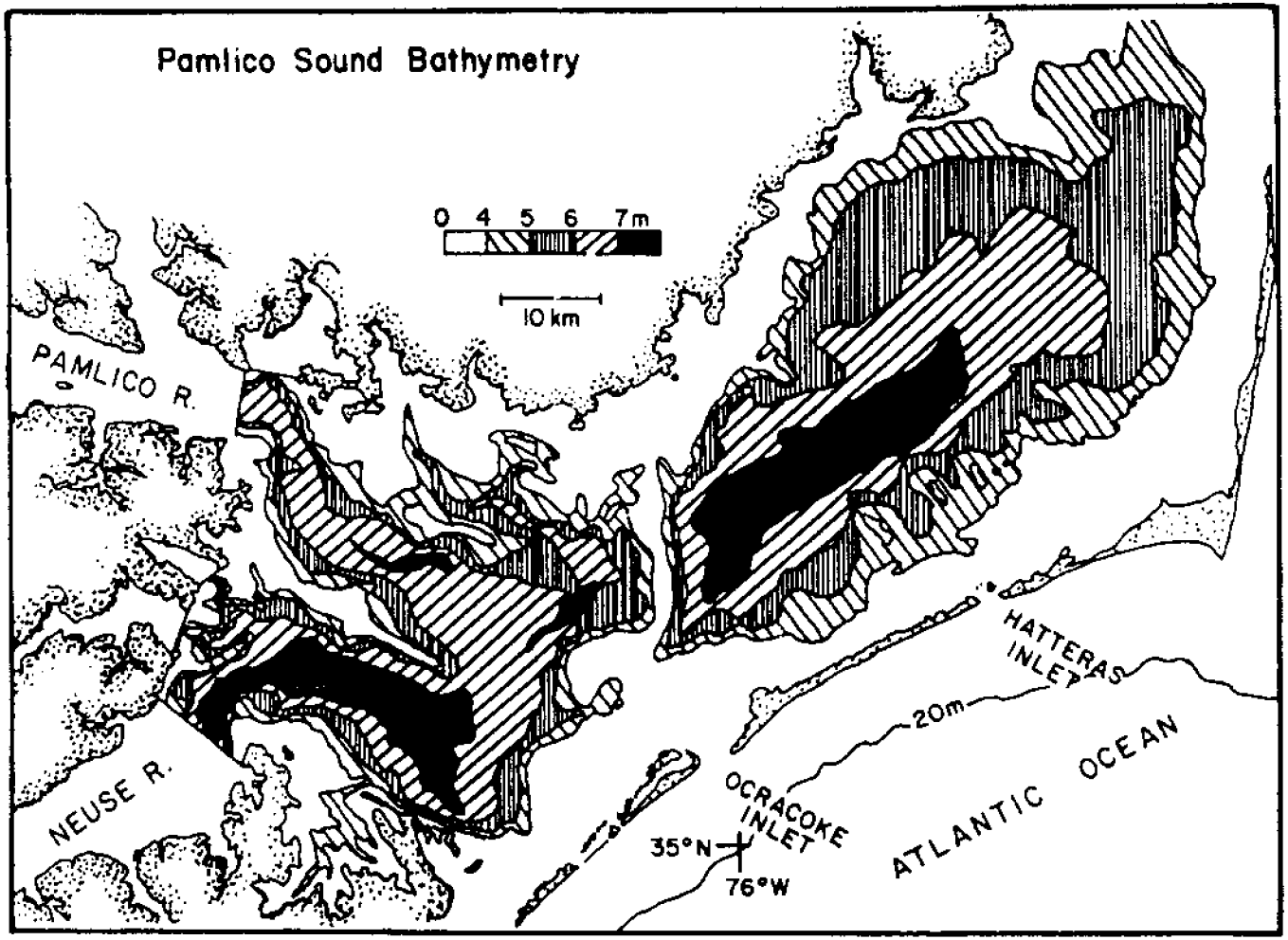

Figure 3. Pamlico Sound Bathymetry.

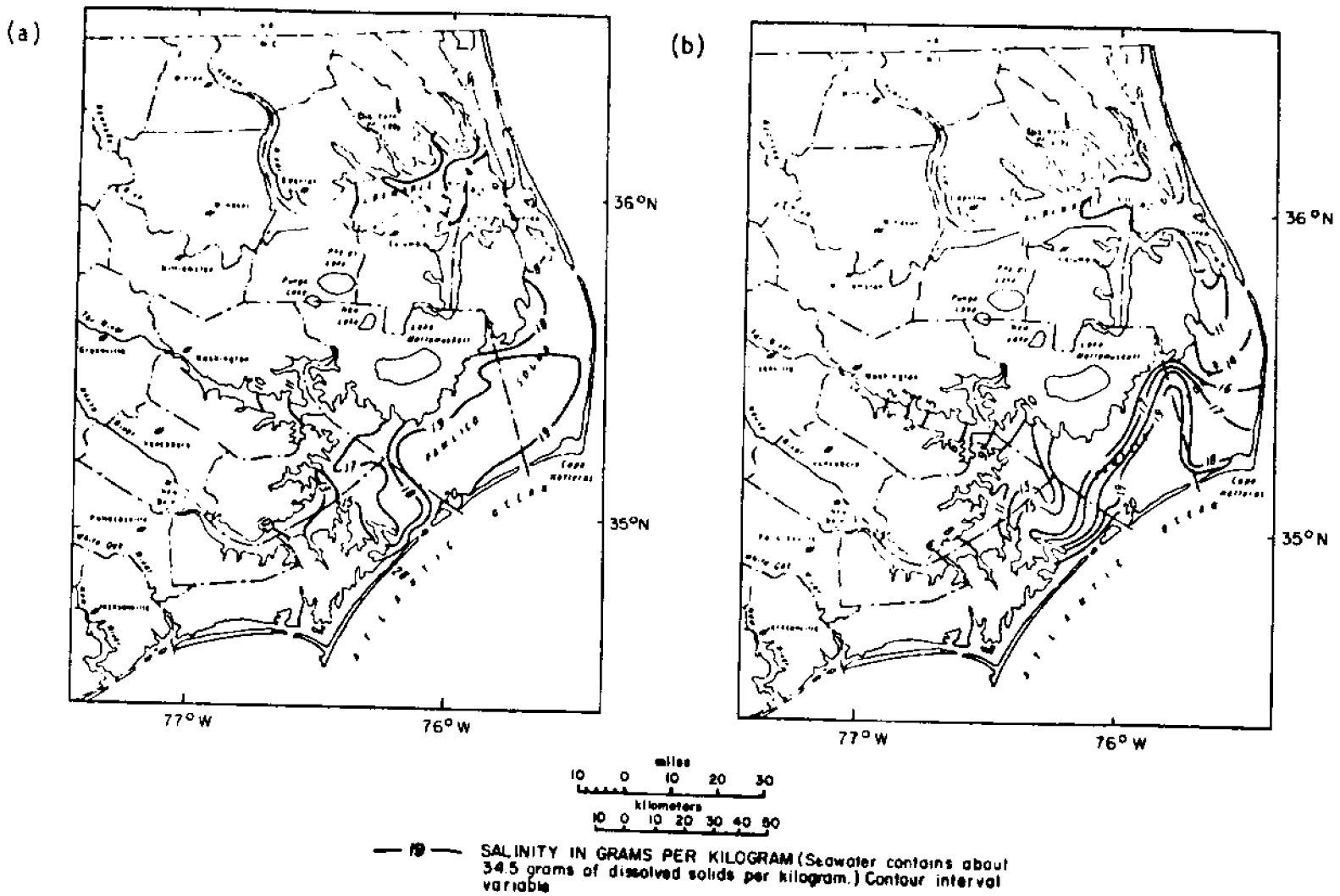

Figure 4a. Average surface salinity of water in Pamlico Sound and vicinity for the month of December. (Adapted from Williams and others, 1967.)

Figure 4b. Average surface salinity of water in Pamlico Sound and vicinity for the month of April. (Modified from Williams and others, 1967.)

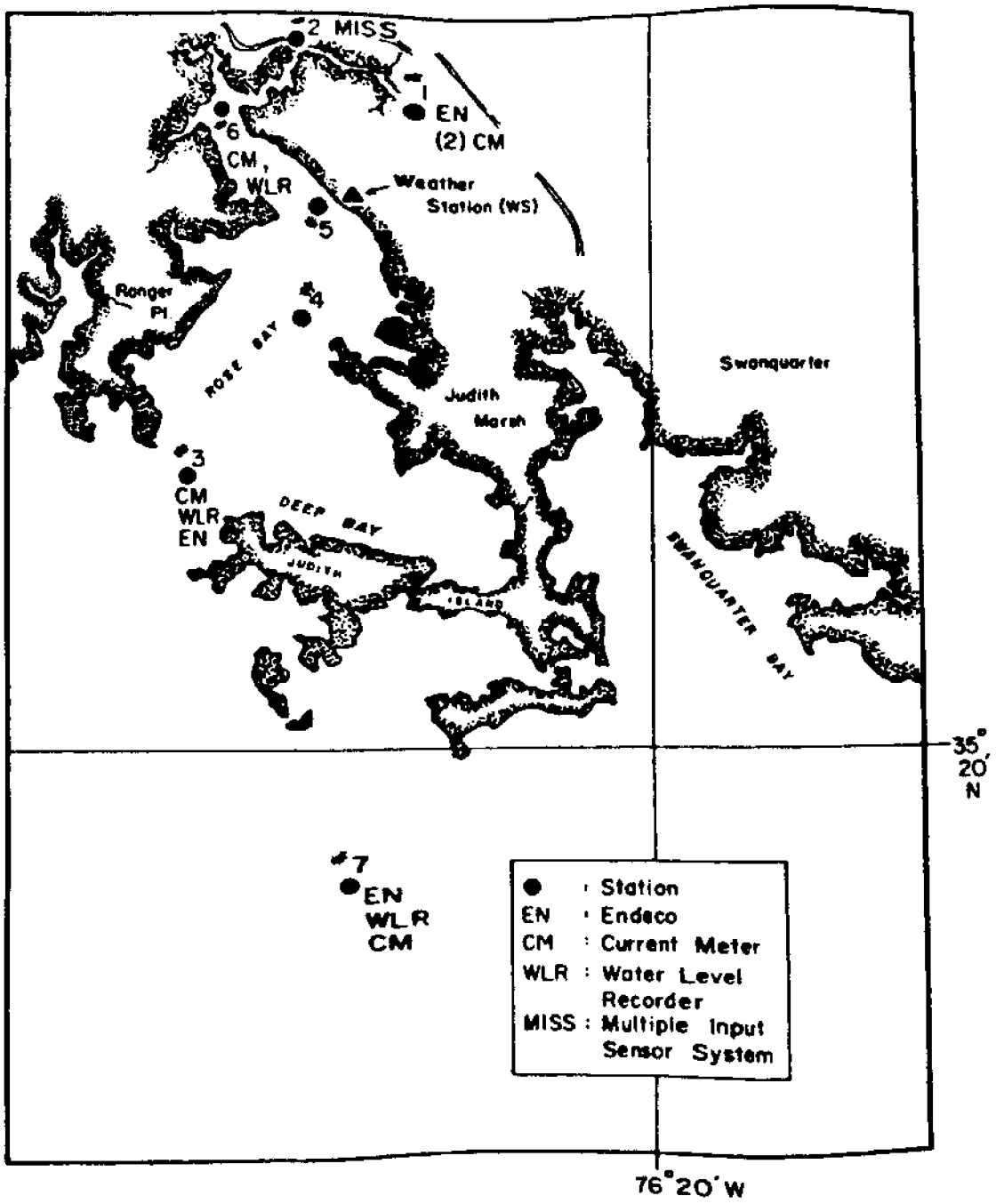

Figure 5. Rose Bay study mooring locations (cf. Figure 1 to locate Rose Bay).

ranges from 7 to 18 ppt; winter S ranges from 6 to 18 ppt; and spring S ranges from 2 to 13 ppt. Figure 6a is representative of the high frequency, large amplitude fluctuations that are evident in this corner of the sound. Figure 6b shows the percent of time that S spent at nearest integer values between 6 12-hour periods during the summer of 1982. The interpretation of this histogram is that, 27.4 percent of the time, S was 16.0 ppt $\pm$<0.5 ppt within any 12 hour period (where the symbol "<" means "less than"). Clearly it is difficult to ascribe a single value of S for any seasonal period given the suggested variability. Figure 6c provides "first differences" of the S data in Figure 6a.

From 6b we conclude that during the summer of 1982, in the southwest corner of Pamlico Sound, 40.5 percent of the time the variations in S were less than $\pm$0.5 during any consecutive 12-hour period. Alternately, 44 percent of the total time variations greater than $\pm$0.5 but less than $\pm$1.5 were observed, and ~15% of the total time S fluctuations of $\pm$1.5 to 4.5 ppt were measured during consecutive half-day periods. It is of note that changes of between $\pm$4.5 to 7.0 ppt in S were observed 0.75 percent of the summer of 1982. While the number of occurrences of such changes were few, the magnitude of these changes was dramatic. The lesson learned from Figures 6a, b and c is that an observer taking a shipboard T,S sample at station x, at time y, on date z may conclude that $S(x,y,z) = S_o$ is representative of S during that season, month, week or day. A second observer making the same measurement at station x but at time y + n hours (where n represents whole integers 1,2,3,4,...) on day z + m, days (where m is 1,2,3,4,...) might find that S(x, y+n, z+m) = So + ΔS where ΔS could be between $\pm$1 ppt to $\pm$6 ppt. Neither observer could reach any definitive conclusion on a representative S. The moral of the story is that if the fluctuations in S are to be understood, then S must be monitored not seasonally, not monthly, not weekly, not daily but at a minimum of one sample every two hours.

The sources of salt water for Pamlico Sound are the barrier island inlets. Saline Carolina coastal water (CCW), with an S range of 34.5 to 37 ppt, enters the sound via Ocracoke and Hatteras Inlets. Virginia coastal water (VCW) ranging from 31 to 34 ppt, relatively fresh compared to CCW, enters through Oregon Inlet. In a recent paper, Pietrafesa and Janowitz (1986) discuss the actual mechanism by which water enters and exits through the inlets. Giese et al (1985) point out that the differences in S between the months of lowest and highest mean S, April and December respectively, is about 5 ppt at the mouths of the feeder rivers and less than 2 ppt at the barrier island inlets. Thus the inlets remain a relatively constant source of salt water.

Factors such as the greater salt content of CCW versus that of VCW, the relative location of Oregon Inlet to the north and Ocracoke and Hatteras Inlets to the south, and the mainland freshwater sources, all contribute to general north-to-south and west-to-east S gradients. Even so, occasional reversals in the horizontal gradient in S have been observed (S. Ross and S. Epperly, NCDMF, personal communication). Unfortunately, there was a lack of synopticity in the sampling schemes used in the hydrographic sampling programs conducted in the sound. This is not to fault those hydrographic programs for being improperly conducted. Rather, this is to point out the difficiencies of shipboard sampling programs in large bodies of water. Creating a snapshot in time of an S field in space is difficult when S is changing rapidly in space as a function of time.

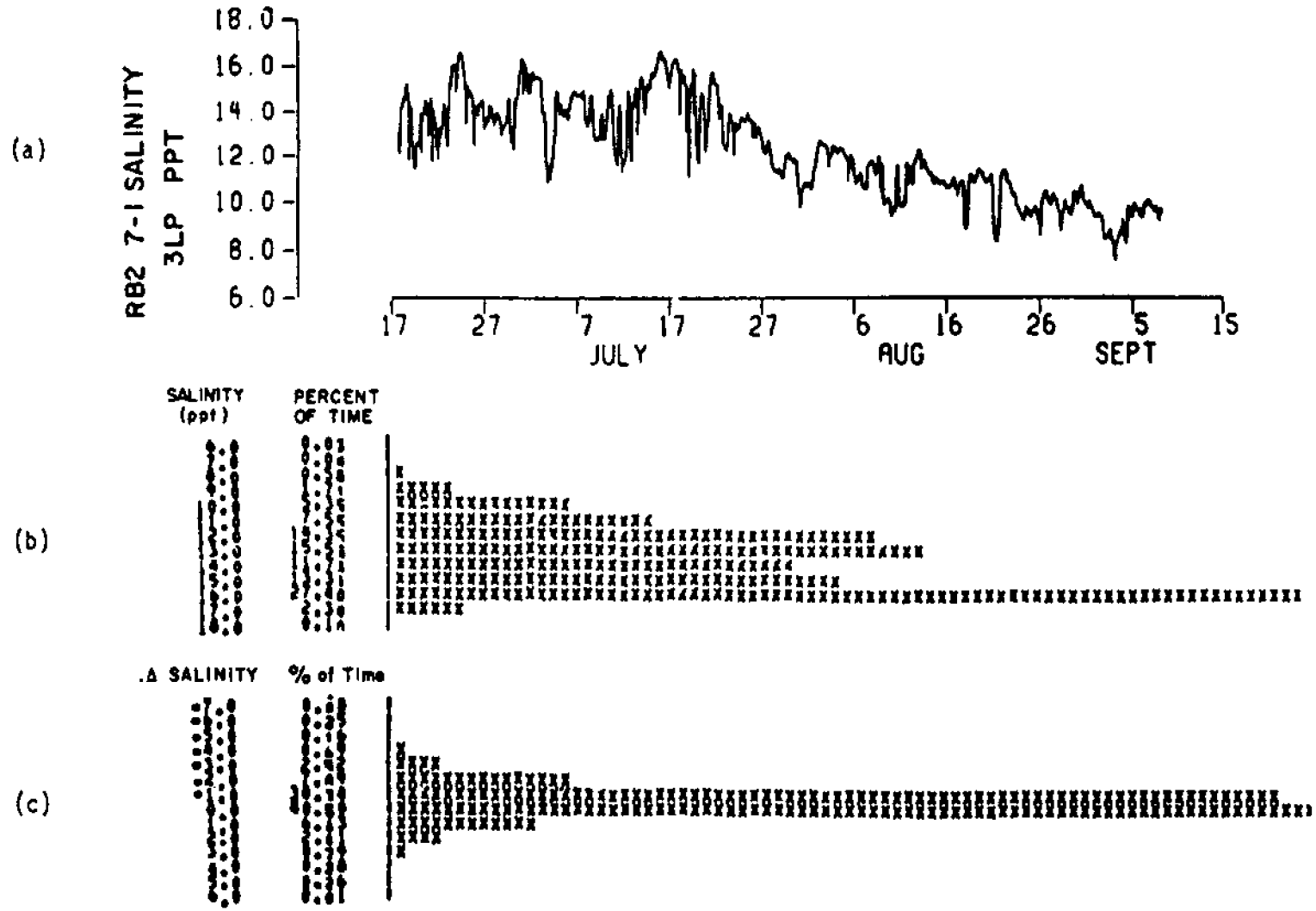

Figure 6. a. Three-hour low pass filtered salinity observations collected at station 7 (cf. Figure 5) in south basin of Pamlico Sound during summer 1982.
b. Salinity values in (a) as a function of percent of time of time series in which S was within ± 0.5 of an integer value.
c. First differences of (a) time series.

The relative importances of wind versus runoff in determining S distributions thoughout the sound over periods of days to weeks to seasons has been addressed but not fully assessed. Giese et al (1985) provides a summary of the previous studies of S within the sound. The literature survey concludes that easterly (from the east) winds generally increase sound S while westerlies are typically associatd with a drop in S. Northerlies are found to cause lower S in the northern basin, while raising S in the southern basin. Winslow (1889) is the source of the latter finding. This classic study also determined that southerly winds created the opposite effect, i.e. S rose in the north basin and dropped in the southern basin. Alternately, Giese et al then refer to the findings of Roelofs and Bumpus (1953) which indicate that S in Core Sound (off of the southern basin) decreases in concert with northerlies and increases with southerlies. The authors point to the existence of Whalebone Inlet, open during Winslow's study and now closed, and Drum Inlet, nonexistent during Winslow's study but open during Roelofs and Bumpus's effort, as a possible explanation for the discrepancy. Unfortunately, insufficient data presently exists to fully answer the basic questions.

Giese et al (1985) position themselves on the side of runoff in the determination of "long-term average net flows at any point," and, as a consequence of this posture, the authors believe that freshwater flow is responsible for longer term S distributions. We now consider freshwater input to Pamlico Sound.

3. Fresh Water

Fresh water input to Pamlico Sound is derived from precipitation, evaporation, land drainage via the Albemarle-Roanoke-Croatan sound system, and by rivers such as the Trent-Neuse and the Tar-Pungo-Pamlico.

From September through May the mean monthly rainfall on the sound is about 10 cm, while from June through August, the rate rises to 14 cm/month. Evaporation falls some 15 cm shy of maintaining a balance with the yearly rainfall, 114 cm versus 129 cm, respectively. Seventy-one percent of the total yearly evaporation occurs from May through October. These data were abstracted from Roelofs and Bumpus (1953).

Runoff input has been estimated by Chu (1970). He found that the mean annual amounts of fresh water from the Neuse River was 145 m^3/sec, from the Pamlico River 130 m^3/sec, and from Roanoke and Croatan sounds, 80 m^3/sec and 448 m^3/sec, respectively. Giese et al (1985) quote values of 173 m^3/sec discharge from the Neuse and 153 m^3/sec from the Pamlico Rivers - fluxes comparable to those of Chu. However Giese et al (1985) also quote values of 906 m^3/sec from Roanoke and Croatan Sounds, taken together a number exactly twice the value given by Chu. In Tables 1 and 2 and Figures 7 and 8, a monthly and annual water budget for Pamlico Sound is presented. These tables were adopted and modifed from Giese et al (1985). The sources of fresh water are direct precipitation, direct net inflow from adjacent land feeding into tributary rivers and direct net flow from adjacent sounds. The principal freshwater sinks are evaporation and the outwelling into the coastal ocean through the inlets. From Table 2 we see that, on the average, it takes approximately 11 months to replace 2.6 (10^{10}) m^3 of storage in Pamlico Sound. Under typical circumstances the S of the system will likely maintain its more typical distribution. But there are other scenarios.

TABLE 1. Monthly and annual gross water budget for Pamlico Sound

Element of Gross water budget	Avg. monthly and annual values in cubic meters												
	Jan	Feb	Mar	Apr	May	Jun	Jul	Aug	Sep	Oct	Nov	Dec	Average annual
Precipitation on Pamlico Sound	191.0	224.56	187.46	152.35	186.61	264.48	356.8	342.64	305.83	190.01	200.49	199.35	233.62
Evaporation from Pamlico Sound	65.98	93.73	138.76	213.23	243.25	263.92	283.17	217.48	173.02	115.53	84.96	56.35	152.54
Freshwater inflow to Pamlico Sound from land areas tributary to Pamlico Sound	481.4	611.66	540.86	373.79	319.99	176.13	253.16	308.66	241.55	223.71	233.34	314.32	339.81
Inflow from Albemarle Sound to Pamlico Sound	645.6	801.38	707.93	603.16	438.92	345.47	402.11	416.27	370.96	303.0	376.62	441.75	487.06
Net outflow from Pamlico Sound to the coastal ocean	1251.6	1543.3	1296.9	917.48	702.27	521.04	727.76	849.52	716.43	600.33	753.24	900.49	897.65

TABLE 2. Monthly and annual gross fresh water input for Pamlico Sound

WATER STORAGE IN PAMLICO SOUND

January---3.35 x 10 to the power of 9

February---3.73 x 10 to the power of 9

March---3.47 x 10 to the power of 9

April---2.38 x 10 to the power of 9

May---1.86 x 10 to the power of 9

June---1.35 x 10 to the power of 9

July---1.95 x 10 to the power of 9

August---2.27 x 10 to the power of 9

September---1.86 x 10 to the power of 9

October---1.61 x 10 to the power of 9

November---1.95 x 10 to the power of 9

December---2.41 x 10 to the power of 9

AVERAGE ANNUAL EQUALS 2.35 X 10 TO THE POWER OF 9

*** NOTE: Basin size in cubic meters equals 2.6 x 10 to the power of 10

Units are in cubic meters.

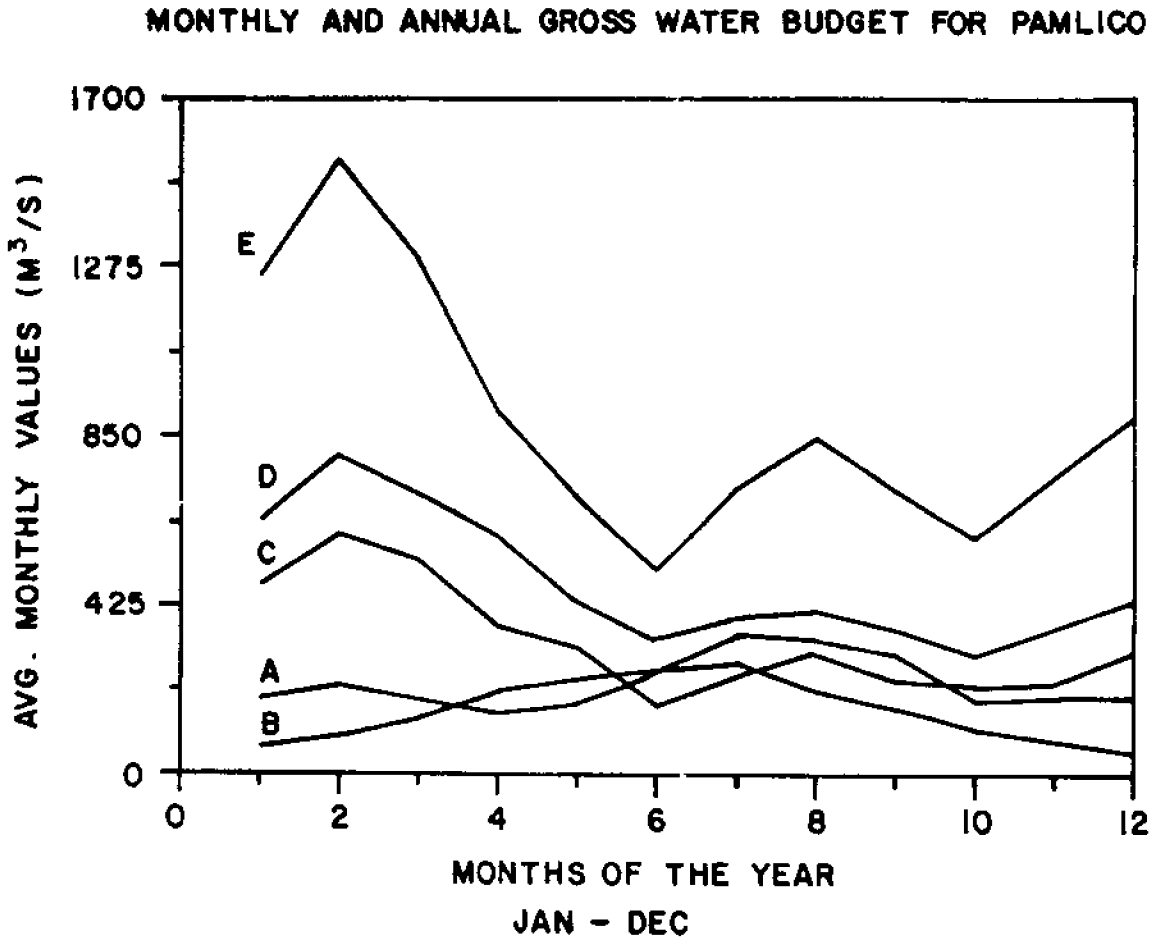

Figure 7. Line A - Precipitation on Pamlico Sound (source).
Line B - Evaporation from Pamlico Sound (sink).
Line C - Freshwater inflow to Pamlico Sound from land areas tributary to Pamlico Sound (source).
Line D - Inflow from Albemarle, Croaton and Roanoke Sounds to Pamlico Sound (source).
Line E - Net outflow from Pamlico Sound to the coastal ocean via the inlets (or outlets).

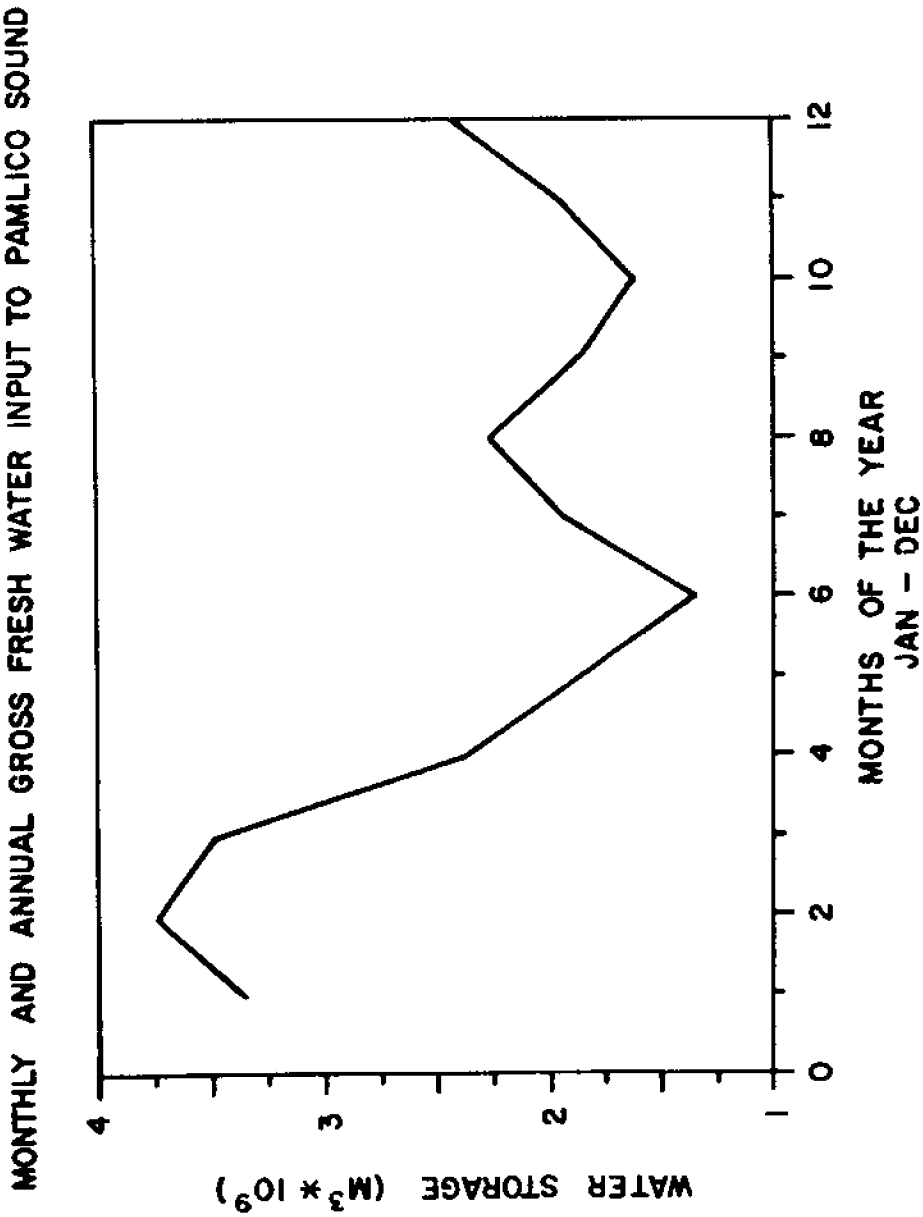

Figure 8. (Refer to Table 2.)

If it were to rain more heavily from October through March, then the demand for water from the coastal ocean would be reduced and the sound would freshen greatly since it would neither be receiving nor demanding salt water. The sound would tend to homogenize both vertically and horizontally. Via the opposite argument, a very dry October through March would result in a much saltier sound - a lagoon with relatively large horizontal and vertical gradients. Evaporation is relatively low during this time of year.

From April through September the evaporative process reaches its annual peak (Figure 7). This process is mainly temperature dependent and constant from year to year. Rainy summers will not only be a source of fresh water but will also be characterized by increased cloud cover and diminishment in the loss of fresh water through evaporation. So, rainy summers increase the source and inhibit the sink of fresh water. The result is a more brackish sound with decreased salt content and gradients thereof. Dry summers have the opposite effect.

4. Temperature

Water temperature in Pamlico Sound is believed to be inexorably coupled to air temperature. Roelofs and Bumpus (1953) found a one-day lagged correlation coefficient between air and surface water temperature to be 0.972 for their data sets based on Cape Hatteras air temperature and surface water temperatures on the sound side of Hatteras Island. In Figure 9a we show a typical plot of air temperature across Pamlico Sound, from Cape Hatteras to Cherry Point. In Figure 9b a representative plot of air and water temperature in Pamlico Sound 1 meter below the water's surface is shown. Roelofs and Bumpus claim that, in general, between the range of 10°C to 29°C, surface water temperature can be directly predicted from air temperature, with a several-day lag sufficient for the surface water to adjust to the air. Between the air temperature range of 0°C to 10°C, the Roelofs-Bumpus study would logically result in a relationship such that water surface temperatures (T_s) vary as two-fifths of the sum of the air temperature (T_a) plus 12.5 °C, i.e. $T_s = \frac{2}{5}(Ta + 12.5)$. The same study also suggests that vertical water column temperature gradients rarely exceed 0.4° c/m and more typically are less than 0.2° c/m. Horizontally, sound temperature gradients are reported to be relatively weak, i.e. between .05-.01 °c/km. However, Figure 9b shows clearly that at 1 meter below the water's surface, water temperature may track that of air but does not display a one-to-one correlation.

At depth, water temperatures look much like their navifacial counterparts but for less high frequency variability and a compressed magnitude of fluctuation. Figure 9a shows the high coherency between Cape Hatteras and Cherry Point air temperatures. The differences between Cherry Point air and Pamlico Sound water temperature, collected 1 m below the surface on a fixed mooring in the southern basin, indicate the need for a more extensive study incorporating fixed temperature sensors at specific locations which can measure temperature (T) every 2 hours for periods of up to a year, if the true response of water temperature to air temperature fluctuations and vertical and horizontal gradients of water temperature are to be ascertained.

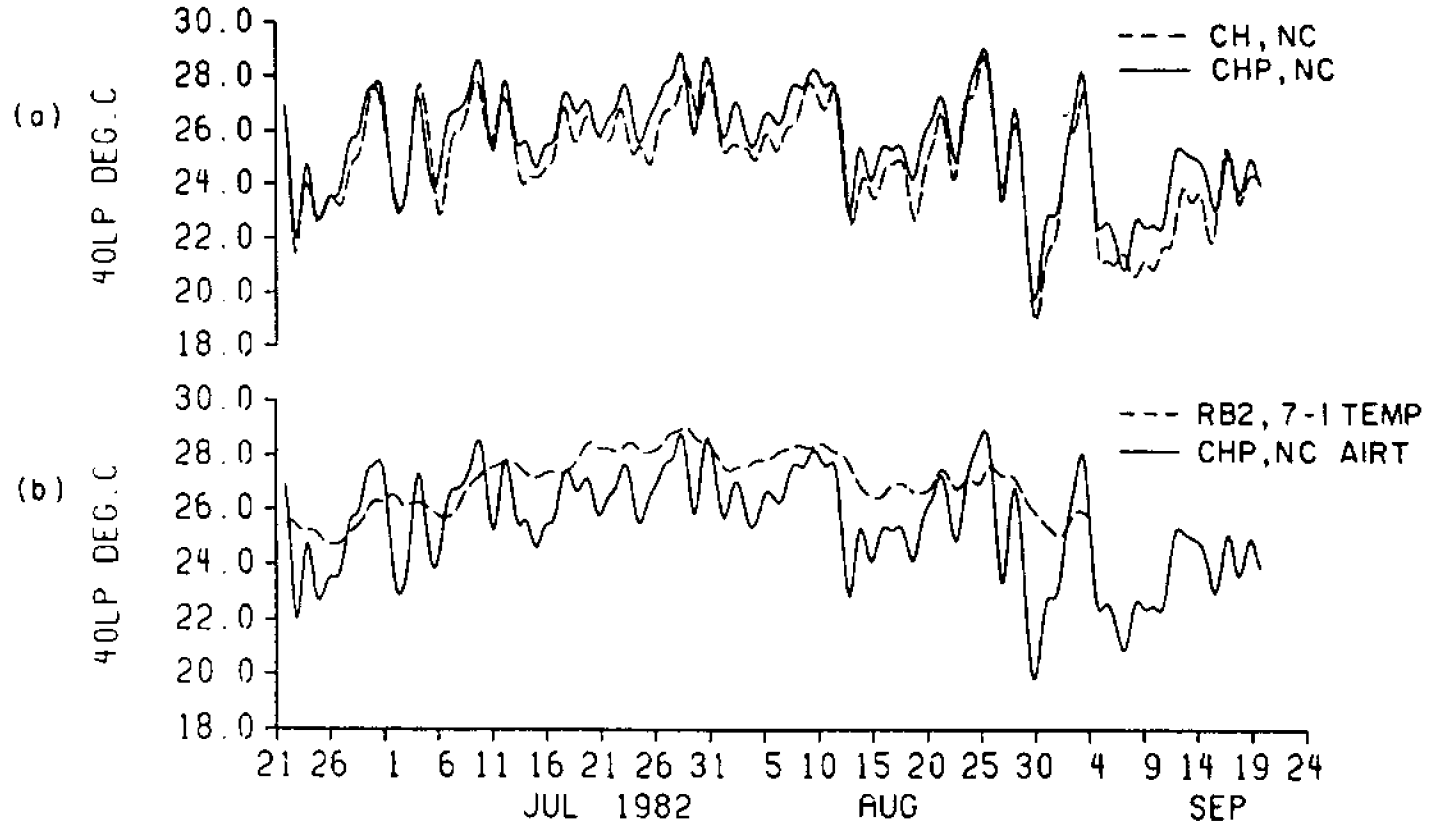

Figure 9. (a) Comparison of air temperatures at Cape Hatteras, NC (CH) and Cherry Point, NC (CP). Cape Hatteras is to the east on the coast while Cherry Point is to the west on the mainland.

(b) Comparison of Hatteras air temperatures and water column temperatures 1 meter below the water surface at Station 7 (cf Figure 5 for location of Station 7).

5. Thermohaline Gradients

It is not presently known whether temperature, salinity or density fronts of any significance exist within Pamlico Sound. Time series of S and T within the sound proper do not exist save for the study by Pietrafesa et al (1986) shown in Figure 5. This latter study provides the only "continuous" (e.g. 10-minute sampling interval) S and T data taken at a fixed station. Unfortunately these data are limited in geographic application because the data was collected as part of a juvenile nursery area study. Consequently, the data sets are concentrated in several bays, namely Rose and Juniper. These data are not necessarily representative of the time series of T or S in Pamlico Sound proper. However, there were several time series of T and S collected soundward of the mouth of Rose Bay, and these data do represent T and S variability in the southwest corner (Station 7) of the sound. The Station 7 S and T time series shown in Figures 6a and 9b, respectively, display the frequency and mangitude of variability of both T and S in Pamlico Sound. They speak to the need for a more concerted hydrographic effort throughout the sound. The once-a-month, spot sampling approach, which has provided us with the only soundwide hydrography to date, clearly creates doubt on the relative worth of past T-S studies given the rapidity and strength of T-S fluctuations shown to exist at Station 7.

A climatological record of temperature, salinity and density averaged over years of monthly observations can be obtained by spatially averaging these data within and without the sound, respectively. Water of depth less than 20 meters in Raleigh Bay, the coastal regime adjacent to Hatteras and Ocracoke Inlets, are hydrographically contrasted with Pamlico Sound southern basin waters in Figures 10 a,b,c. Sound waters are colder from November through March by 2° to 9°C and warmer from April through August by 1° to 6°C than are adjacent coastal waters. Coastal waters are always more saline and dense than sound waters, with relative differential highs occurring during the period November through June and relative lows from July through October. However, bottom waters achieve their yearly minimum difference in both S and σ_t during February, a month sandwiched between high ΔS and $\Delta\sigma_t$ differentials.

The implications of the mean monthly salinity, temperature and density gradients between sound and coastal waters as they might provide for or inhibit finfish larval transport pathways are not known. However, the hydrographic cycles suggest that perhaps larvae are hydrographically cued and may be recruited when ΔT and ΔS are in tune with a convenient flow field. It is conceivable that large scale T and/or S fronts may propagate across the shelf during either stormy or quiescent periods which may be tracked by larval fish.

Mini-thermohaline fronts may also exist, particularly near the inlets, within or beyond the mouths of the bays and rivers, as suggested in the study of surface chlorophyll and salinity in the Neuse River as perceived in several Landsat satellite images (Khorram et al, 1985), near shoaling areas, and during small scale atmospheric storms. Unfortunately such a study requires mapping with a towed thermosalinograph and no such investigation has been conducted to date. The need, resources and manpower are there; however, various government and management agencies have lacked the insight to endorse such studies to date.

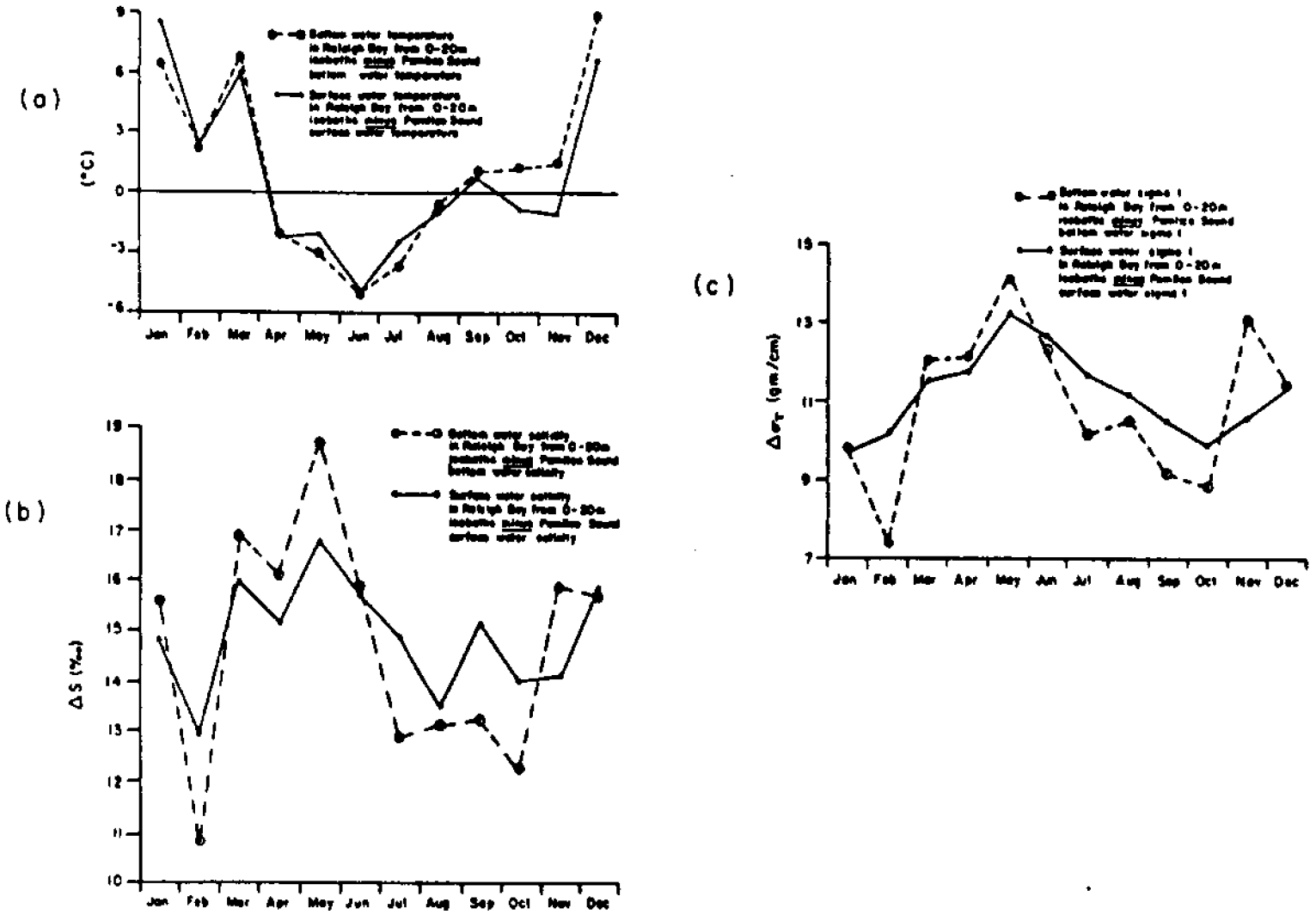

Figure 10. Monthly surface and bottom S, T, and Sigma t differences between Raleigh Bay inner shelf and Pamlico Sound waters.

6. Tides

Marshall (1951) and Posner (1959) concluded that astronomical tides in Pamlico Sound proper are negligible. The rationale was that the sound is too shallow vertically and narrow laterally to be directly forced by the tidal potential. Consequently, tidal forcing can only occur via the barrier island inlets through which the adjacent continental margin tides must make entry.

North Atlantic East Coast USA tides have been described variously by Redfield (1958), Pietrafesa (1983), Moody et al (1984) and Pietrafesa et al (1985). In summary, the principal tidal constituent, in both the Mid and South Atlantic bights is the semi-diurnal lunar or M2 component which has a period of 12.42 hours or approximately 12 hours, 25 minutes, 12 seconds. The M2 tide is a co-oscillation of the Atlantic Ocean tide and appears on the ocean sides of the barrier island inlets as consecutive highs and lows in water level elevation every 6.21 hours. The tidal wave (a "Poincare" wave) cannot propagate freely into and out of the sound, but rather sets up a boundary condition whereby the water elevation fluctuation due to the rise and fall of coastal sea level associated with the M2 tide creates pressure gradients along the axis of inlet, so that as the water level rises with an incoming or "high" tide, a downhill tilt of the water surface is created. The gravity force affected by this tilt eventually drives a current, the flooding tide, into the sound. Given the mound of water which builds outside of the inlets and the narrow widths and shallow depths of these sea-sound connectors, the flood tide appears to "jet" in. The exiting tide, the ebb, occurs similarly in that, as the shelf tide begins to recede from the coast during the transgression from high to low, a drop in coastal sea level occurs and a downward tilt of the water's surface from within to without the sound, along the axis of the inlet, eventually drives a current out. Marshall (1951) speculated that the tide is damped rapidly away from the inlets. Support for this assumption is obtained by a comparison of Ocracoke Inlet and the Ocracoke Coast Guard Station tidal heights. There is a 3.55 cm/km drop in mean tidal range away from the inlet or a drop of 4.35 cm/km during spring tides.

In Table 3, representative tidal ranges and ebb and flood currents for Oregon, Hatteras and Ocracoke Inlets are presented.

If the assumption is made that the drop in range of tide from the Ocracoke Inlet to the Ocracoke Coast Guard Station (separated by a distance of 7.73 km) is representative of the general spatial attenuation of tidal height, then both "mean" and "spring" tides would lose recognition within 16.3 km of the inlet. However, Singer and Knowles (1975) and Pietrafesa et al (1986) have reported a semi-diurnal tidal signal in current measurements made in both the Neuse River and in the southwest corner of Pamlico Sound, respectively. Chao (1981) reported an M2 signal in sea level collected at various locations in the sound. Representative examples of the Neuse River along axis current data are shown in Figures 11a, and b and the sea level testimony is left for the section "Sea Level" (I-8). It may well be that the M2 tide in Pamlico Sound is manifested as a simple longitudinal reversing pattern aligned with the major axis of the basin. Unfortunately current meter data which could be used to interrogate the true character of the M2 tide in the sound are nonexistent and need to be collected in a systematic study.

At this time it can only be assumed that tidal motions in Pamlico Sound will be less significant with distance from the inlets. A tidal wave

TABLE 3. Oregon Inlet flood and ebb data

Inlet	Date of Observation of Tidal Flow data	Mean Tidal Range (in cm)	Spring Tidal Range (in cm)	Tidal Flow Data Representative currents in cm/sec	
				Flood	Ebb
Oregon	28 June, 1973(a)	61.0(c)	73.2(c)	75.8(a)	64.7(a)
Hatteras	25 May, 1958(b)	61.0(c)	73.2(c)	109.7(b)	103.6(b)
Ocracoke	25 May, 1958(b)	57.9(c)	70.1(c)	80.8(b)	86.6(b)
	14 Oct., 1962(b)			106.6(b)	140.9(b)
	1977 (c)			88.4(c)	121.9(c)

The sources of information are:

(a) Singer and Knowles, 1975

(b) U.S. Army Corps of Engineers Report

(c) National Ocean Survey Tide and Tidal Current Tables - 1977

(a)

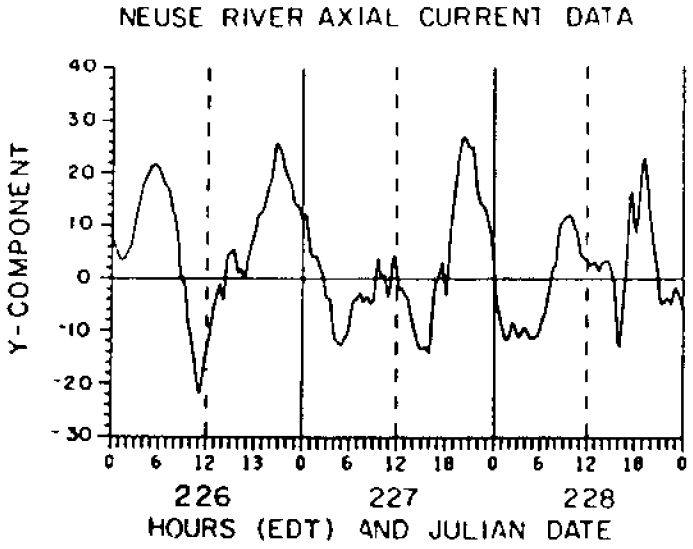

(b)

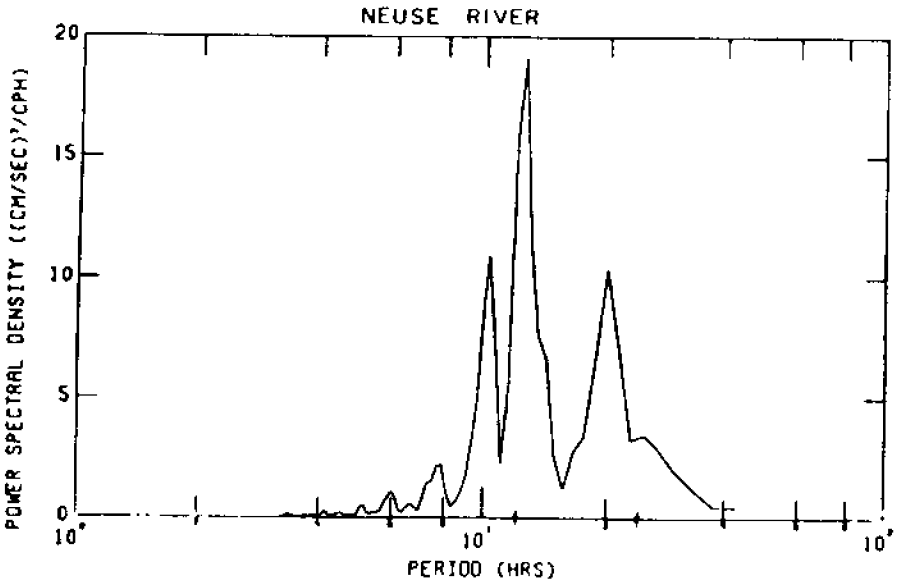

Figure 11. (a) Time series of along axis currents in the Neuse River indicating presence of semi-diurnal signal.
(b) Power spectra of along axis currents in the Neuse River indicating presence of semi-diurnal signal.
(From Knowles, 1975.)

progressing through the sound would be damped frictionally by each successive shoal or channel. The complex nature of the bathymetry of the sound is suggested in Figures 4 and 12.

Previously it was noted that the astronomical tidal wave produces a slope in the water surface at the opening to the inlet. The magnitude of the resulting flood or ebb current will be directly dependent upon the magnitude of this slope. However, wind-induced motions in either the coastal ocean or the sound can also create water surface slopes. Pietrafesa and Janowitz (1986) have recently shown that these wind-induced slopes may either enhance or diminish the tidal flows into and out of the inlets. As a function of the relative strengths of the pressure gradient forces associated with the tidally-induced vs. wind-induced water surface slopes, floods and ebbs may be greater than normal or may appear to not occur at all.

The barrier island inlets can, by the very nature of their formation and maintenance, be sufficiently narrow to produce fluid jetting. The incoming tide creates a jet-like motion, whereas the flow associated with the falling tide is like a potential flow toward a sink (Milne-Thompson, 1968). Over a complete tidal cycle, the circulation would simulate a double vortex sheet along the edge of a widening jet. Using these concepts, Lee and Rooth (1972) estimated a radius of inlet jetting to be approximately 500 times the mean depth of the inlet. A depth of 5 m would yield a jetting radius of 2.5 km while 11 m gives 5.5 km. Given inlet complexity, the simple formula of "Radius of jetting = 500 Mean Inlet Depth" is at best a ballpark estimate. Nonetheless, the evidence is there. The Pamlico Sound satellite image depicted in Figure 13 suggests a plume extending several kilometers from the inlet.

7. Winds

Pietrafesa and Weisberg (1979) and Weisberg and Pietrafesa (1983a,b) provide an overview of the synoptic meteorology of the South Atlantic Bight. There were several important findings in these studies which are germaine to a discussion of the physical oceanography of Pamlico Sound. First, these authors found a low-frequency rise in wind energy toward a seasonal time scale; second, a mid-range wind energy plateau exists at synoptic wind scales; and third, a sharp energy peak exists at the sea breeze time scale. The highly energetic snyoptic range lies between time scales of 2 to 30 days centered at 4 to 6 days. Averaging over an entire year the authors found a northeastward vector. Winter and summer were found to be seasons of maximum and minimum in both means and variances with fall and spring being transitional. During the winter, cyclones are most active, with storms progressing toward the east-northeast and mean monthly winds directed southeastward. The mean wind vector rotates cyclonically through the spring transition to occupy a northeastward set during the summer. August denotes a period of minimum wind magnitude. September and October are transitional months, and by November mean winds are directed southwestward. However, the most important findings concerning the disposition of the wind field in Pamlico Sound derive from a study of the relationship between water level fluctuations and wind conducted during the period January 1978 to February 1979 and presented in Section II.

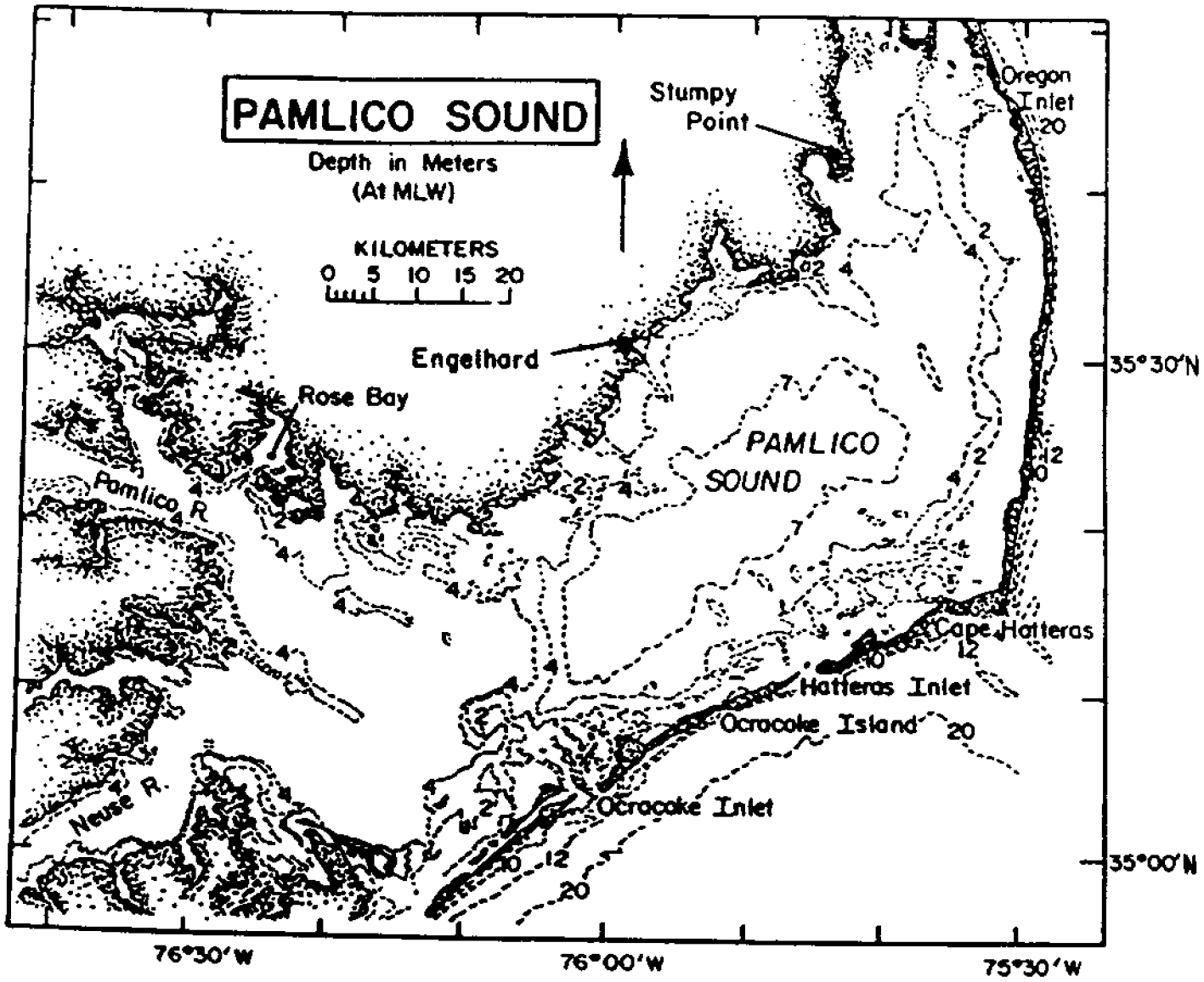

Figure 12. Pamlico Sound Bathymetry.

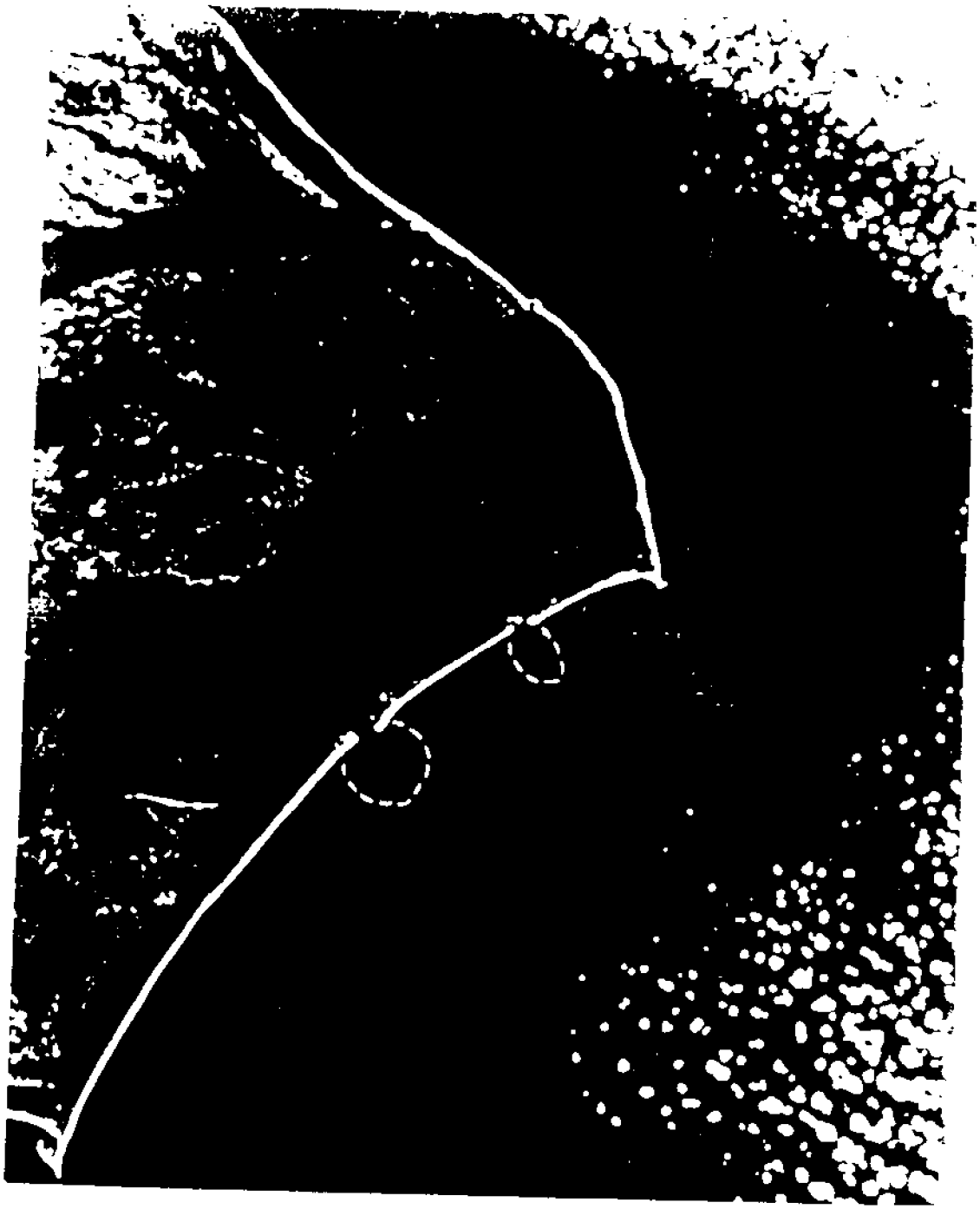

Figure 13. NOAA satellite image of: Pamlico Sound; Portsmouth, Ocracoke and Hatteras Islands; and Ocracoke, Hatteras and Oregon Inlets. The dashed lines depict the perimeter of the plumes which form during the tidal ebb jetting process.

8. Sea Level

The principal factors which affect sea level in Pamlico Sound include atmospheric winds, changes in coastal sea level, water density, precipitation and evaporation, river discharge, atmospheric pressure and astronomical tides. We have not yet addressed atmospheric wind or pressure effects, the influence of the rise and fall of the coastal ocean nor the effects of water density changes.

Atmospheric pressure changes over the water's surface can create an inverse barometer effect wherein a 1 millibar rise or fall in pressure exacts either a -1 cm (drop) or +1 cm (rise) change in sea level. This is not the result of compressibility, but rather an isostatic adjustment. However, the effect breaks down when the spatial scale of the atmospheric pressure system is much larger than the size of the local basin. This, as we will show, appears to be the case in Pamlico Sound.

The limited hydrographic time series collected in Pamlico Sound indicate that it is well mixed in the vertical direction but that horizontal salinity changes can be appreciable. Consequently, the vertical integral of the horizontal density gradient can be an important local factor in sea level variations. But given the paucity, i.e. virtual lack of serial observations of density, the consequences of its spatial gradients cannot be assessed at this time.

Monthly to seasonal to annual variations in sea level, due to thermal variability of the Atlantic Ocean, i.e. the heat content of North Atlantic central water, can significantly affect sea level in the coastal ocean and, subsequently, Pamlico Sound. During the period January to February, water temperatures are the lowest of the year on the North Atlantic shelf due to atmospheric cooling, and sea level is at its yearly minimum, standing 20 to 25 cm below zero datum as shown in Figure 14. However, during the period of late winter to early spring, the heat content of North Atlantic central water increases down to a pressure depth of about 100 db corresponding to a spatial depth of about 100 m. Sea level begins to rise, due not to wind but rather to density structure alone. This point is well documented by Pattullo et al (1955).

The higher frequency fluctuations, i.e. 2 to 10 day perturbations superimposed on the seasonal, low frequency background change in sea level, shown in Figure 14, are caused by atmospheric cyclones and anticyclones, which spin through the system every 5 to 10 days (Weisberg and Pietrafesa, 1983). Since the North Carolina coast is on the southerly side of these storms, the winds observed at the coastal stations generally rotate clockwise as the storm passes by a specific locale. Since sea level variance is strongly tied to wind speed and direction (Pietrafesa et al, 1978), water surface heights can obviously rise and fall dramatically over a several-day period.

During mid-spring there is a substantial strengthening of the Azores-Bermuda (atmospheric) High, and as the high pressure system expands west and north, a southwesterly wind system develops over the North Carolina coast and migrates northward up the Carolina Capes coast to the Virginia shelf. The southwesterly winds drive near coastal waters offshore, causing a set-down of sea level at the coast. This sequence of falling sea level occurs in the southerly portion of the coast and proceeds to the north, with the

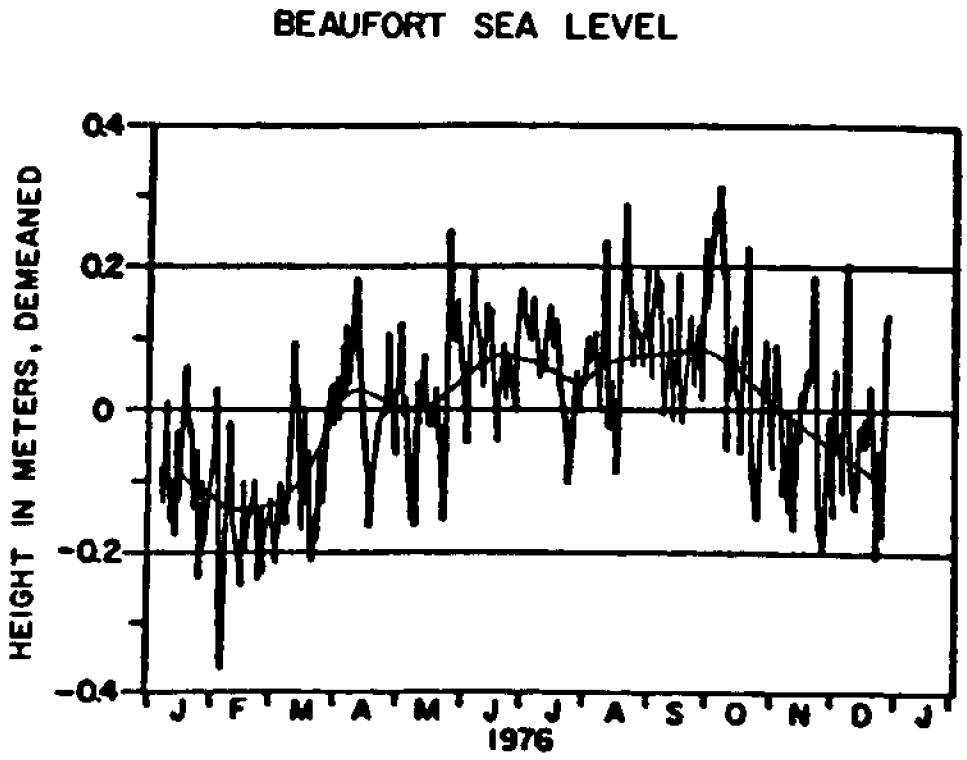

Figure 14. 1976 annual sea level time series indicating the synoptic scale wind-induced variations superimposed on the seasonal rise (expansion) and fall of North Atlantic Central Water.

advent and progression of the southerly to westerly predominant wind fields. When a southwesterly wind blows, sea level slows its rise as the wind-driven transport of water away from the coast counteracts and eventually overwhelms the rise of sea level due to the increase of North Atlantic central water heat content, as described previously.

The monthly to annual cycle of water level in Pamlico Sound mimics the rise and fall of open ocean coastal sea level in the Carolina Capes region. In Figure 15, sound sea level obtained in the south (Minnesott Beach) and north (Stumpy Point) basins during 1978 are compared to coastal station data from Beaufort, Wilmington and Cape Hatteras. Over periods of 1 to 14 days, sound sea level shows occasional agreement with the coastal data. The nuances of the daily to weekly variations will be addressed below, but we first note that the monthly to seasonal to annual rise and fall of sound water level shows the same pattern as the coastal data with approximately a 2-week to 1-month lag. However, the magnitude of the rise and fall are comparable.

The relationship between coastal sea level and wind stress along the North Carolina coast has been the subject of several previous investigations. Coastal geometry and prevailing winds result in basic principle relationships which make for local application. Pietrafesa et al (1980) and Chao and Pietrafesa (1980) have established the basic tenets of of the response of open ocean coastal sea level to wind forcing. These studies found that coastal sea level responds to local alongshore wind stress forcing at synoptic time scales, i.e. 2 days to 2 weeks as shown in Figure 16, and to non-local forcing at longer time scales, i.e. 3 weeks to a year. We shall test the verity of these relationships in Section II of this report.

Sea level studies within Pamlico Sound consist mainly of the numerical modeling results derived from the efforts of Jarret (1966), Smallwood and Amein (1967), Hammack (1969), Chu (1970), Amein (1971), Airan (1974) and Amein and Airan (1976). All of these investigators produced sea level (η) versus wind stress (τ) from various vertically integrated momentum and continuity governing equations. However, the only systematic study of actual response characteristics of water level to wind forcing in the sound was conducted in 1978 and 1979 by the authors of this report and first reported on by Chao (1981) in an MS thesis. Chao (1981) concluded that the previous numerical modeling studies were correct in that they all showed that wind is the major factor in controlling sea level (and as a correlary, circulation, $\bar{v}$, as well) in Pamlico Sound. Of course, Roelofs and Bumpus (1953) had speculated this to be true years earlier. We will show that the numerical modeling results alluded to above are extremely limited in their application to characterizing η and $\bar{v}$ in the sound. Basic tenets of the following discussion appear in the Chao thesis as well as in Pietrafesa et al (1986a, 1986b).

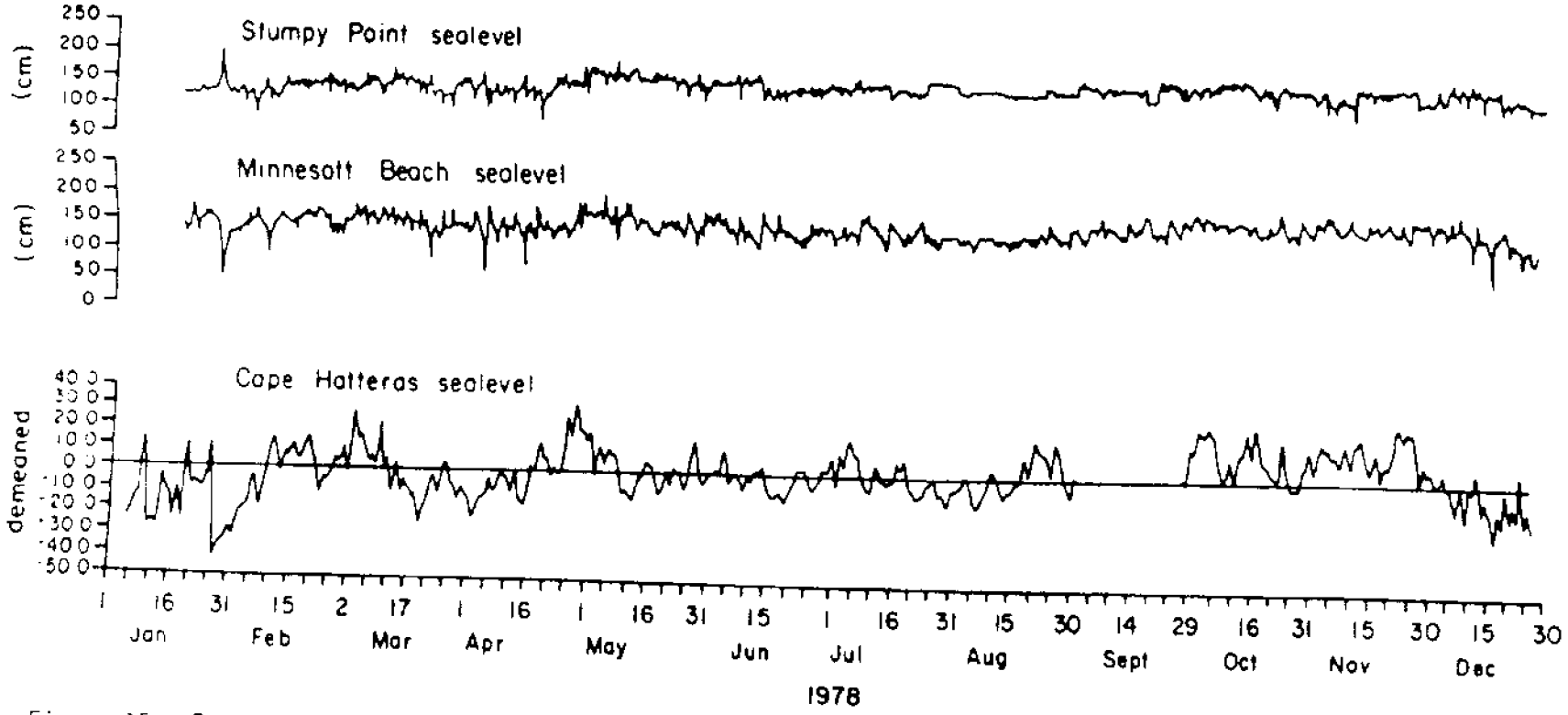

Figure 15. Forty-hour low-pass filtered time series of water height data collected at:

(a) Cape Hatteras (an open ocean coastal station),
(b) Minnesott Beach (in the south basin of Pamlico Sound),
(c) Stumpy Point (in the north basin of Pamlico Sound)

during the North Carolina State University 1978 12-month experiment.

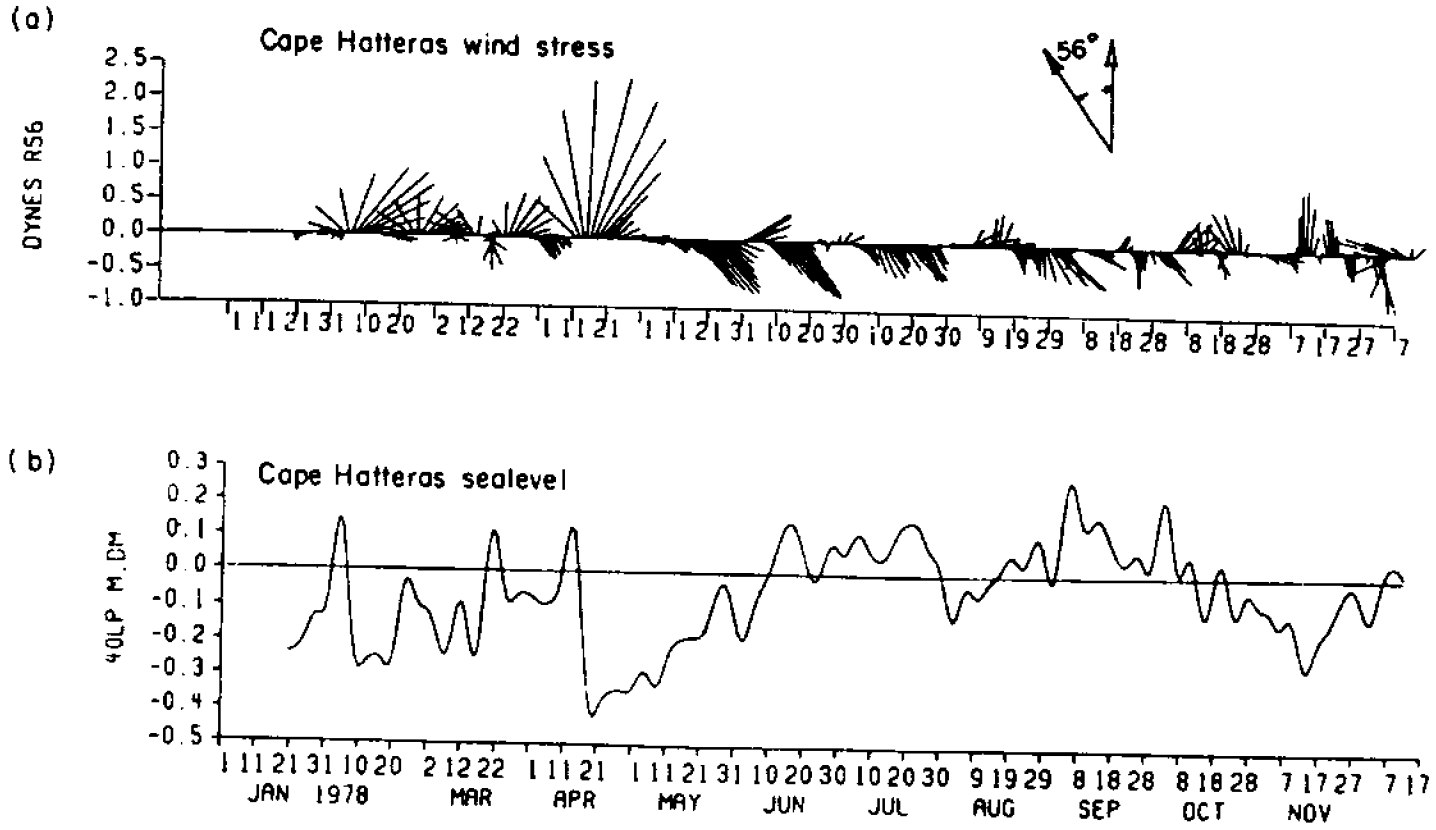

Figure 16. 1978 monthly average (a) wind stress vectors and (b) sea level from Cape Hatteras.

II. The 1978 to 1980 NCSU Study

1. Data

Data collected in the 1978 to 1979 Sea Grant study included atmospheric wind velocity and atmospheric pressure and temperature and water level from several locations in Pamlico Sound. The study periods included a year-long or 346-day data set, from 17 January to 28 December, 1978; an intensive summer set of 72 days from 22 June to 2 September, 1978; and an intensive winter set of 71 days from 18 December, 1978 to 26 February, 1979. Cumulative data collection locations are summarized in Figure 17, while specific study period data locations are shown in Figures 18 to 20 for the three separate measurement periods. In Table 4, a summary of the data is presented. Atmospheric data for New Bern (NB) and Cape Hatteras (CH) were obtained from the National Climatic Center in Asheville, N.C., and water level data for stations at Stumpy Point (SP), Washington (W), Engelhard (E), Manteo Harbor (MH), Cedar Island (CI), Minnescott Beach (MB) and Hatteras Inlet (HI) were obtained from the U.S. Army Corps of Engineers, Wilmington, N.C. Bottom mounted General Oceanics pressure gages were deployed at Ocracoke Shoals (OI), Bluff Point (BP), Hatteras Shoals (HS), Avon (A), Bomb Tower (BT), Brant Island (BI) and Gull Shoal (GS). Data was sampled every 2 hours. Unfortunately the BP, HS and GS instruments failed. Figures 21 to 25 present the time series of the good data sets. The eastward wind component is denoted by +u and the northward wind component is denoted by +v. The mean values of sea level for each data set define local datum.

2. Atmospheric Pressure and the Wind Field for the 1978 Twelve-Month Study

The spatial and temporal variability of the atmosphere local to Pamlico Sound can be assessed by comparing data from the inland station at New Bern, NB, to that at Cape Hatteras, CH, a coastal station (cf Figure 18 for relative locations).

The effect of atmospheric pressure on changing water level was discussed previously. However, we briefly reiterate the arguments. If atmospheric loading, in the form of pressure (P_A), is applied differentially spatially to the water surface, then for every ± 1 mb changes in P_A there will be a ∓ 1 mb change in η. The same argument could be made for a P_A which is not only spatially variable, but varies temporally, as well. So it is conceivable for Pa to vary sufficiently to create relative hills and depressions of η around the sound. These spatial gradients in η create pressure gradient forces (PGF_s), proportional to $g\frac{\partial \eta}{\partial x}$ and $g\frac{\partial \eta}{\partial y}$, where g represents gravitational acceleration (~980 cm/sec^2) and $\frac{\partial}{\partial x}$ and $\frac{\partial}{\partial y}$, are partial derivatives with respect to x and y, respectively. These PGFs drive currents. Alternatively, if there are no gradients in P_A or if the timing of a change in P_A occurs simultaneously across the entire sound, then no gradients in η will be created so the change in P_A is of no dynamical importance.

Figure 26 displays the coherency and phase relations between the wind velocity components u and v and P_A observed at the meteorological stations at

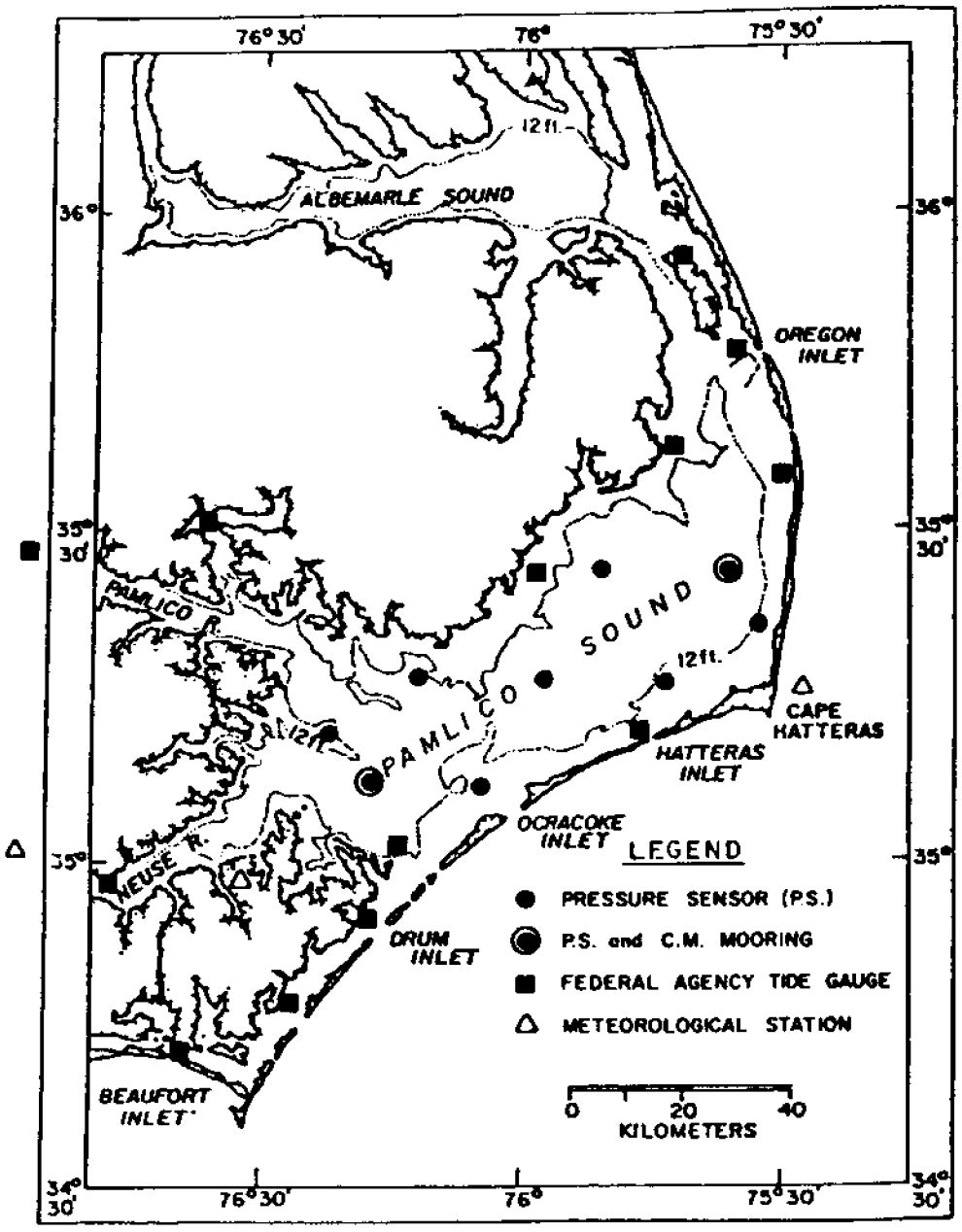

Figure 17. Measurement sites of 1978-1979 North Carolina State University Pamlico Sound Study.

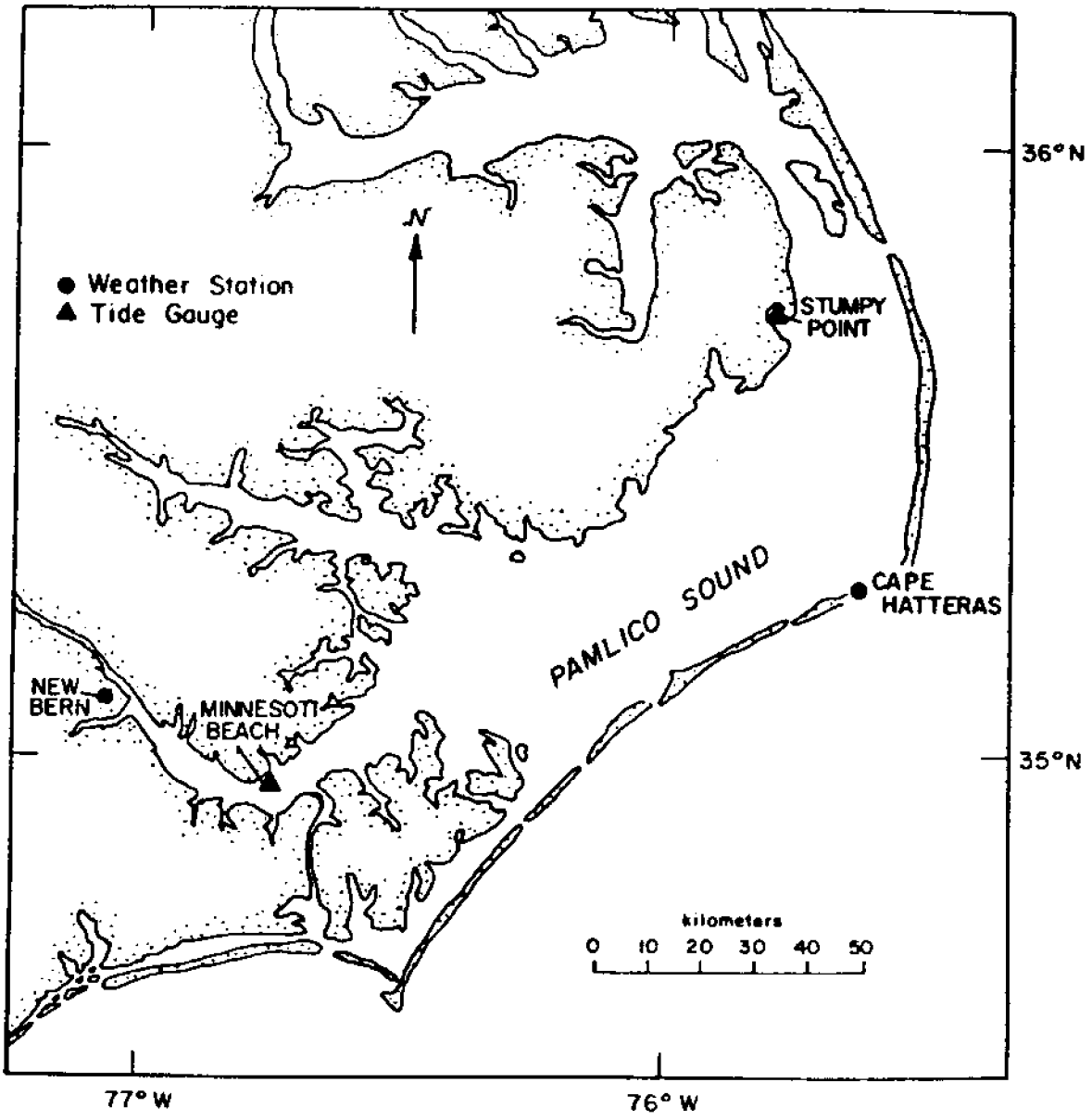

Figure 18. Measurement sites for 1978 12-month sea level study.

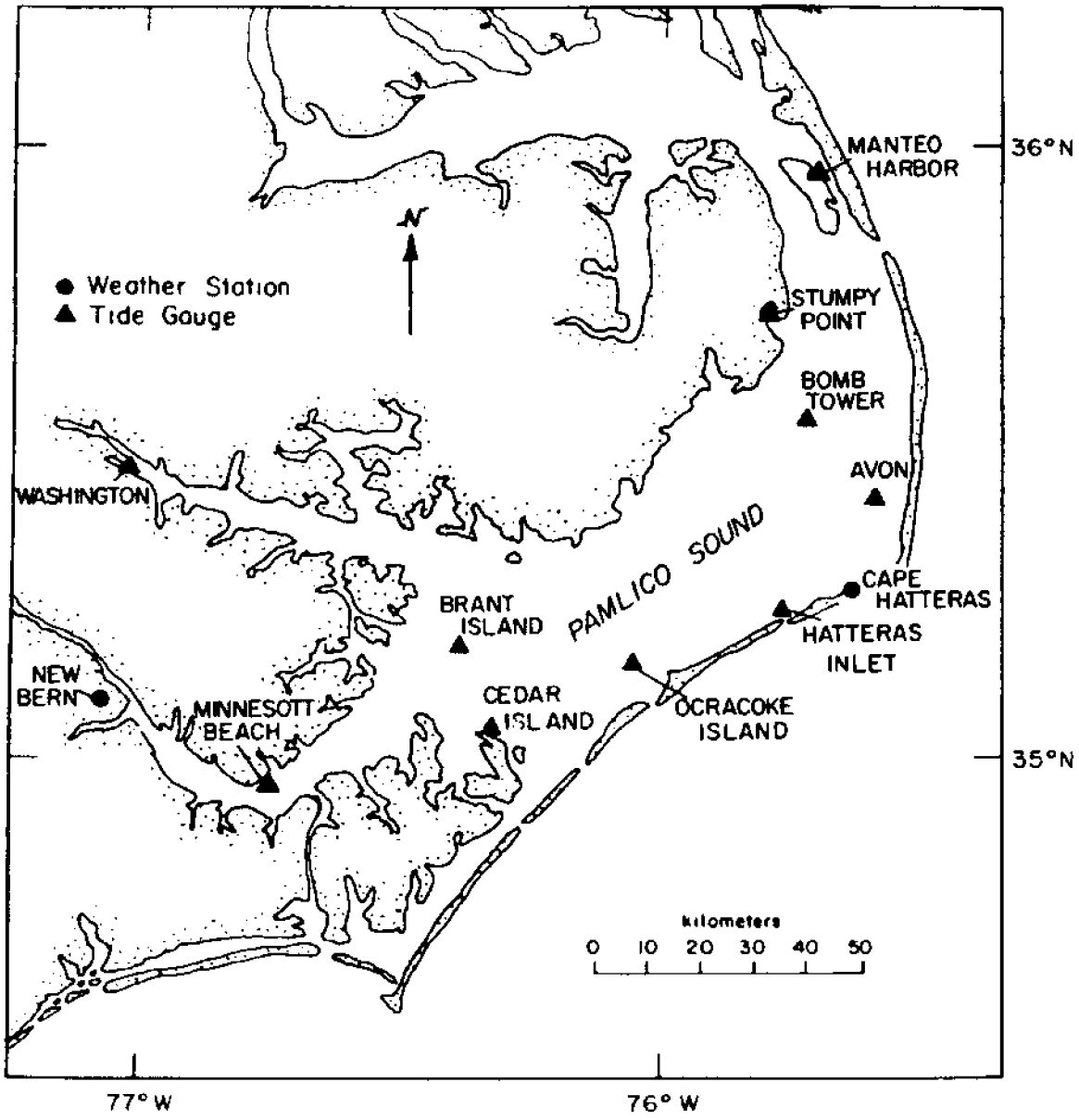

Figure 19. Measurement sites for summer 1978 sea level study.

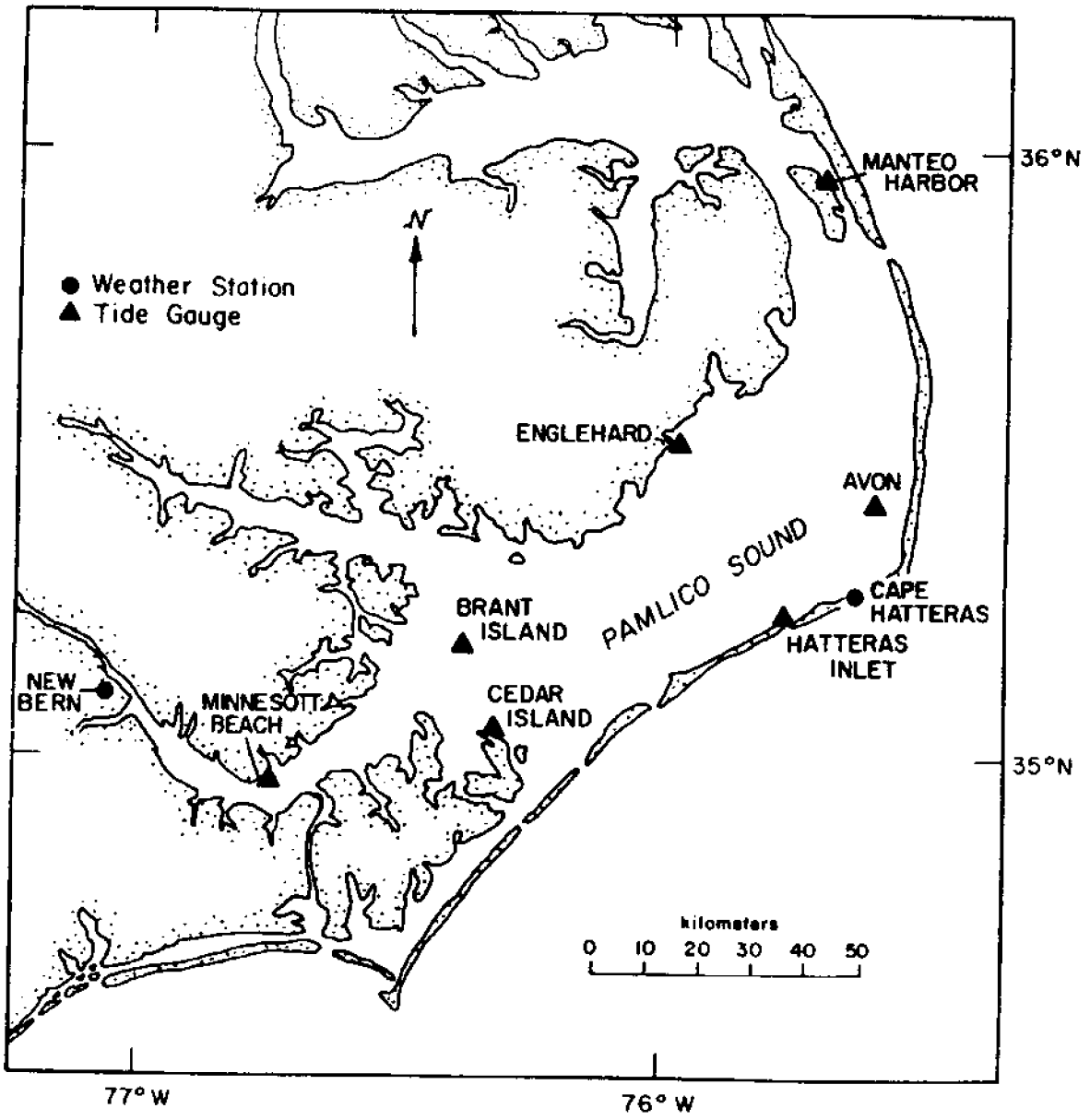

Figure 20. Measurement sites for winter 1978/79 sea level study.

TABLE 4 **Station indices, sampling duration, and location of examined stations during 1978-79 Pamlico Sound sea level study**

Station Index	Station Name	Sampling Duration 0000 01/17/78-2200 12/28/78	Sampling Duration 1200 06/22/78-0200 09/02/78	Sampling Duration 0000 12/18/78-2200 02/26/79	Location Long.	Location Lat.
SP	STUMPY POINT	X	X		77.73°W	35.67°N
W	WASINGTON		X		77.02°W	35.53°N
E	ENGLEHARD			X	77.99°W	35.52°N
M	MANTEO HARBOR		X	X	75.66°W	35.93°N
CI	CEDAR ISLAND		X	X	75.33°W	35.02°N
MB	MINNESOTT BEACH		X	X	75.81°W	34.94°N
HI	HATTERAS INLET		X	X	75.76°W	35.19°N
OI	OCRACOKE ISLAND		X		76.04°W	35.14°N
A	AVON		X	X	75.56°W	35.38°N
BT	BOMB TOWER		X		75.68°W	35.51°N
BI	BRANT ISLAND		X	X	75.96°W	35.18°N
NB	NEW BERN	X	X	X	72.22°W	35.17°N
CH	CAPE HATTERAS METEOROLOGY AND SEALEVEL	X	X	X	75.61°W	35.38°N

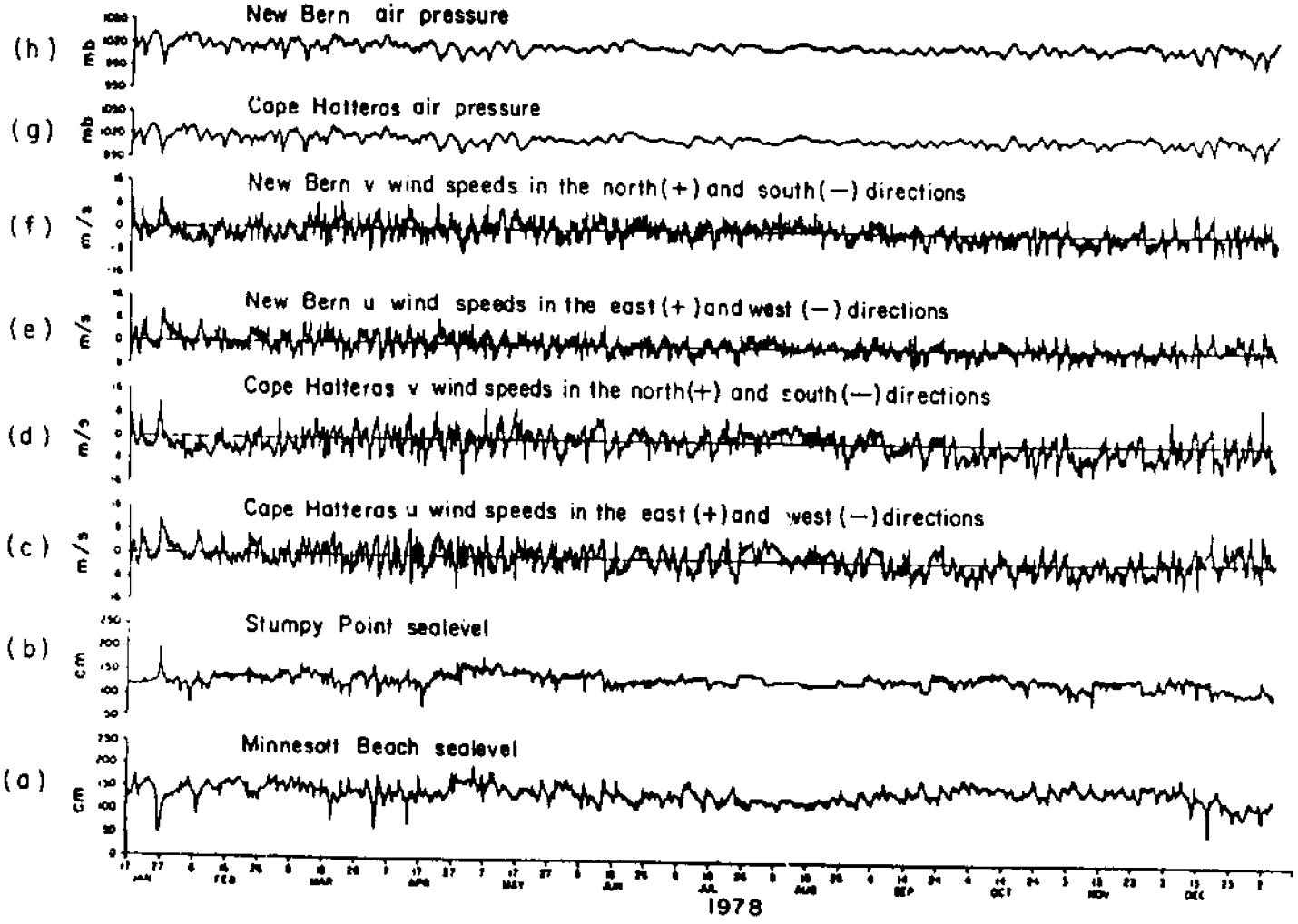

Figure 21. Time series of data collected during North Carolina State University 1978 Pamlico Sound study.

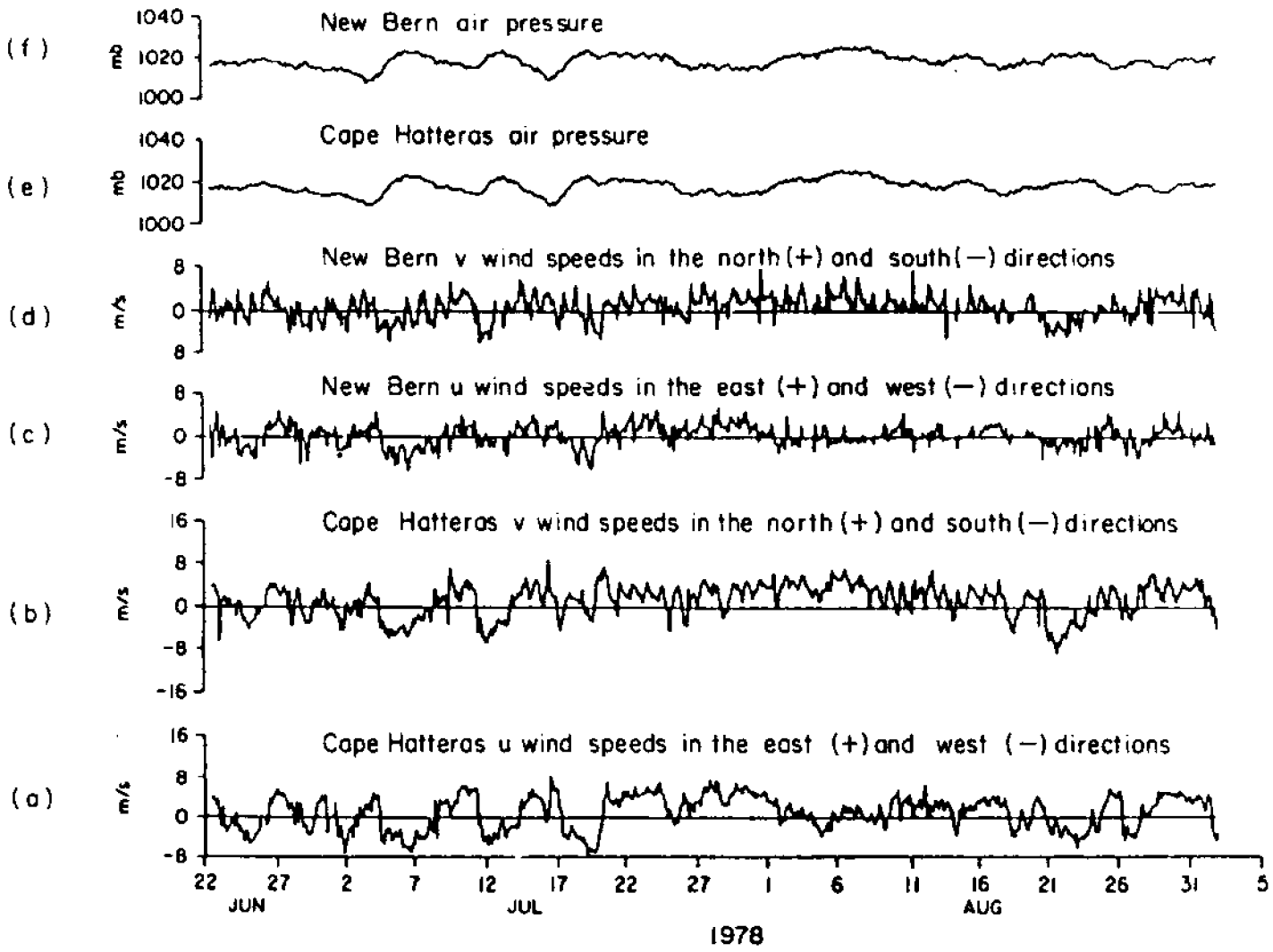

Figure 22. Time series of data collected during North Carolina State University 1978 summer study of sea level in Pamlico Sound.

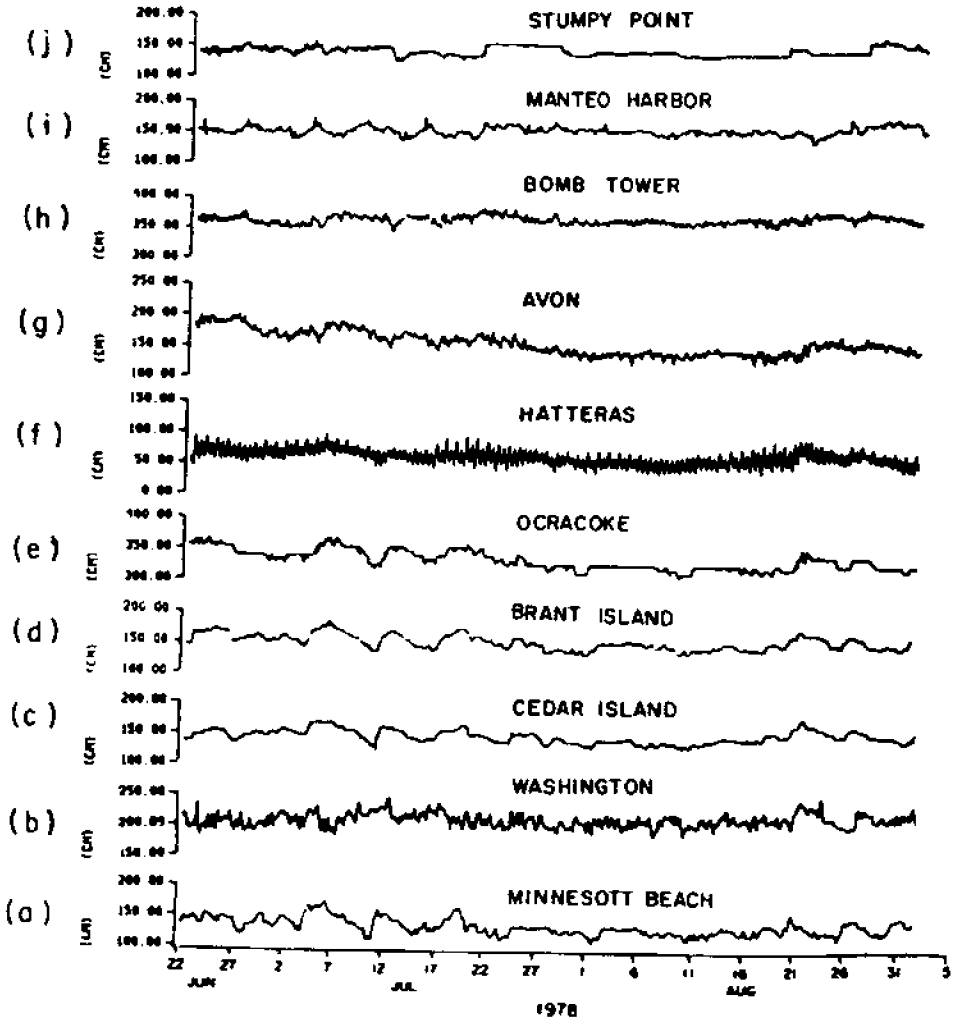

Figure 23. Time series of sea level collected during North Carolina State University 1978 summer study in Pamlico Sound.

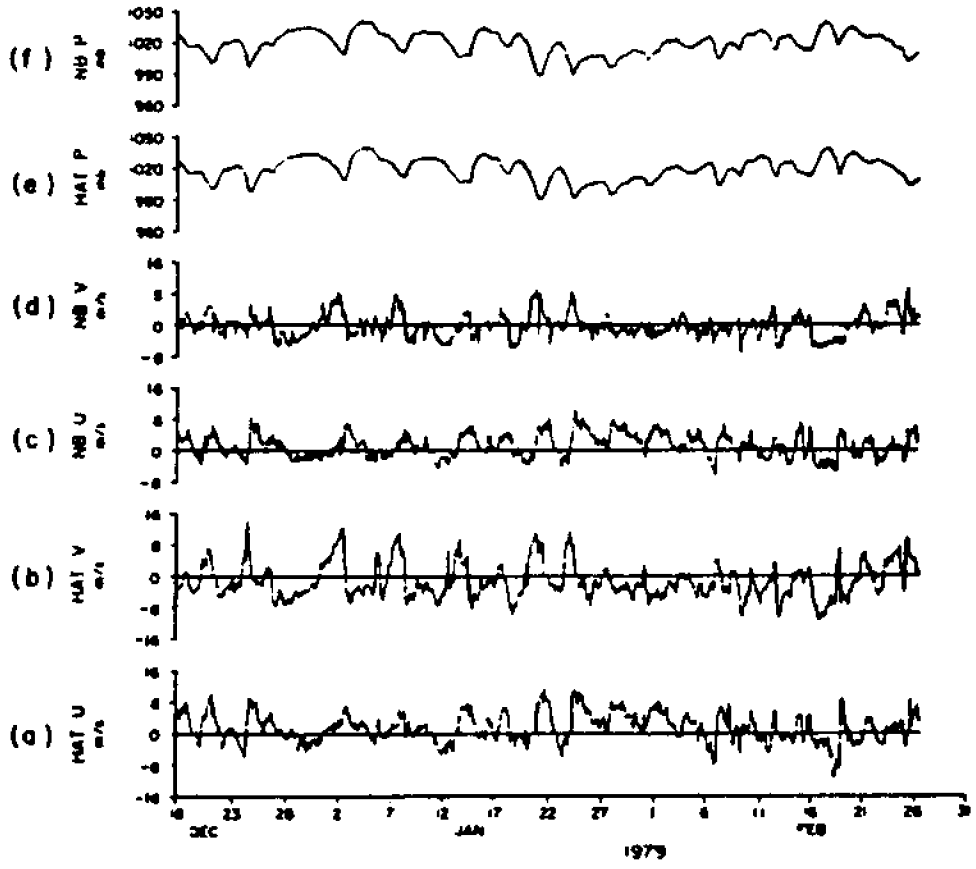

Figure 24. Time series of data collected during North Carolina State University 1978/79 winter study of sea level in Pamlico Sound.

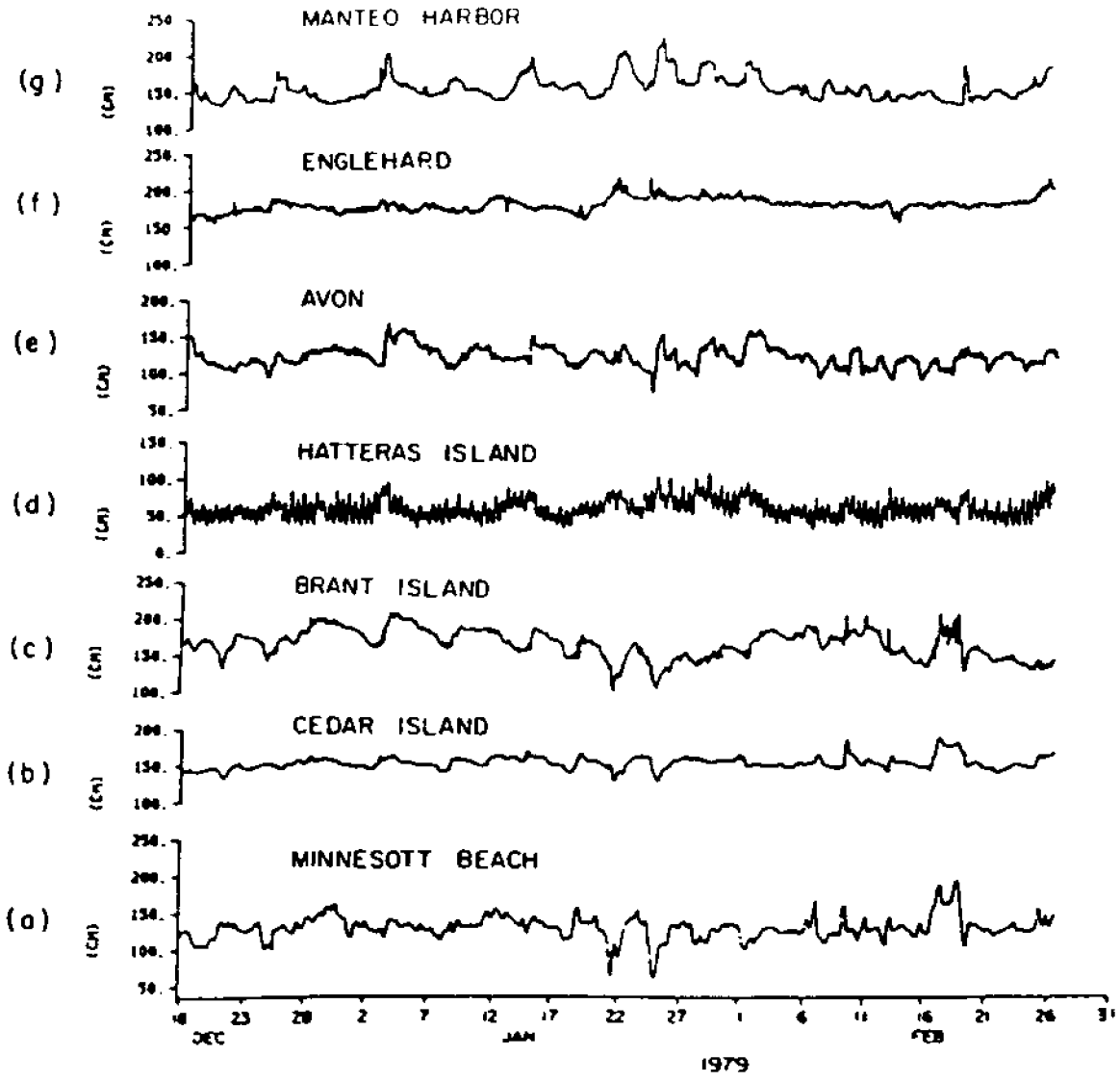

Figure 25. Time series of sea level collected during North Carolina State University 1978/79 winter study in Pamlico Sound.

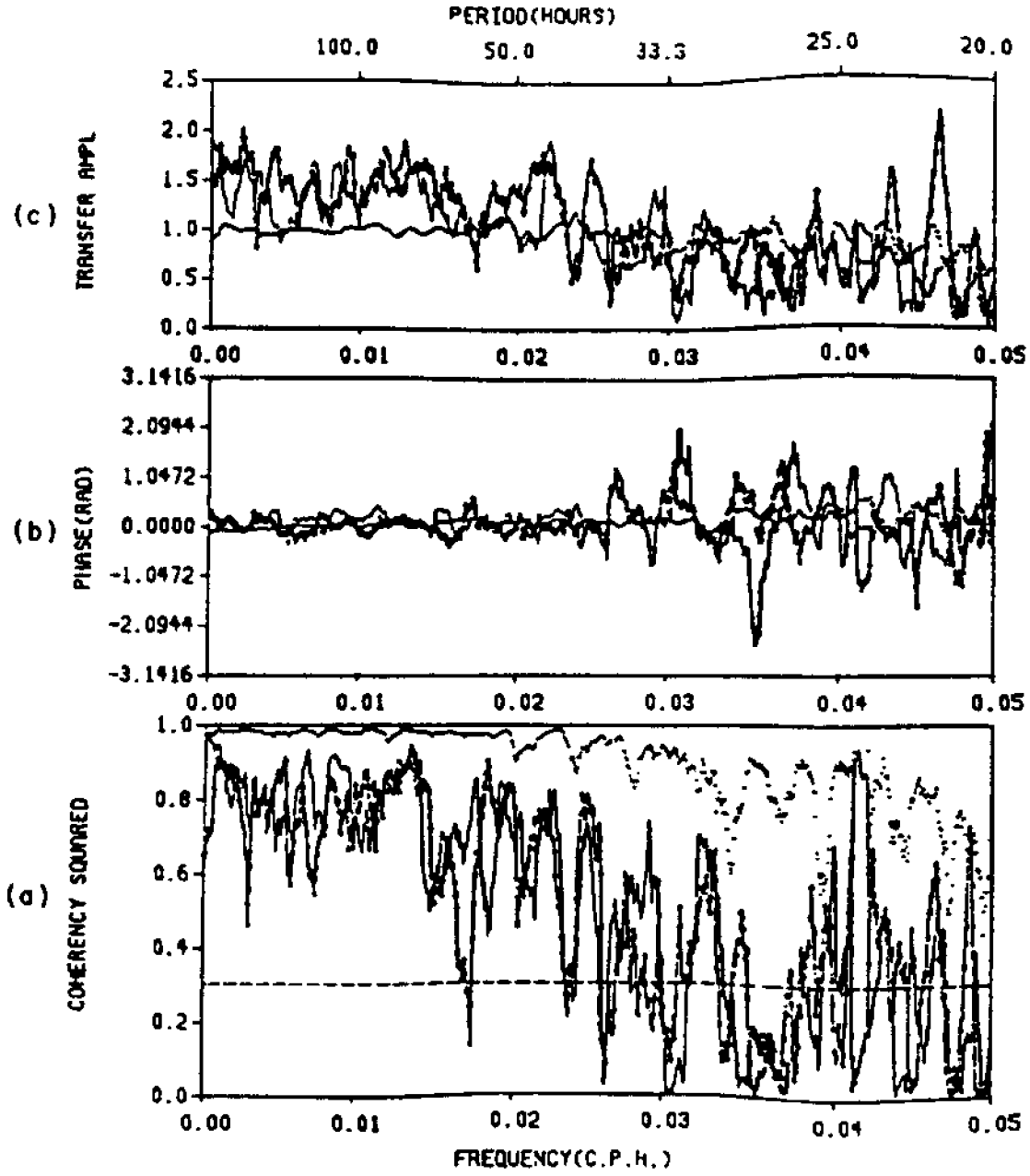

Figure 26. (a) Coherency squared, (b) cross-phase and (c) transfer function amplitudes between U(E-W) and V(N-S) wind velocity components and air pressure at Cape Hatteras and New Bern. (Uch vs. Unb (•—•—•), Vch vs. Vnb (——), Pch vs. Pnb (——).

NB and CH during the 340-day period in 1978. The time series of u, v and P_A for NB and CH were presented in Figure 21. From Figure 26, we see that P_A is coherent and uniform across the sound for events with periods greater than 1 day. Likewise, wind velocity components, i.e. the u's and v's, are highly coherent with their counterparts at time scales longer than 2 days. The near zero phase differences indicate that fluctuations in both wind velocity and atmospheric pressure occur contemporaneously at both stations. The amplitudes of P_A were the same at both NB and CH as shown by the transfer function amplitude. Albeit, the wind velocity at CH is approximately 50 percent higher than at NB. The norm of the wind acting on Pamlico Sound is that barrier island winds have a larger magnitude and are more energetic than mainland winds. In Figure 27, we see that Hatteras winds are always larger than Cherry Point winds. The case rests.

We conclude that atmospheric pressure presents a forcing function of no dynamical consequence. Alternatively, the wind stress has very clear spatial gradients and these "curls" and "divergences" of the wind stress vector field may be of significance to the circulation in Pamlico Sound. For our purposes, an average wind stress vector field, derived from the New Bern and Cape Hatteras wind data, will be used.

The averaged east-west (u) and north-south (v) wind velocity vector component kinetic energy densitites (KEDs) are presented in Figure 28 for the year 1978. The fluctuation of kinetic energy of both components is approximately equal up to periods of ~ 40 days where the north-south component dominates somewhat. For motions with periods between 1 and 40 days, the average KED aligns itself with the major topographic axis of the sound, which tends to be NE-SW (refer to Figure 1). At seasonal time scales the KED has a decided N-S tendency.

In Figure 29 the rotary spectra, i.e. the tendency for clockwise vs. counterclockwise (or anti-) rotation of the wind velocity, vector is shown. Once again for periods of a month or less, there is no tendency for rotational motion other than at a period of 4 to 5 days, where clockwise peaks appear. The rectilinear nature of the rotary spectra suggests that Pamlico Sound is aligned with the leading edge of atmospheric fronts. To further investigate the character of the wind field, we consider the kinematical descriptors shown in Figure 30. Such descriptions of environmental time series were first presented by Fofonoff (1969).

Kinematical descriptors of the wind field u and v (east-west and north-south) components are presented in Figures 30 a,b,c, and d. The descriptor shown in 30a indicates the orientation of the "principal axis" of motion, as a function of frequency. In 30b, the "stability" of this motion is presented. The stability (actually the coherence squared relationship between clockwise and anticlockwise rotating velocity vector components computed as a function of frequency or period of motion) is a measure of the steadiness or repeatability of a motion, occurring at a certain period, being aligned in a particular direction. Note that whenever the stability is relatively high, i.e. the peaks are above the 90 percent confidence level signified by the dashed line, the motion tends to be aligned at approximately $\pi/4$ radians or at 45° north of east (or vice versa). This happens to be the approximate topographic alignment of the sound (cf Figures 1,2). In 30c the ratio of the semi-minor axis of preferred motion to the semi-major axis of preferred motion is shown. If the ratio is nearly zero, then the motion lies along a straight

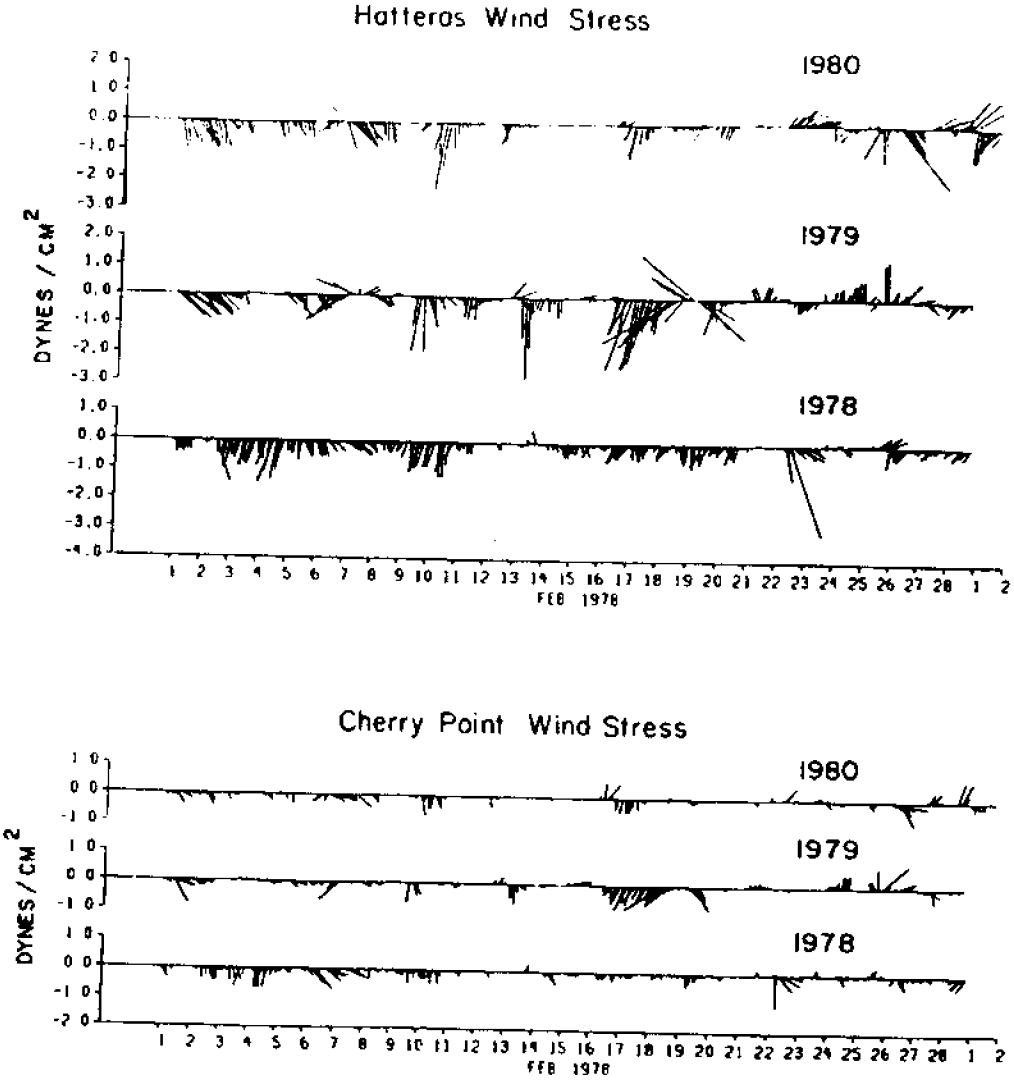

Figure 27. Time series of wind stress vectors during the month of February for three different years showing: repeatability of winds; consistency of direction between Cape Hatteras and Cherry Point winds; and larger magnitude of Cape Hatteras wind stress vectors.

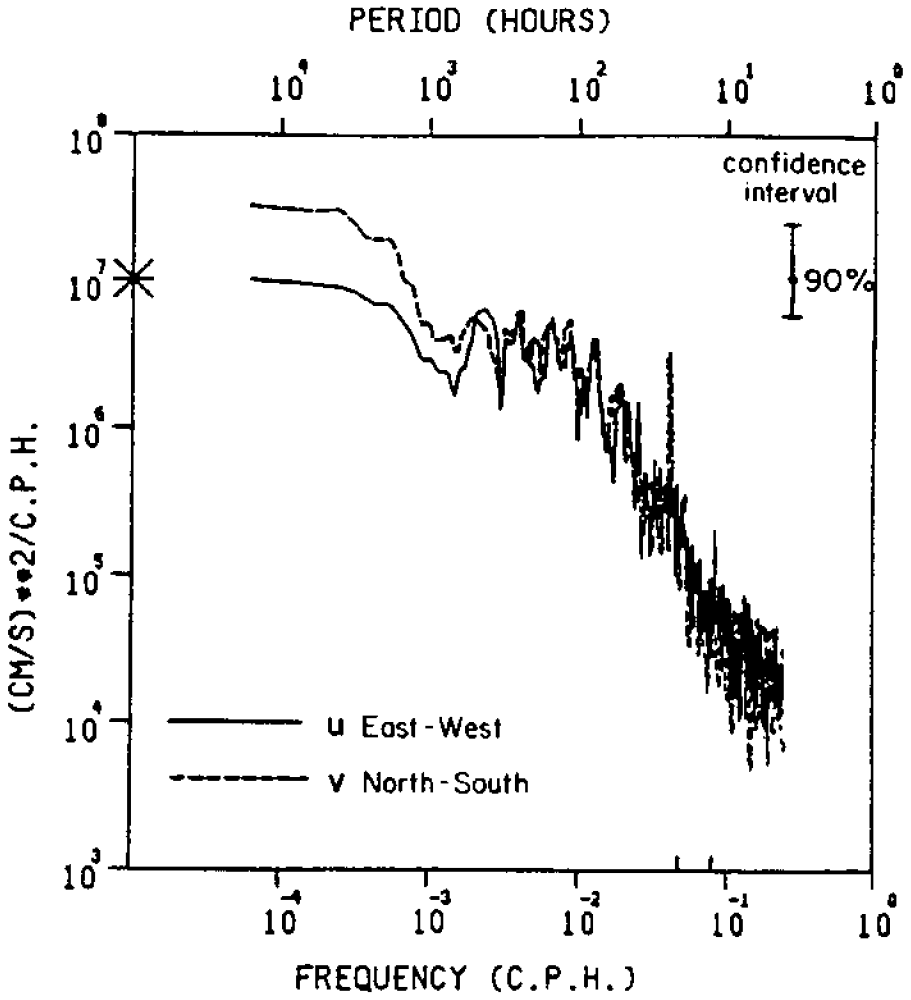

Figure 28. Energy density spectra for averaged New Bern and Cape Hatteras wind velocity component time series for 1978.

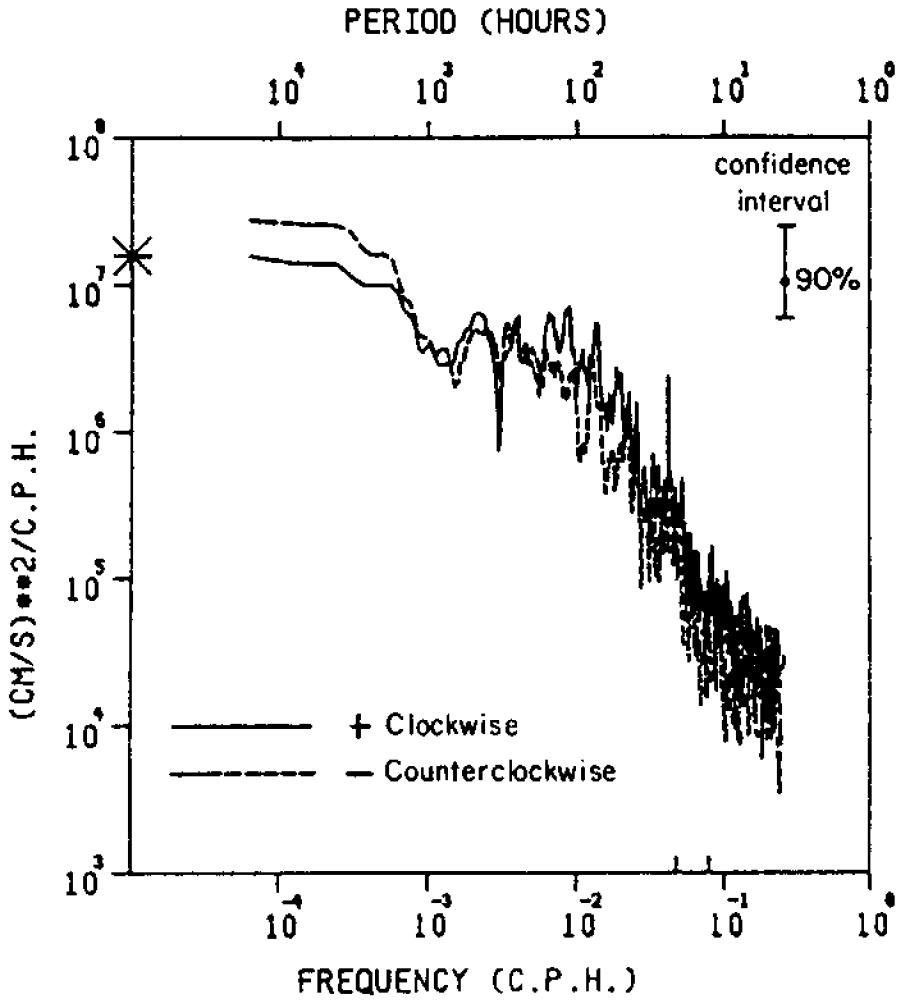

Figure 29. Rotary energy density spectra for averaged New Bern and Cape Hatteras wind velocity time series during North Carolina State University 1978 study.

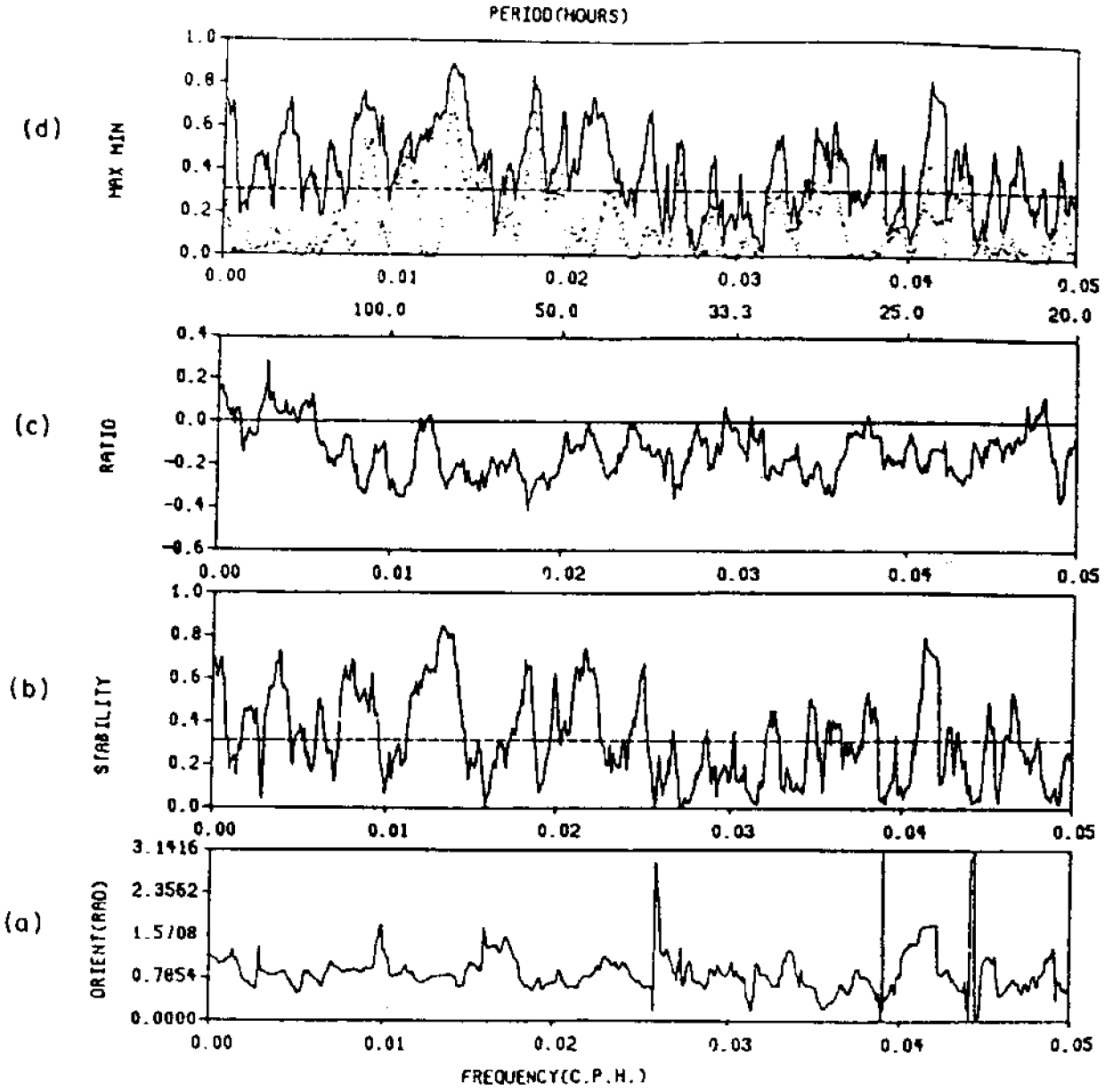

Figure 30. Hodograph, kinematical descriptors of the New Bern/Cape Hatteras wind velocity time series during North Carolina State University 1978 study. See text for figure discussion.

line and is deemed "rectilinear." At a ratio of unity the motion would be perfectly circular while ratios between 0 and 1 signify elliptically polarized windfield particle motions. Finally, in 30d, the minimum (....) and maximum (----) coherencies of the wind field particle motions are depicted. Where the maximum coherency is high (above the 90 percent level) and the minimum is low (below the 90 percent level), then coherent, or well-defined rectilinear motions are suggested. Alternatively, if the maximum and minimum coherencies are both high, then well defined wavelike or elliptically polarized motions are indicated. So what do the four kinematical descriptors tell us about the wind field which was present during 1978 and is the principal forcing agent for the circulation in Pamlico Sound?

At the period of 24 hours (or frequency of 0.0417 cycles hour^{-1}), a well defined, stable, coherent, clockwise rotating motion aligned at about 26° west of north with an axis ratio of about 0.12 is indicated. This is the "seabreeze" phenomenon. At periods between 25 and 40 hours, wind motions are incoherent and unstable, i.e. there is disorganized or undefinible wind motion. Motions with periods between 2 days and 1 week are well organized, clockwise rotating, stable, wavelike motions, with an ellipse axis ratio of about 0.3 and an alignment which varies between 45°-54° east of north. Motions of 10-to 15-day periods tend to be well organized, stable, rectilinear motions with an orientation or alignment which is also about 39° east of north while coherent wind motions of 15-25 day period align at 48° east of north. There is a spectral gap in u,v coherency between 26 and 45 days suggesting either a lack of energy or disorganization in the windfield. Motions with time scales of 45 to 90 days are coherent, stable, energetic and tend to align at between 30° and 22° east of north.

In general, coherent motions of the windfield at all periods in excess of 1 day tend to be aligned with the major axis of Pamlico Sound in a northeasterly-southwesterly direction. At the diurnal period, the seabreeze phenomenon is evident and its orientation is NNW-SSE or across the sound. The fact that the majority of the wind energy is aligned NE-SW may have much to do with the fact that the sound itself is aligned NE-SW.

3. Sea level Fluctuations During the 1978 Twelve-Month Period

The sea level time series obtained for stations Minnesott Beach and Stumpy Point for the period 17 January to 28 December 1978, were presented previously in Figures 15 and 21. Some immediate revelations about η at the two different stations, which are located on opposite longitudinal (or axial) sides of the sound, can be obtained by considering energy densities and kinematical descriptions of the two.

First, consider the spectral distribution of variance shown in Figure 31. Sea level variance is shown to be 80 percent greater at Minnesott Beach than at Stumpy Point as indicated by year-long averaged values of 309 cm^2 and 172 cm^2, respectively. Thus, energy density at Stumpy Point, in the northern half of the sound, is only 56 percent of that at Minnesott in the southern half. At both locations, variability at time scales in excess of 25 days displays a "red" spectrum, or monotonic rise up to time scales of 90 days, with a flattening or "whitening" thereafter. The variance flattening is more evident at Stumpy Point, where the spectra becomes "white" or evenly distributed for event periods in excess of 3 months.

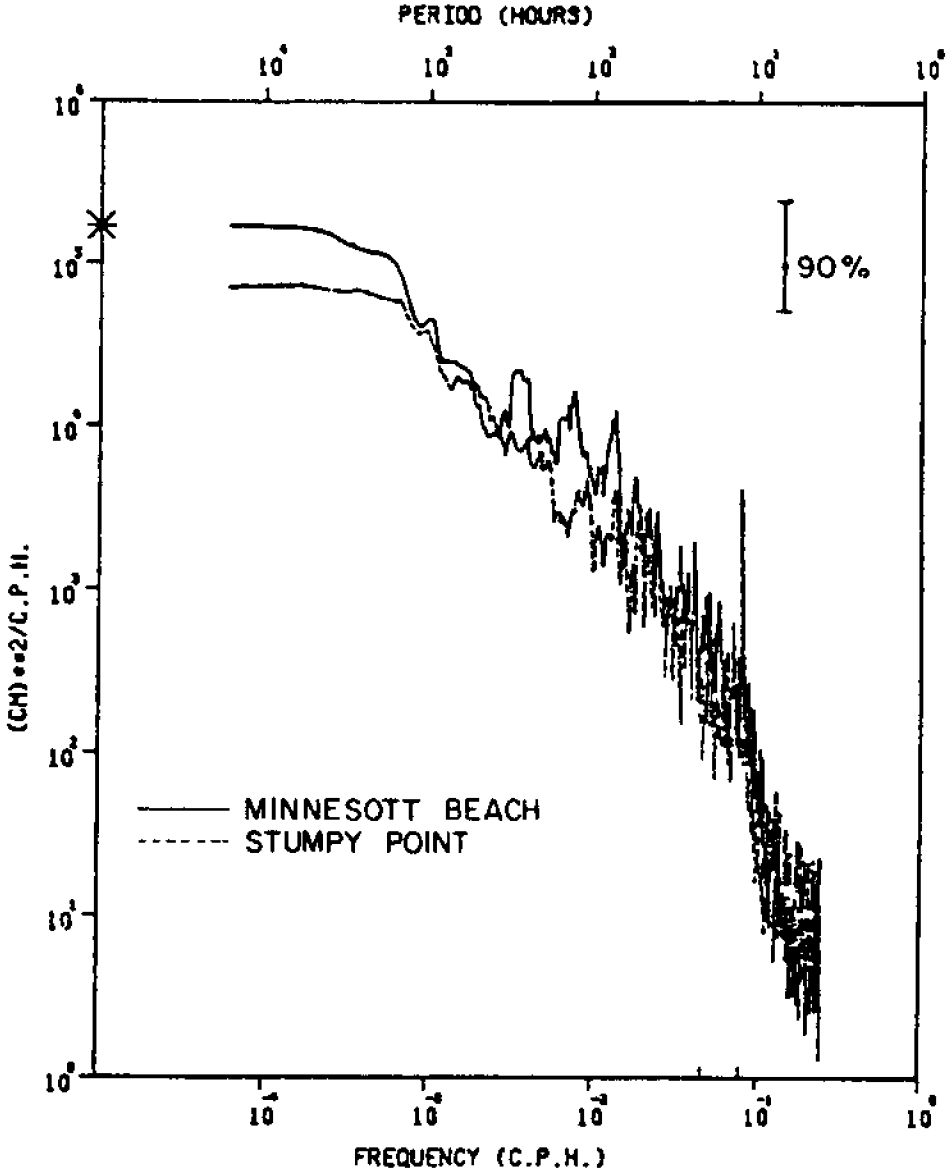

Figure 31. Potential energy density for Minnesott Beach and Stumpy Point water height time series during North Carolina State University 1978 study.

At time scales of 2 to 25 days, the inhomogeneity in sea level variance between the two sites is quite evident. At periods less than 2 days, sea level energy is comparable at both sites, except for the semidiurnal period where a large peak is evident at Stumpy Point, but essentially absent from Minnesott Beach. Albeit, this response to the lunar, M2 tide accounts for only 1 percent of the total sea level variance at Stumpy Point and is thus not significant.

A comparison of sea level fluctuations at the two-year-long stations is shown in Figure 32. From Figures 32a and 32b we see that at time scales in excess of 32 days, the fluctuations are coherent and virtually in phase, i.e. the rises and falls occur in conjunction simultaneously. Over the period range of 7 to 30 days, the vertical rise and fall of sea level at the two sites are incoherent with each other save for the range of 8.7 to 10.7 days where the fluctuations bear a modicum of coherency. At time scales of less than 7 days, the oscillations are typically coherent and 180° out of phase. That is, sea level rises at Stumpy Point in concert with sea level falling at Minnesott Beach.

What is suggested by Figure 32 is that different physical, and environmental processes affect the synoptic, or 1 to 7 day, fluctuations versus those with monthly to seasonal, or greater than 30 day, variations. At periods of 1 to 7 days, sea level sets up at one axial end of the sound while setting down at the other end. At periods greater than 30 days, sea level sets up and down simultaneously along the axis of the sound. At time scales of 7 to 30 days there is a spectral gap in sea level coherency (cf Figure 32a) which appears as a drop in energy in η at both sites as shown in Figure 31. Note that there was a similar gap in the wind field energy density at like periods as evidenced by the energy density and rotary spectra of the wind shown previously in Figures 28 and 29, respectively.

The seabreeze phenomenon exacts a soundwide response of sea level as suggested in the strong coherency and high transfer function amplitude between Stumpy Point. and Minnesott Beach sea level (Figures 32 a,c).

4. Sea Level Fluctuations vs. Atmospheric Forcing During the 1978 Twelve-Month Period

Coherence between atmospheric pressure over Pamlico Sound and sea level in the sound were generally quite low over most of the spectrum of variability during the period 17 January to 28 December 1978. In Figure 33, the coherence squared (C^2), phase relationship and transfer function amplitude between the sea level time series obtained at Minnesott Beach and an atmospheric pressure time series created by averaging Pa from the meteorological stations at New Bern and Cape Hatteras, are presented. Several isolated peaks are evident in the C^2 plot. Within the energy-bearing portions of the spectrum of Minnesott sea level (refer to Figure 31) we see coincident, coherent peaks at the periods of 1, 2.75, 3, 5 and 64 days. The bimonthly peak is accompanied by a negative 180° phase difference signifying the previously discussed inverse barometer effect. The 180° out-of-phase effect does not appear throughout the rest of the coherency spectrum for reasons discussed in Section II-2. The bimonthly peak will be discussed later in the text.

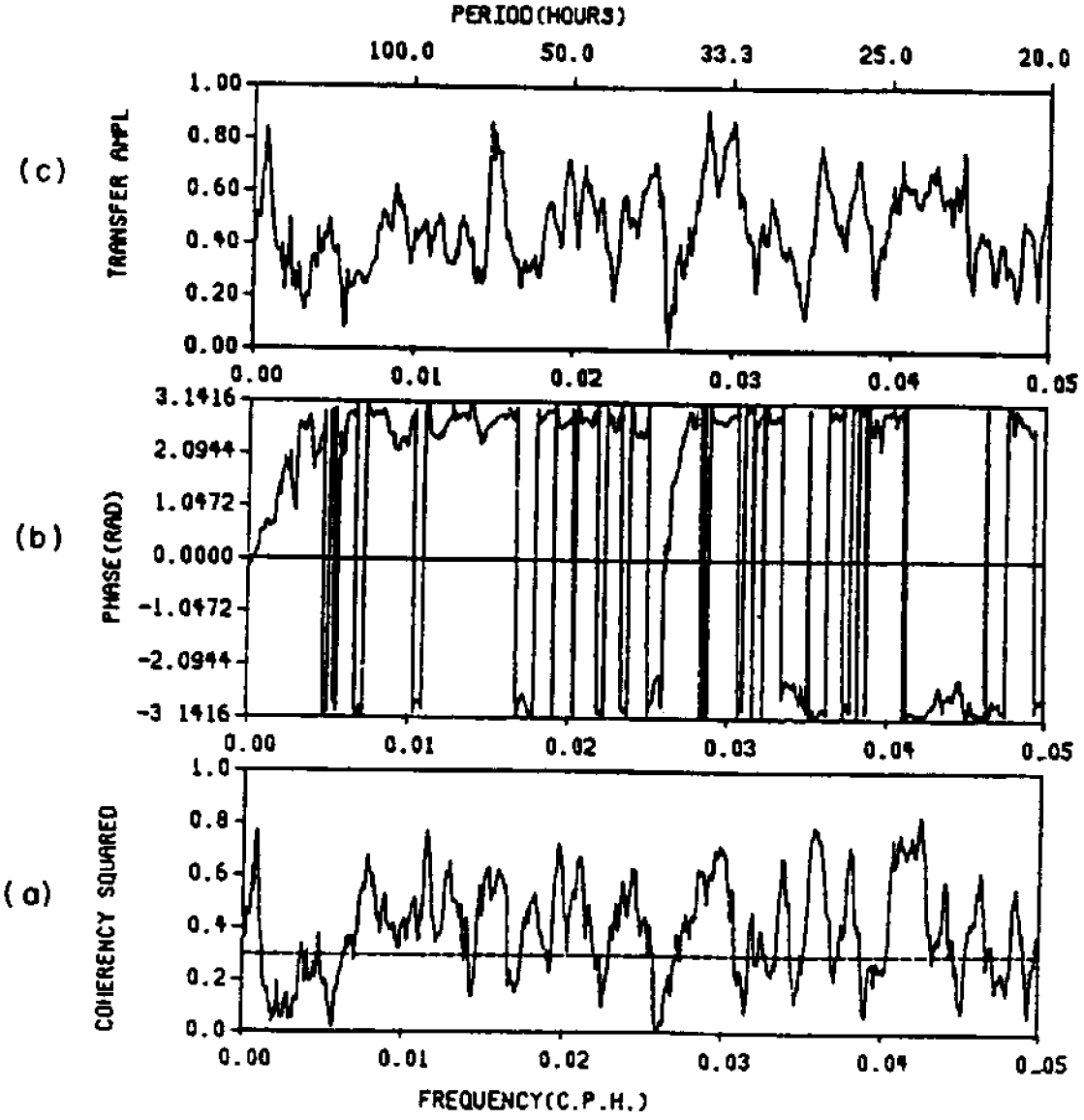

Figure 32. (a) Coherency squared, (b) cross-phase and (c) transfer function amplitudes between sea level at Minnesott Beach and Stumpy Point during North Carolina State University 1978 study.

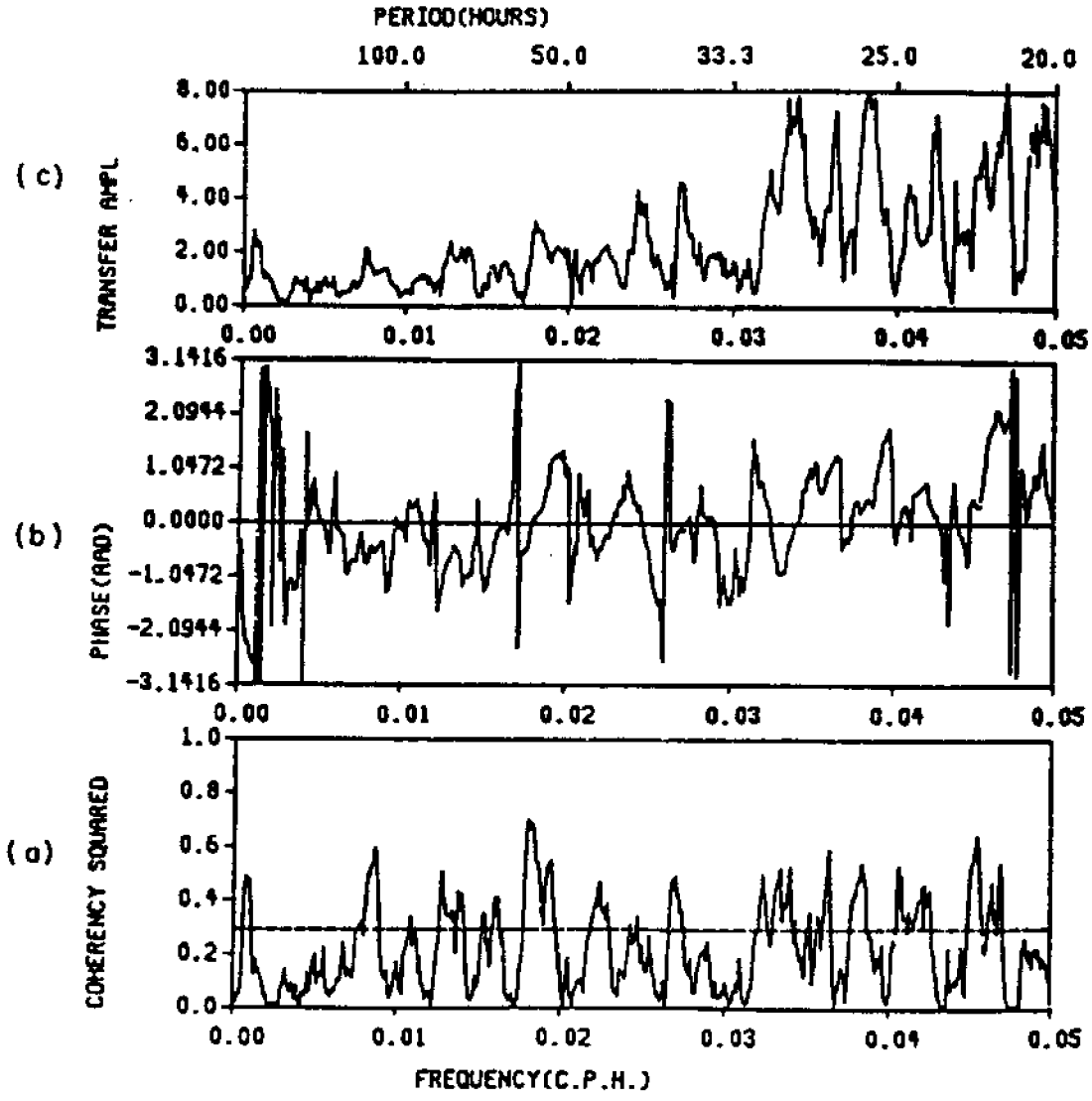

Figure 33. (a) Coherency squared, (b) cross-phase and (c) transfer function amplitudes between atmospheric pressure versus Minnesott Beach sea level during North Carolina State University 1978 study.

Since the principal axis of the wind field tends to be aligned with the major topographic axis of Pamlico Sound, we reconstruct the wind stress vector component time series accordingly, i.e. the zero axis is aligned 45° east of north. In Figures 34 and 35, we present coherency and phase relationships between sea level fluctuations at Stumpy Point and Minnesott Beach, separately, with the major axial or longitudinal or NE-SW wind velocity, τy, (the solid lines) and the minor axial or lateral or NW-SE component of the wind stress vector τx, (the dotted lines).

Sea level fluctuations at both Minnesott and Stumpy Point are highly coherent with the axial component of the wind stress vector but not so with the cross-sound component. While fluctuations at Stumpy Point were practically in phase with fluctuations in the longitudinal component of the wind stress vector, those at Minnesott were 180° out of phase with the NE-SW wind component. In Section II-4, we found that sea level fluctuations at the two locations were 180° out of phase so this finding that τy and $\eta_{Minnesott}$ are 180° out of phase while τy and η_{Stumpy} are either 0° or 360° out of phase is entirely consistent. A northeasterly wind will set water up in the southwestern side of Pamlico sound and down in the northeastern end. Alternatively, a southwesterly wind will set up the northeastern end with water drawn from the southwestern end of the sound. From this simple relationship, we conclude that a relationship between slope of the water surface along the axis of the sound and the NE-SW wind may exist. In Figure 36 we compare the sea level difference between Stumpy Point and Minnesott Beach to both the major axial wind component, τy (--), and the cross-sound wind component, τx (.....).

Figure 36 provides the coherence squared, phase relation and transfer function amplitude frequency domain relationships between the year-long time series of sea level slope along the axis of Pamlico Sound from Stumpy Point to Minnesott Beach, a crow's flight distance of approximately 128 km., to the time series of wind stress vector components τy and τx. In summary, $\eta_{SP}(t) - \eta_{MB}(t)$ is correlated with $\tau y(t)$ and $\tau x(t)$, separately. Once again, extremely good correlation is shown to exist between τy and the sea level difference or slope time series over virtually the entire spectrum. Amazingly, a straight line can be drawn, as a best fit linear regression, through the phase diagram (Figure 36b) from the frequency of 0.0 cycles per hour to 0.00949 cph. Since the phase relationship is positive (in our frame of reference) then τy is shown to lead $\eta_{SP} - \eta_{MB}$ and the best fit line suggests a sea level slope setup-setdown response time of 2 hours 45 minutes. Alternatively, coherent peaks between τx and η_{MB} lie along the dashed line in Figure 36b between the frequencies of 0.0 - 0.03 cph. This suggests a response lag of approximately 24 hours at the coherent period of 5 days, 22.5 hours at the period of 3 days, 3 hours and 19.6 hours at the period of 2 days, 7 hours. The axial setup and setdown of water level occurs within 3 hours of the onset of the NE-SW component of the wind at any frequency. So, a temporal response relationship such as $\tau_{\Delta\eta}(t) \alpha\ T\tau_y(t) + 2^{hr}47^{min}$ will yield the time lag, time-series of $\Delta\eta = \eta_A - \eta_B$ where $T\Delta\eta_{AB}$ is the time for the axial sea level slope between stations A and B, $T_\tau y$ is the time of the onset of the axial windstress component and α is a proportionality symbol.

Consider the transfer function amplitude relationship between $\eta_{SP} - \eta_{MB} = \Delta\eta_{SM}$ and τy shown in Figure 36c. Note that at frequencies where the $\Delta\eta_{SM}$ time series is most coherent with τy, i.e. if we only consider the peaks in coherency, that the transfer function amplitude, which we will call

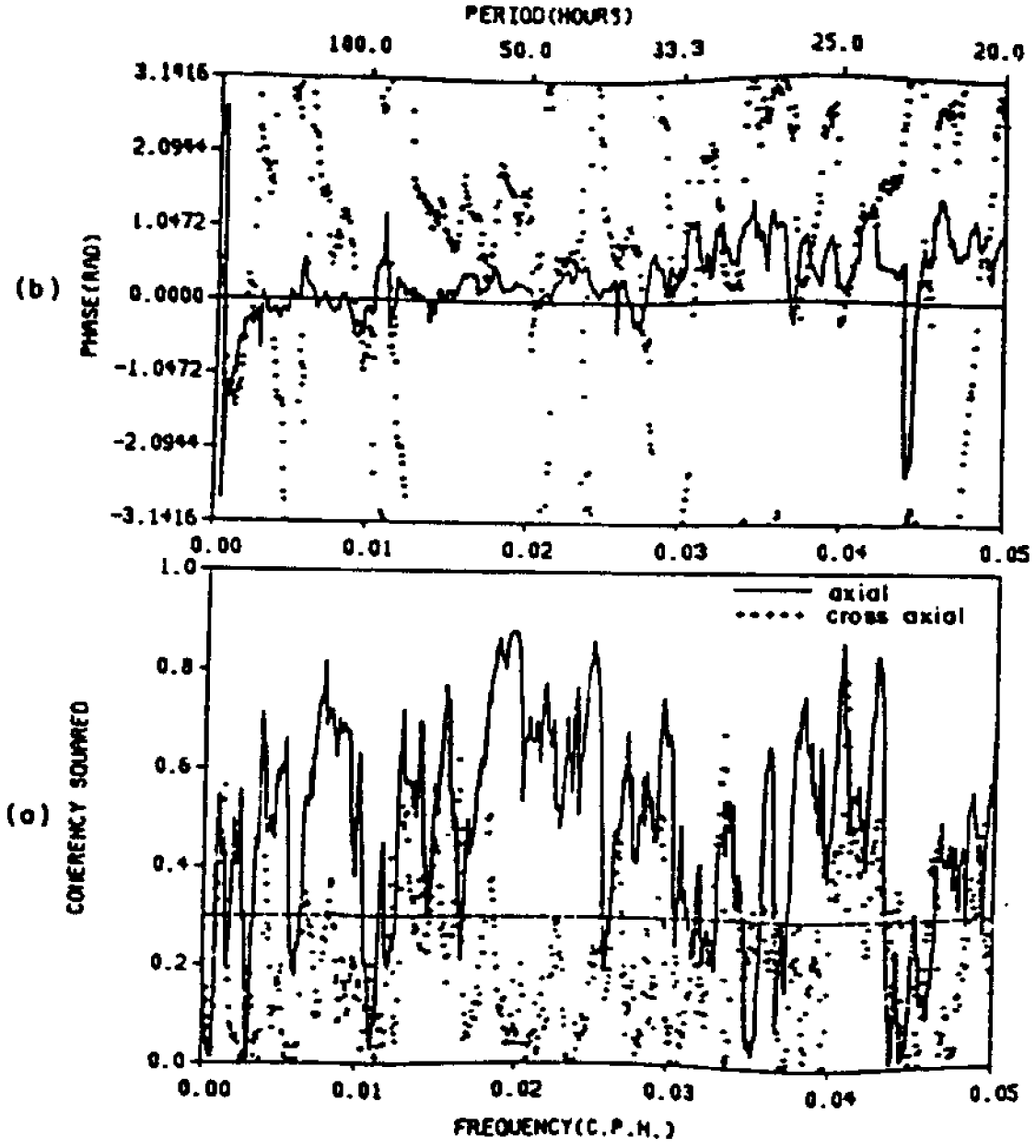

Figure 34. Coherency squared and cross-phase between axial and cross-axial wind stress components of Stumpy Point sea level during North Carolina State University 1978 study.

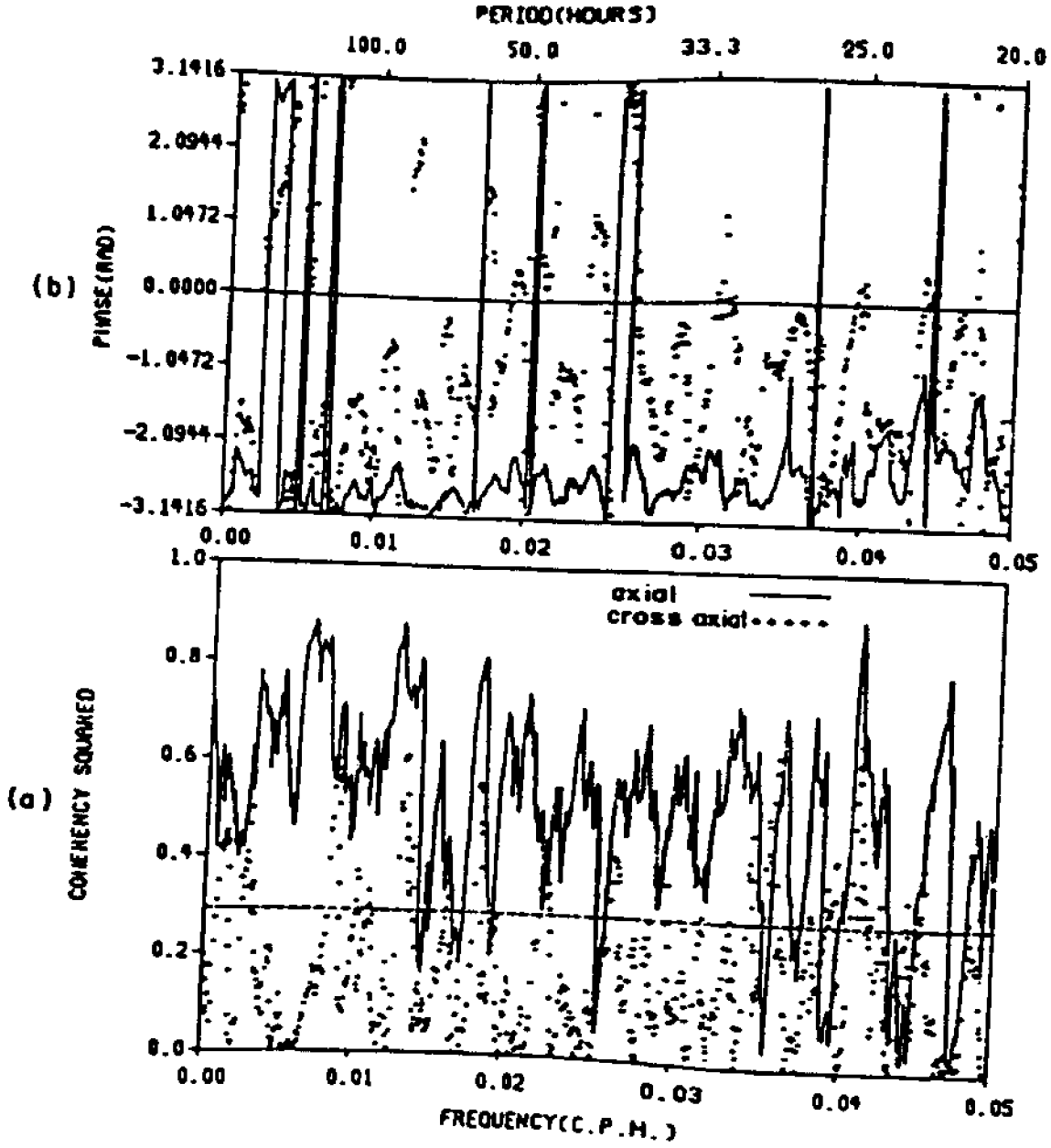

Figure 35. (a) Coherency squared and (b) cross-phase between axial and cross-axial wind stress components and Minnesott Beach sea level during North Carolina State University 1978 study.

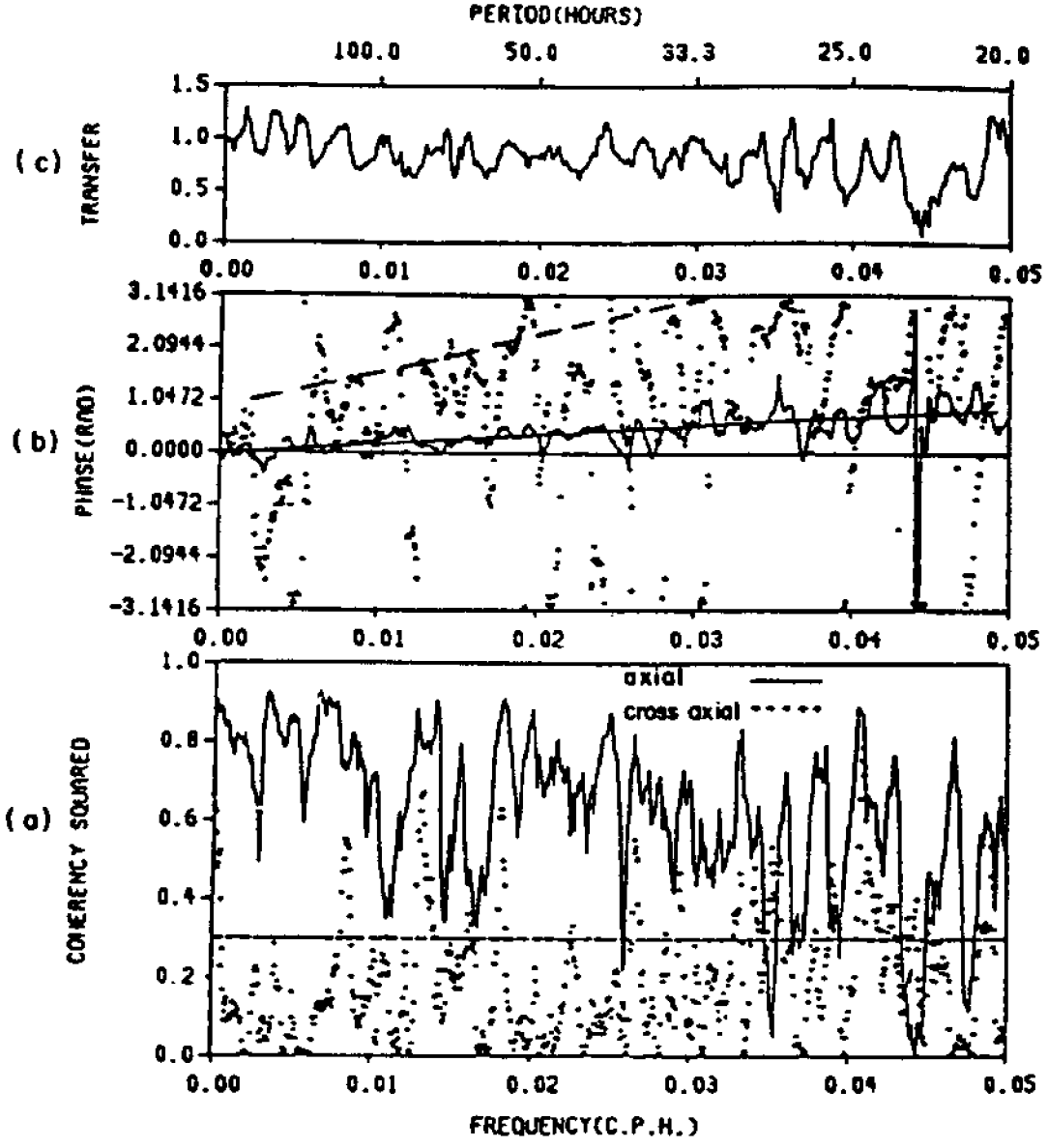

Figure 36. (a) Coherency squared, (b) cross-phase and (c) transfer function amplitudes between axial and cross-axial wind stress components and the Stumpy Point minus Minnesott Beach sea level difference during the North Carolina State University 1978 study.

TFA, is about 1.12. This means that there is a 1.12 cm sea level difference between water height at Stumpy Point and that at Minnesott Beach for every 1.0 msec-1 of longitudinal wind speed. If one takes a more conservative approach and simply does a linear regression fit of TFA over the range of frequencies shown, then the absolute value of 0.85 cm for $\eta_{SP} - \eta_{MB} = \Delta\eta_{SM}$ for each 1.0 m s^{-1} of $\bar{v}_W$ results.

Let us now consider the relationship between sea level slope and axial windstress, τ^y, directly rather than simply with the windspeed of which τ^y consists. Wind stress can be calculated from wind velocity using the conventional drag law $\tau = \rho_a c_D V_W V_W$ where ρ_a is the density of air taken as $1.3(10^{-3})$ (Pond, 1975). We then solve the relationship for sea level slope, $\Delta\eta_{SM}$, in cm per km of separation distance between stations at Stumpy Point and Minnesott Beach per unit wind stress, which can be expressed as

$\Delta\eta_{SM}/\Delta y_{SM} = \frac{(TFA)uw^2}{\tau y \Delta y}$, where Δy is the separation distance and v_W is the axial wind speed. Using the TFA obtained by averaging values of the peaks in the coherency spectrum of $\Delta\eta_{SM}$ versus the axial component of V_W, a 0.26 (cm/km)/(dyne/cm^2) sea level slope per c.q.s. unit of wind stress results. The "least square" TFA yields a value of 0.2 (cm/km)/(dyne/cm^2). Alternatively stated, for every knot of axial wind there will be an axial slope of sea level of 0.698 to 0.907 cm/km and thus with a 20 knot wind will create an 83 to 109 cm sea level difference between Stumpy Point and Minnesott Beach. A 43-inch water height difference down the axis of Pamlico Sound is significant.

The dynamical implications of a $2(10^{-6})$ slope of sea level can be assessed by considering the implications of the 30-year-old study of Welander (1957) in his investigation of the response of a shallow sea or large lagoonal embayment to wind forcing. In an extension of the work of Welander, Pietrafesa (1984) showed that the flow field, driven by seasurface slopes set up by wind forcing in a shallow embayment like Pamlico Sound is proportional to the sea level height difference divided by the distance between the sea level stations times $(10)^7$ or u,v α 10^7 $\Delta\eta/\Delta y$. So a 1 dyne/cm^2 wind stress (or a wind of 5.44 m/sec or 10.7 knots) creating a $2(10^{-6})$ slope, will drive a 20 cm/sec or 17.3 km/day current. Ten-knot winds are quite common to Pamlico Sound as suggested by Figures 22 and 25 where speeds are typically $\pm$ 5-6 m/s, i.e. approximately 10 knots.

We next consider the coherency between wind stress components and sea level as a function of month of the year. In Figures 37 and 38 the squared coherencies between the axial, (τy) at 45° east of north, and lateral or cross-axial (τx) at 135° east of north, wind stress components and sea level at Minnesott Beach and Stumpy Point, respectively, are presented as a function of periodicity of dependent variables and time of the year, 1978. The cross-hatched areas signify C^2 below the 90 percent significance level. Obviously, the coherency between sea level fluctuations and the along-axis wind is very high throughout the year at Stumpy Point, with some seasonal modulation such that maxima C^2's are reached during the late fall through early winter. Coherency between η_{sp} and τ^x are generally not significant. Minnesott Beach sea level bears about the same relative relationships to τy and τx as a function of period of motion and month of the year, but the C^2's are lower in general.

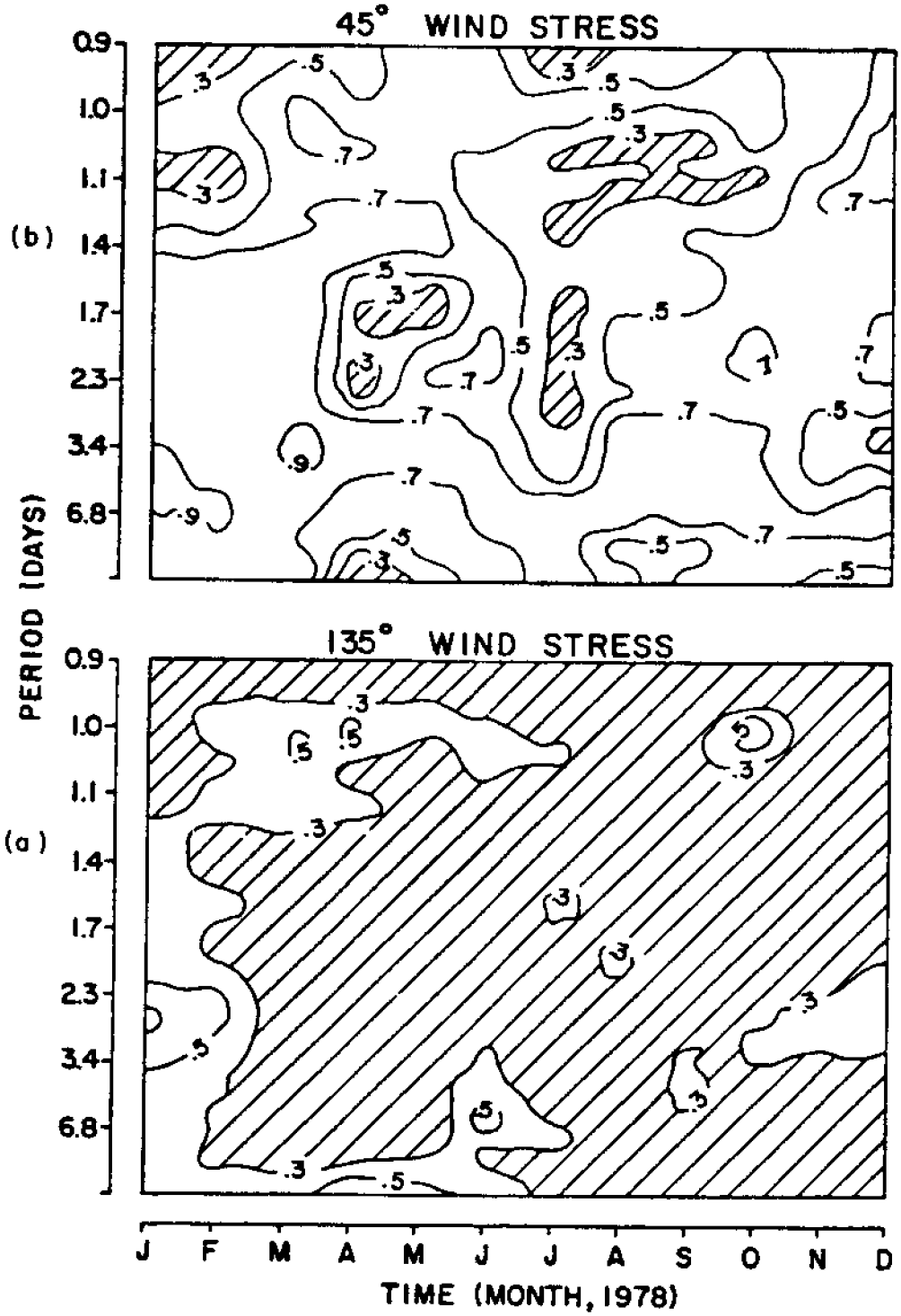

Figure 37. Squared coherency between (a) cross-axial (135°) and (b) axial (45°) wind stress components and Minnesott Beach sea level as a function of period of event and month of the year. Hatched areas are below 10 percent significance level.

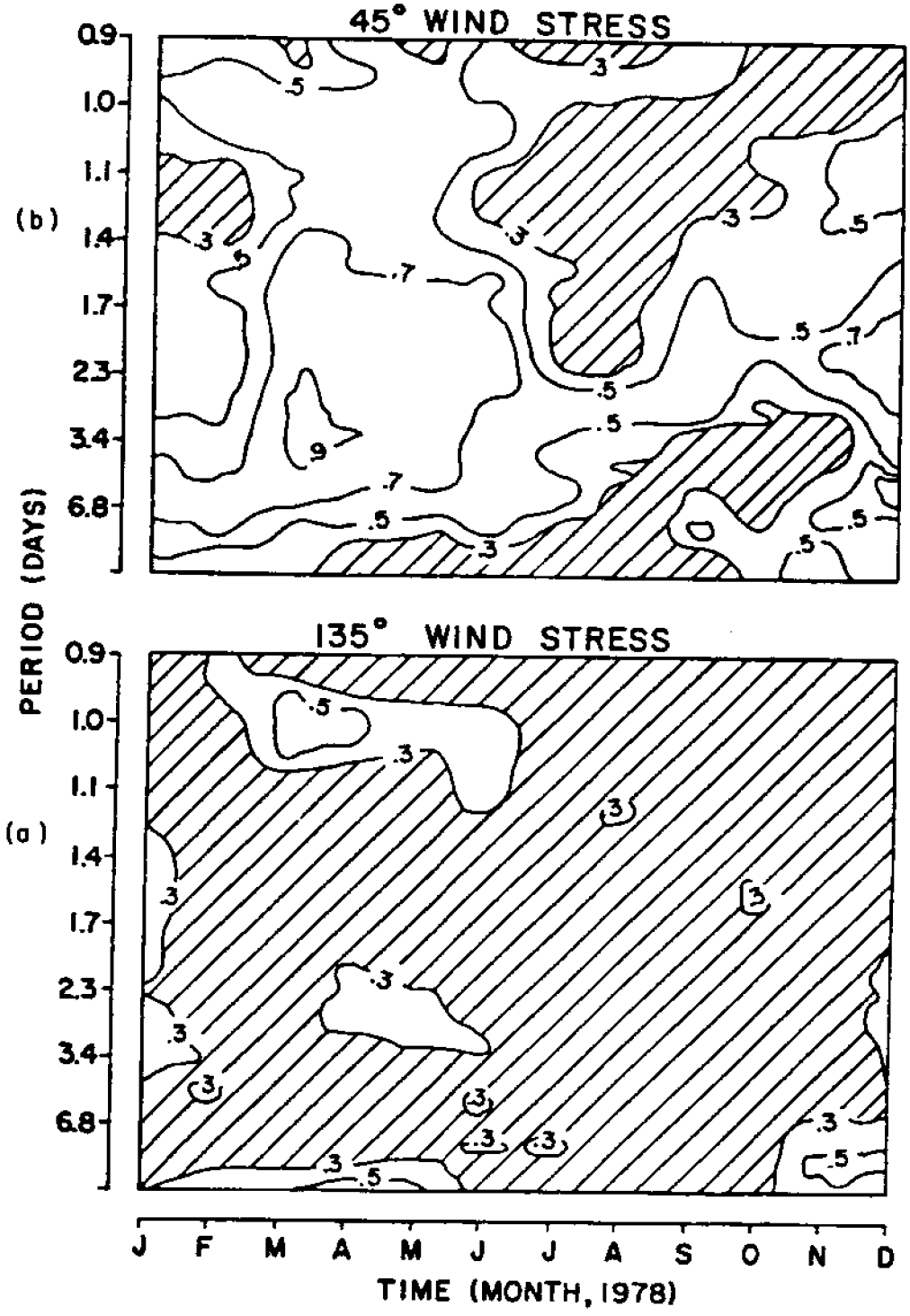

Figure 38. Squared coherency between (a) cross-axial (135°) and (b) axial (45°) wind stress components and Stumpy Point sea level as a function of period of event and month of the year. Hatched areas are below 10 percent significance level.

A curious phenomenon is the seabreeze which aligns itself north-south and peaks, in effect in causing sea level fluctuations during the late winter through early summer centered around spring.

In Figure 39 we see the coherency of the Stumpy Point-Minnesott Beach sea level difference versus τ^y and τ^x as a function of synoptic scale period and month of the year. The C^2's are similar to those for the individual stations save for the fact that the "$\Delta\eta$ vs τ^y C^2's are larger than are the individual "η vs τ^y's".

5. Seasonal Sea Level Fluctuations

In the discussion of the coherency between the 1978 year-long time series of sea level at Stumpy Point and Minnesott Beach (Section II-3) we noted that in general the rise at one site occurs simultaneously with a drop at the other site (cf Figure 21). This is true up to monthly time scales. However, for time scales of months to seasons, water level at the two stations rises and falls in concert, actually with a few days phase lag of each other.

In Figure 40, overlapping 60-day averages of both η_{SP} and η_{MB} 1978 data as well as averaged atmospheric pressure are presented. While Stumpy Point has a lower low from January to March, Minnesott Beach has a higher high from September to November. However, the seasonal oscillations are clearly in phase. There are spring and fall peaks and summer and winter lows in water elevations. The maximum range at both stations is about 25 cm. The monthly to seasonal oscillations at both locations bear little resemblance to the monthly-annual gross water budget presented previously in Figure 8 save for the fact that the net influx of fresh water, accounting for all sources and sinks to Pamlico Sound, occurs in July, which is a relatively low point in the water level at Stumpy Point and Minnesott Beach. Atmospheric pressure appears to match up, i.e. the inverted barometer effect appears to be operative during the spring in causing the seasonal high in sea level. However, at 1 cm of η per 1 mb of P_a, the inverted barometer effect can account for at most 3 cm of the 20 cm spring rise in η. What then is responsible for the monthly to seasonal to annual variations in η?

The answer to the question of the cause of monthly to seasonal to annual variations in sea level lies in a consideration of coastal sea level (e.g. sea level at Cape Hatteras, Figure 41), as discussed previously in Section 8 of Part I. The raising and lowering of the North Atlantic as a function of its heat content and the seasonality of predominant winds provide the causal functions for the effect displayed in Figure 40.

6. The Summer, 1978

During the period 22 June to 5 September 1978, 10 sea level stations were established around Pamlico Sound. The field program is synopsized in Table 4 and Figure 19. The data sets collected during that experiment are shown in Figures 22 and 23. The 40HLP Cape Hatteras wind stress vectors during this period are shown in Figure 41a. The time series of sea level from without the sound at the Cape Hatteras coastal station as well as from within the sound at Stumpy Point and Minnesott Beach are shown in Figures 41b and 42, respectively. Kinematical descriptors of the wind field are shown in Figure 43 and the potential energy spectra of sea level at stations Brant Island,

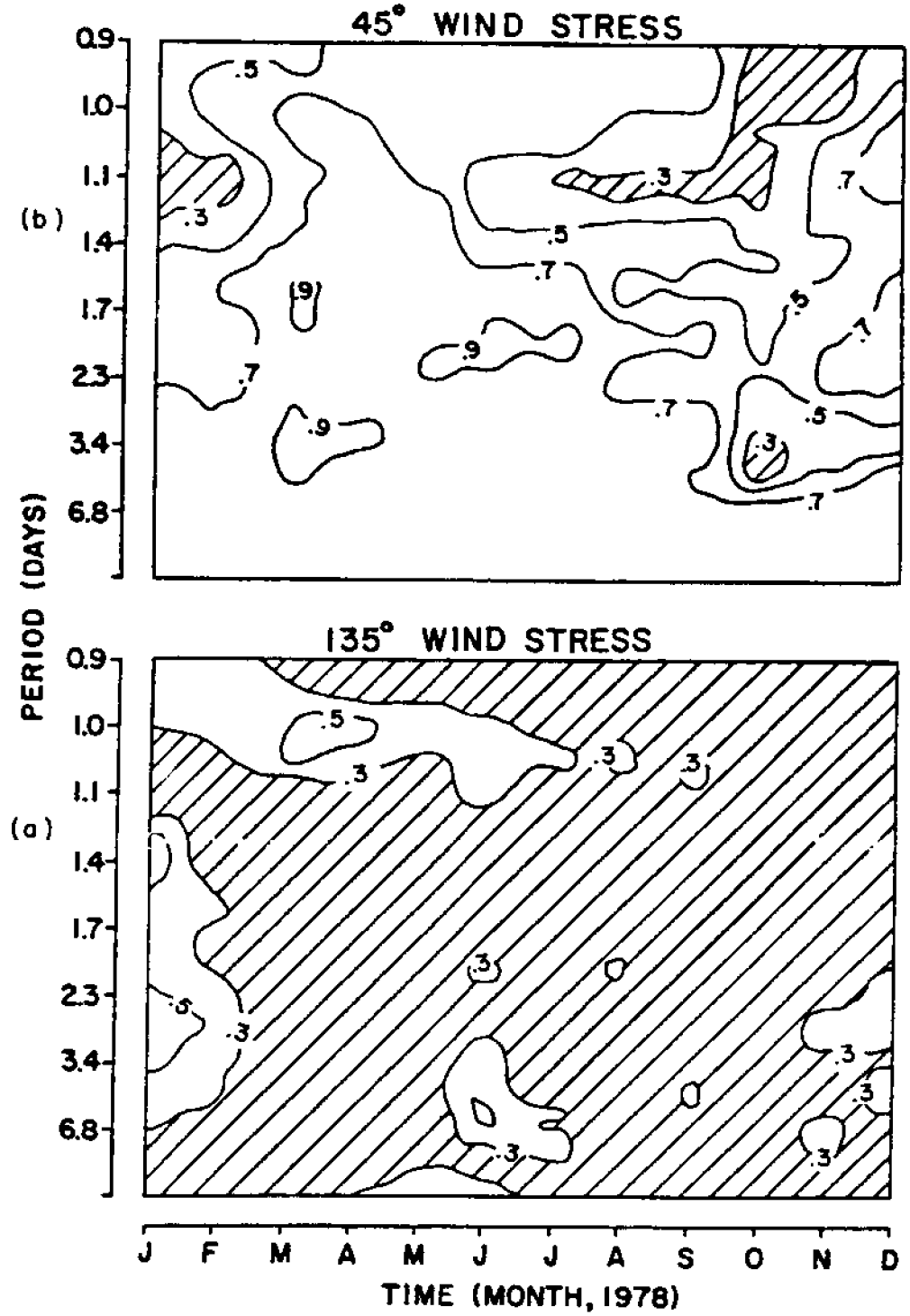

Figure 39. Squared coherency between (a) cross-axial (135) and (b) axial (45) wind stress components and Stumpy Point minus Minnesott Beach sea level difference as a function of period of event and month of year. Hatched areas are below 10 percent significance level.

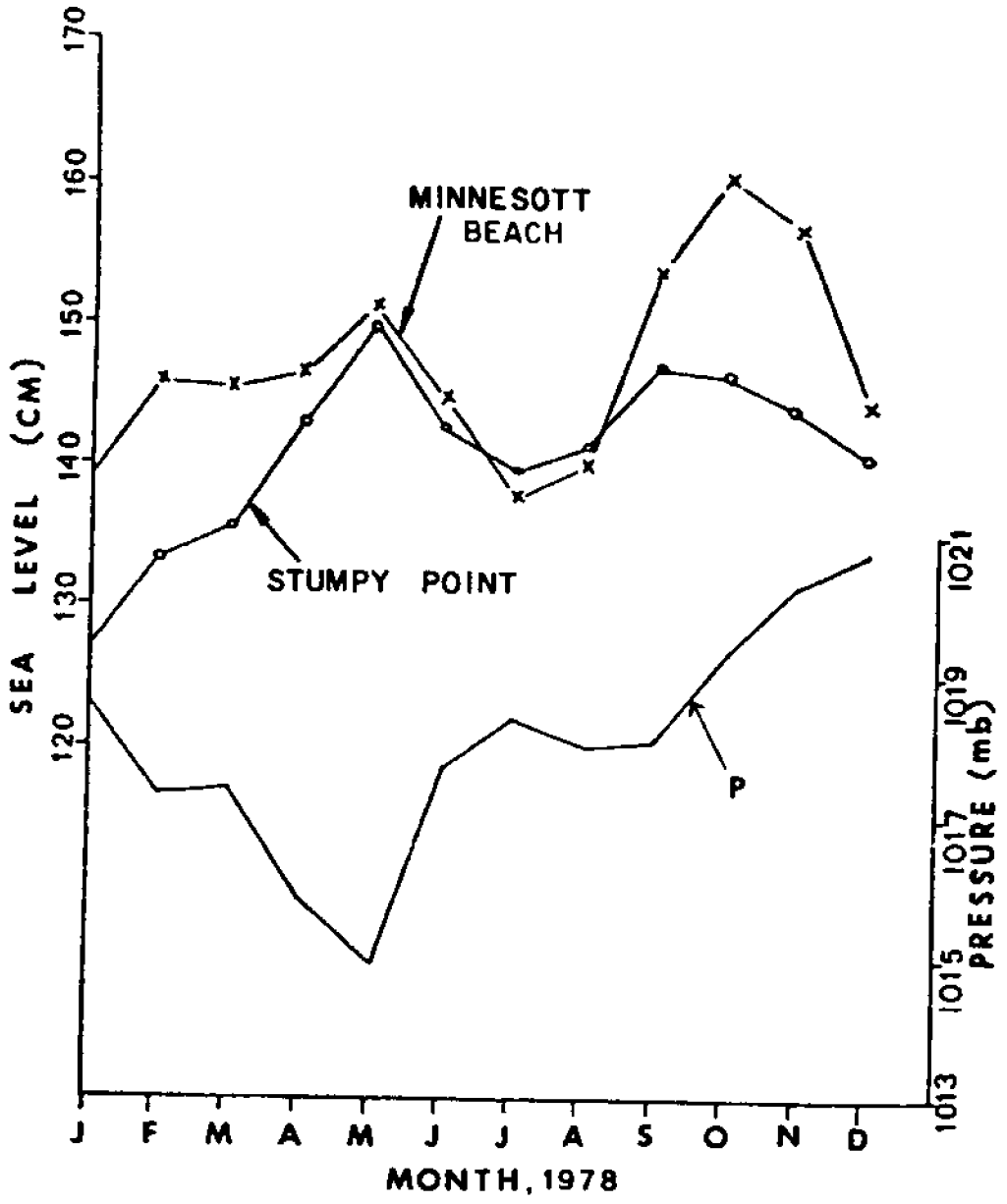

Figure 40. Monthly averaged sea level at Minnesott Beach and Stumpy Point versus air pressure during North Carolina State University 1978 study.

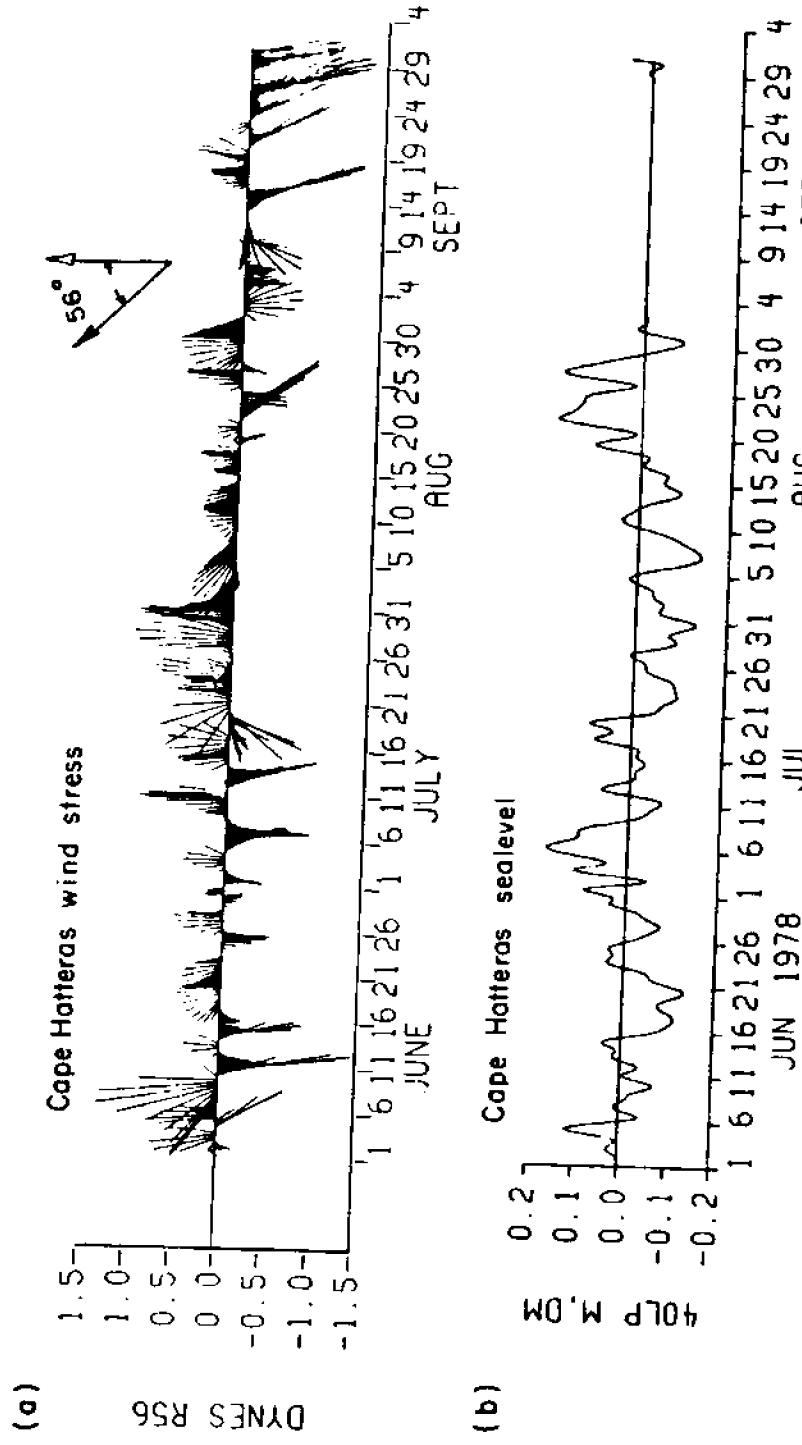

Figure 41. Cape Hatteras 40 HRLP filtered time series of (a) wind stress vectors and (b) sea level during the North Carolina State University 1978 summer study.

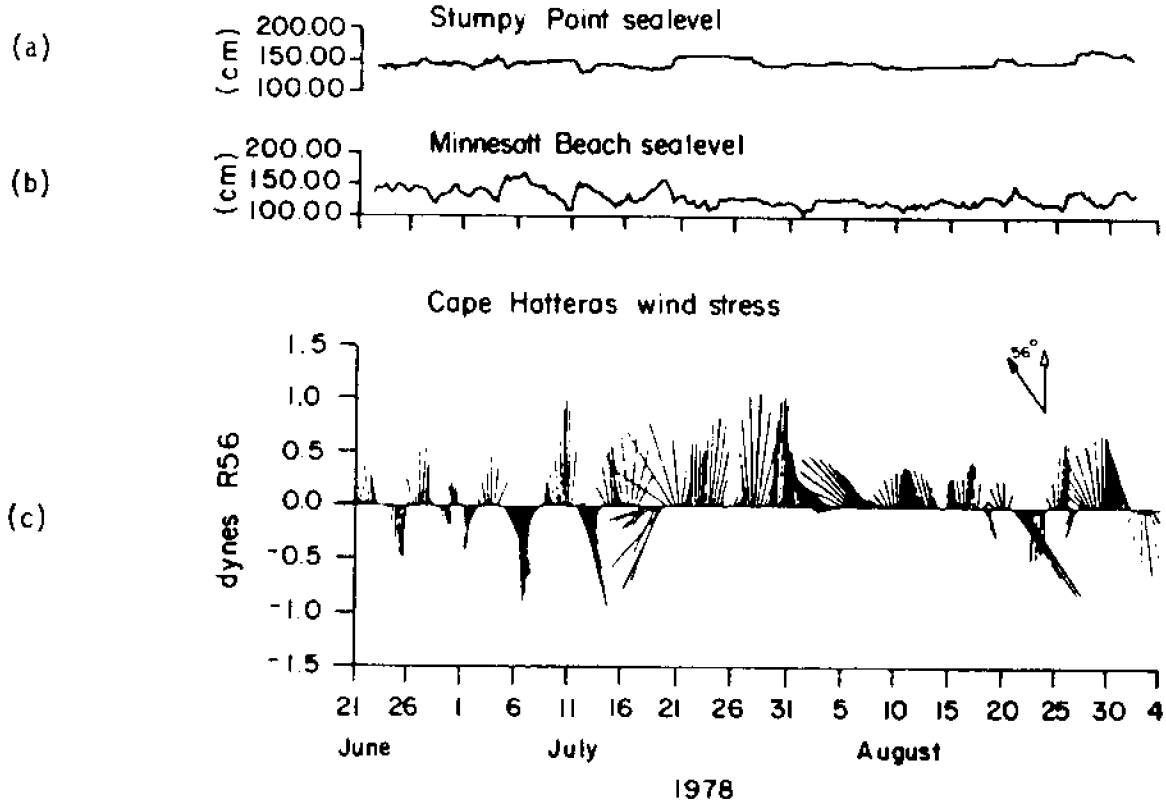

Figure 42. (a) Coastal winds versus Stumpy Point and Minnesott Beach during North Carolina State University summer 1978 study.

(b) Northward winds are seen to cause a rise (drop) at Stumpy Point (Minnesott Beach).

(c) Southward winds cause a rise (drop) at Minnesott Beach (Stumpy Point).

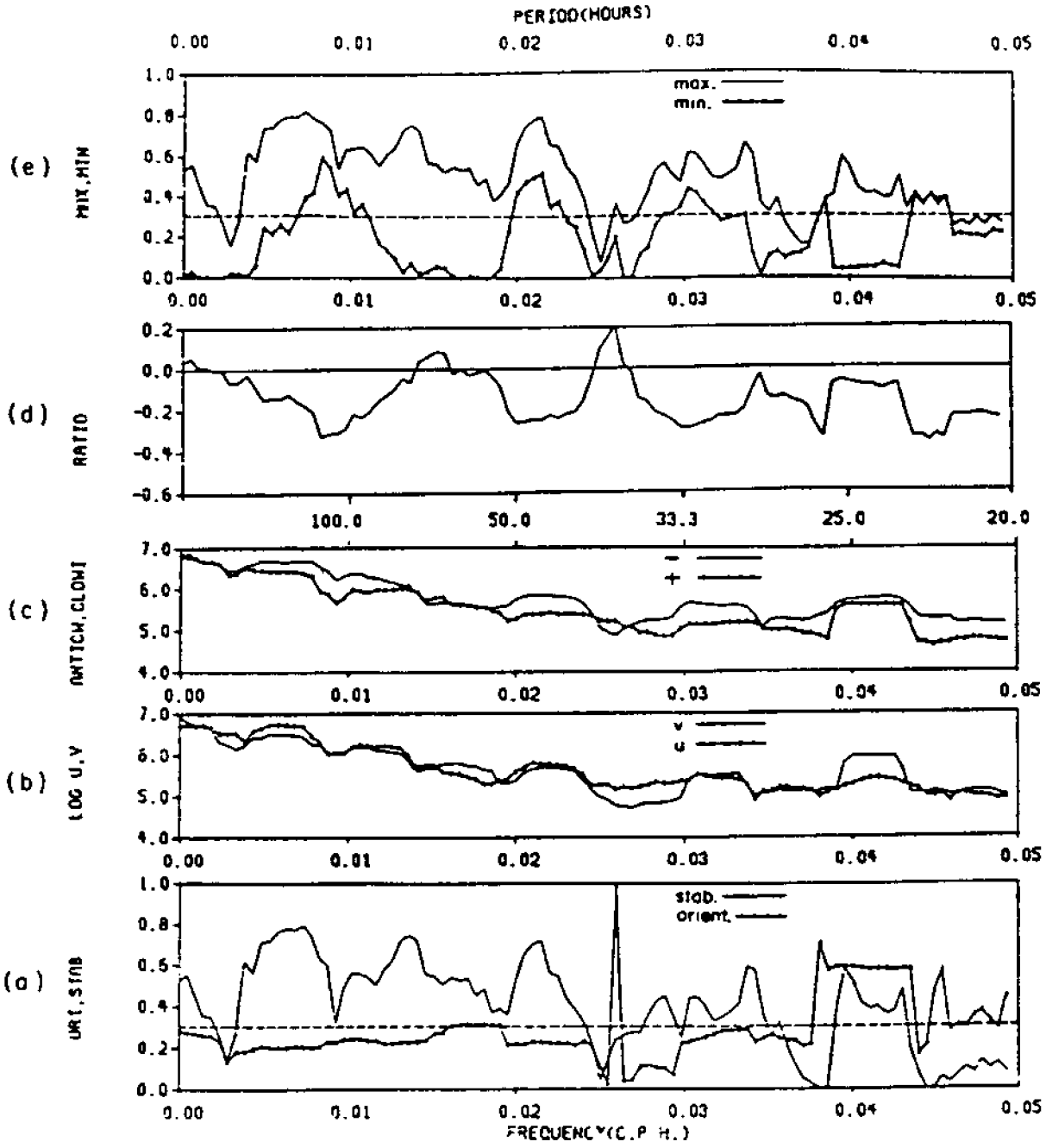

Figure 43. Hodograph, kinematic descriptors of averaged Hatteras and New Bern wind velocity vector components (+v, north; +u, east) during North Carolina State University 1978 summer study.

Washington, Manteo and Stumpy Point are shown in Figure 44. The kinetic energy density of the Hatteras wind field and the potential energy density of Hatteras sea level are both shown in Figure 45.

From Figures 41 a, and b we see that coastal sea level responds to the alongshore component of the wind within 8 to 10 hours and follows coastal Ekman dynamics as discussed by Pietrafesa et al (1980), Chao and Pietrafesa (1980) and Pietrafesa and Janowitz (1986). In effect, northward to northeastward winds cause sea level to drop at the coast in concert with a surface Ekman transport offshore and vice-versa for winds which are southward to southwestward, i.e. sea level rises at the coast. Also note from Figure 41 that persistently northward winds create longer-term net drops in coastal sea level and persistent southward winds cause a net rise. In Figure 42 we see that northward winds cause a rise of water elevation at Stumpy Point and a drop at Minnesott Beach. Southward winds cause the opposite scenario to occur; η_{SP} falls and η_{MB} rises. We will consider the implications of the rise and fall of both coastal, i.e. open ocean, sea level and the contemporaneous vertical excursions of water level on the soundside of the barrier islands in Section III. Transport through the inlets can be modified or controlled by the surface slopes created by the differential rises and falls of water level on the sound side versus the ocean side of barrier island inlets.

From Figure 43, we see that the motions of the wind field were counter-clockwise rotating, elliptically polarized over periods of 3.7 to 6 days and rectilinear, i.e. the wind parcels generally moved back and forth along a straight line over the synoptic scales of 1.5 to 2 days or motions with periods greater than 6 days. The orientation of the principal axis of wind motion varied between 35° and 60° or approximately northeast-southwestward. Once again, the sea breeze is shown to be aligned at 18° west of north and is found to be a very stable prominent feature characterized by rectilinear particle motion.

The potential energy densities of sea level at several diverse, yet representative 1978 summertime sites are shown in Figure 44. They are for the stations at Washington (up the Pamlico River), Brant Island (in the southern basin), Manteo Harbor (in Roanoke Sound north of the northern basin), Oregon Inlet), Stumpy Point (on the mainland side of the north basin) and Cape Hatteras (an open ocean, coastal station). At Cape Hatteras, the lunar, astronomical, semi-diurnal or, rather, M2 tide, accounts for 49 percent of the total variance of sea level. However, within the sound the M2 constituent, which is the major tidal component, accounts for only a small percentage of the total variance. For a further discussion of the tides in the sound refer to Section I6. In general, the PEDs display a sea breeze peak and a monotonic increase in energy (or red spectrum) up to periods of 8.4 days at both Washington and Brant Island and 20.8 days at Manteo Harbor, Washington and Stumpy Point. While all of the PEDs show very similar slopes, Manteo Harbor and Washington display more definite changes in slope at 8.4 and 20.8 days.

In Figure 45, we consider the PED of sea level at Cape Hatteras and the KEDs of the τ_y and τ_x wind velocity vector components. It is vividly obvious that the axial component of the wind field contains the 90 percent of the total KED at periods of 2.7 to 35 days or throughout the spectrum of fluctuation kinetic energy from days to weeks, up to a month.

Figure 46 displays the coherency between the axial (-) and lateral (----)

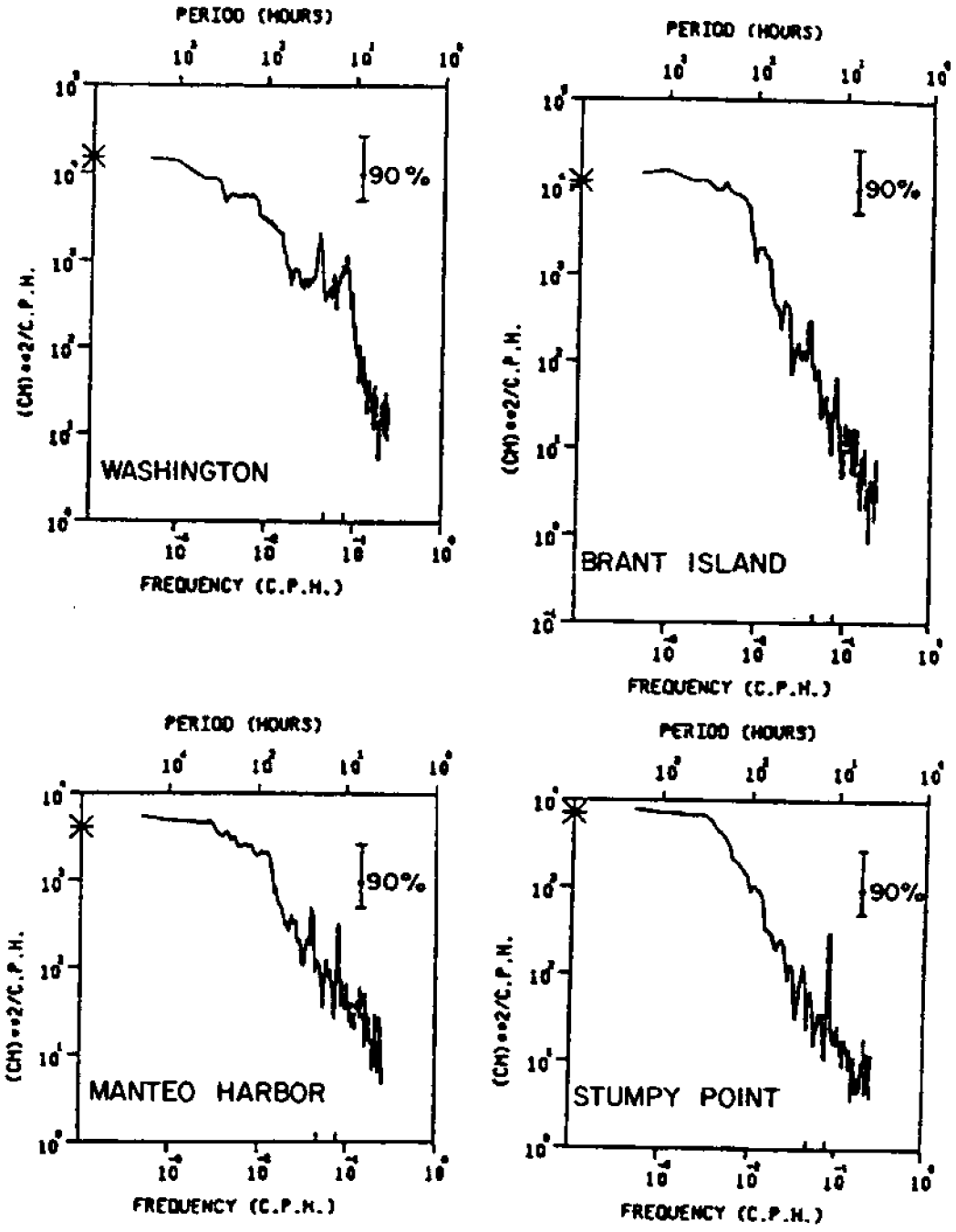

Figure 44. Potential energy spectra of sea level during North Carolina State University 1978 summer study. Manteo Harbor and Stumpy Point are in north basin. Washington and Brant Island are in south basin.

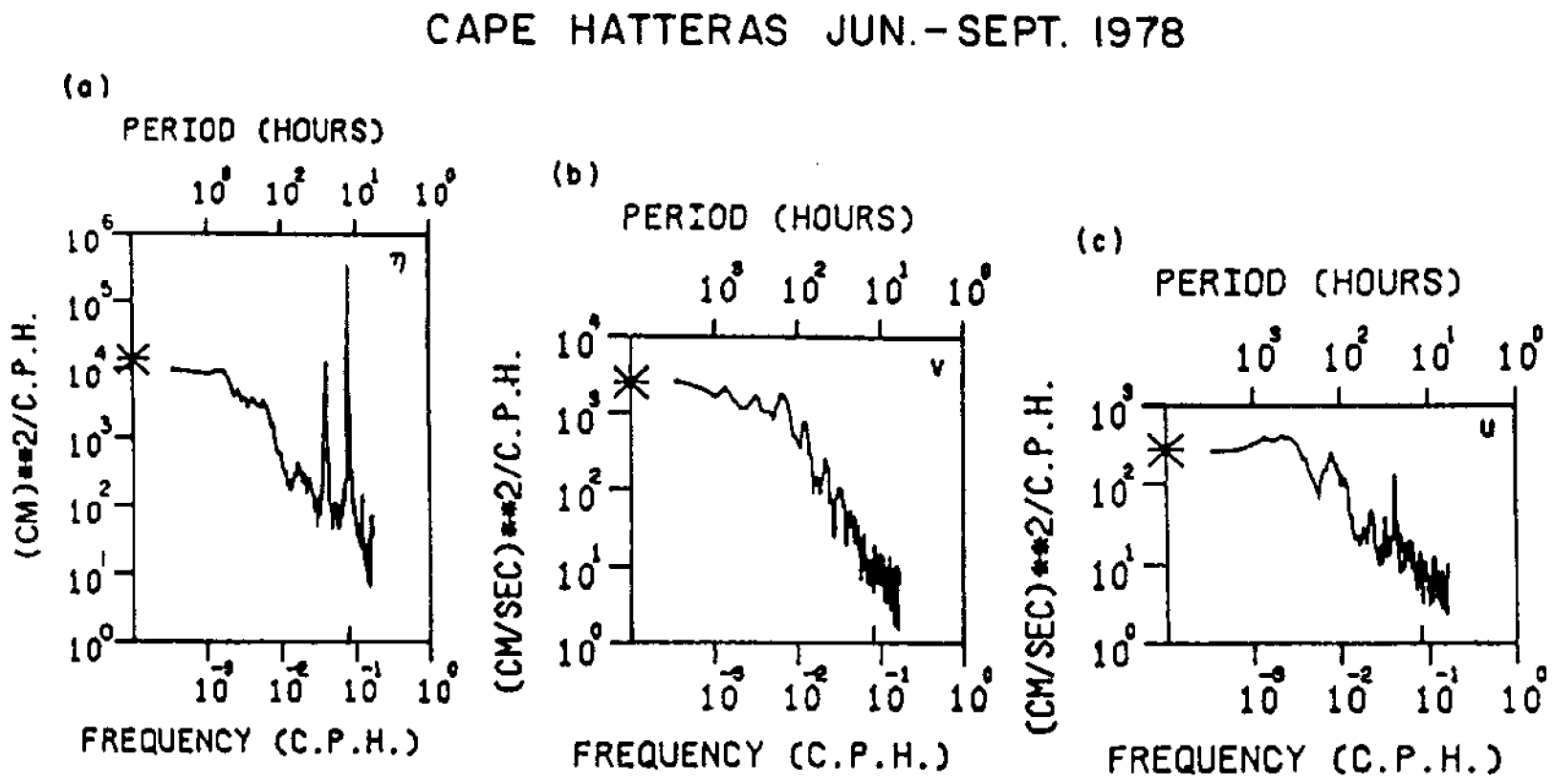

Figure 45. Potential and kinetic energy densities of (a) sea level, (b) the NE-SW wind velocity vector component and (c) the SE-NW wind velocity component at Cape Hatteras during the North Carolina State University 1978 summer study.

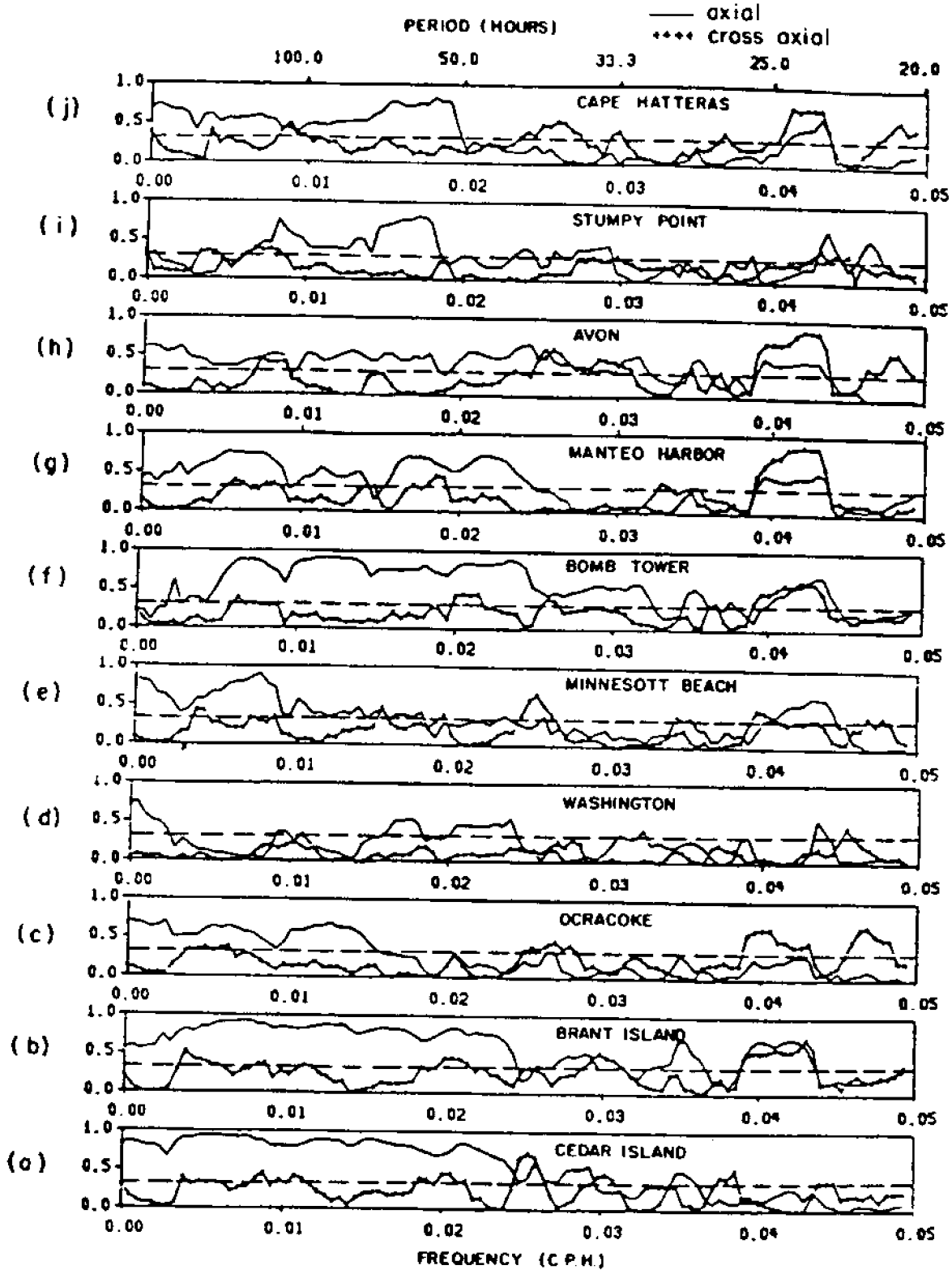

Figure 46. Coherency squared between sea level and axial and cross-axial wind stress components during North Carolina State University 1978 summer study.

components of the wind stress vector and the sea level time series from the 1978 summer experiment.

In the southern end of the Pamlico Sound basin, Cedar Island, Brant Island, Ocracoke and Minnesott Beach all display good coherency with the axial wind component with η_{CI} vs τ^y highest, η_{BI} vs τ^y second, η_O vs τ^y third and η_{MB} vs τ^y fourth. Washington, also in the "southern" basin shows good coherency between η_W and τ^y at superdiurnal periods of 2-3 days, 4 days, and greater than 16.5 days. Cedar and Brant Islands are located in the sound proper. Ocracoke is on the back side of a barrier island on the eastern flank of the sound and Minnesott Beach is 40 km (mi) upstream of the mouth of the Neuse River. Washington is on the Pamlico River, 60 km (mi) from the connection of the river's mouth to Pamlico Sound.

In the northern end of the sound, sea level is most coherent with the axial windstress at Bomb Tower, Manteo Harbor, Avon and Stumpy Point, in order of highest to lowest C^2. At Cape Hatteras, which is an open ocean, coastal station, η and τ^y are highly coherent at all periods in excess of two days. Curiously, stations on the north and eastern side of the northern basin, including Manteo Harbor and Avon indicate high C^2 at all periods greater than 2 days, while at Bomb Tower, in the middle of the northern basin, C^2 becomes insignificant at periods greater than 20 days. At Stumpy Point, η is highly coherent with τ^y between periods of 2 to 6.8 days only. It was speculated by Chao (1981) that the degradation in coherency between τ^y and η at Stumpy Point and Bomb Tower at lower frequency was due to the influence of water exchange between Albemarle, Roanoke, Croatan and Pamlico Sounds and the flux of coastal and sound waters through Oregon Inlet.

Coherency between lateral or cross-sound winds, τ^x, and sea level is generally low throughout the sound with several notable exceptions. At the diurnal period, η and τ^x are highly coherent everywhere except for Washington and Cedar Island. Within the period band of 4.8 to 7.5 days there is marginal coherency between η and τ^x at Minnesott Beach, Cedar Island, Brant Island, Ocracoke, Avon, Hatteras, Bomb Tower, Stumpy Point and Manteo Harbor.

In Figure 47 we consider the coherency squared (C^2), phase relation (ϕ) and transfer function amplitude (TFA) frequency domain relationships between the summer, 1978 time series of sea level slope along the axis of Pamlico Sound between the north and south basins using the Bomb Tower and Brant Island time series vs. τ^x and τ^y, the lateral and axial wind components. In summary, $\eta_{BT}(t) - \eta_{BI}(t)$ is correlated with $\tau^y(t)$ and $\tau^x(t)$ separately. Extraordinary C^2's exist between $\eta_{BT}-\eta_{BI}$ and τ^y over most of the spectrum of summertime motions, particularly for motions with periods greater than 2 days. As was found with the year-long, 1978, time series of $\eta_{MB} - \eta_{MB}$ vs. τ^y, we see that a straight line can be drawn as a best fit linear regression, through the phase diagram (Figure 47b). Positive ϕ (negative ϕ) indicate that τ^y ($-\tau^y$) leads (leads) $\eta_{BT} - \eta_{BI}$ ($\eta_{BI} - \eta_{BT}$). The straight line suggests an axial water level slope set up-set down time of 3 hours 36 minutes. Alternatively, τ^x leads $\eta_{BT}-\eta_{BI}$ by 16 hours 20 minutes at the coherent period of 2 hours and by 28 hours 45 minutes at the high C^2 period of 4.7 hours.

The result that $T_{\Delta\eta}(t) \alpha T_{\tau^y}(t)+3.6$ hours during the summer of 1978 is almost identical to the $T_{\Delta\eta}(t) \alpha T_{\tau^y}+2.8$ hour finding for the entire 1978 year. The transfer function amplitude, TFA, is 0.667, i.e. a sea level difference of 0.667 cm between water level at Bomb Tower and Brant Island occurs for every

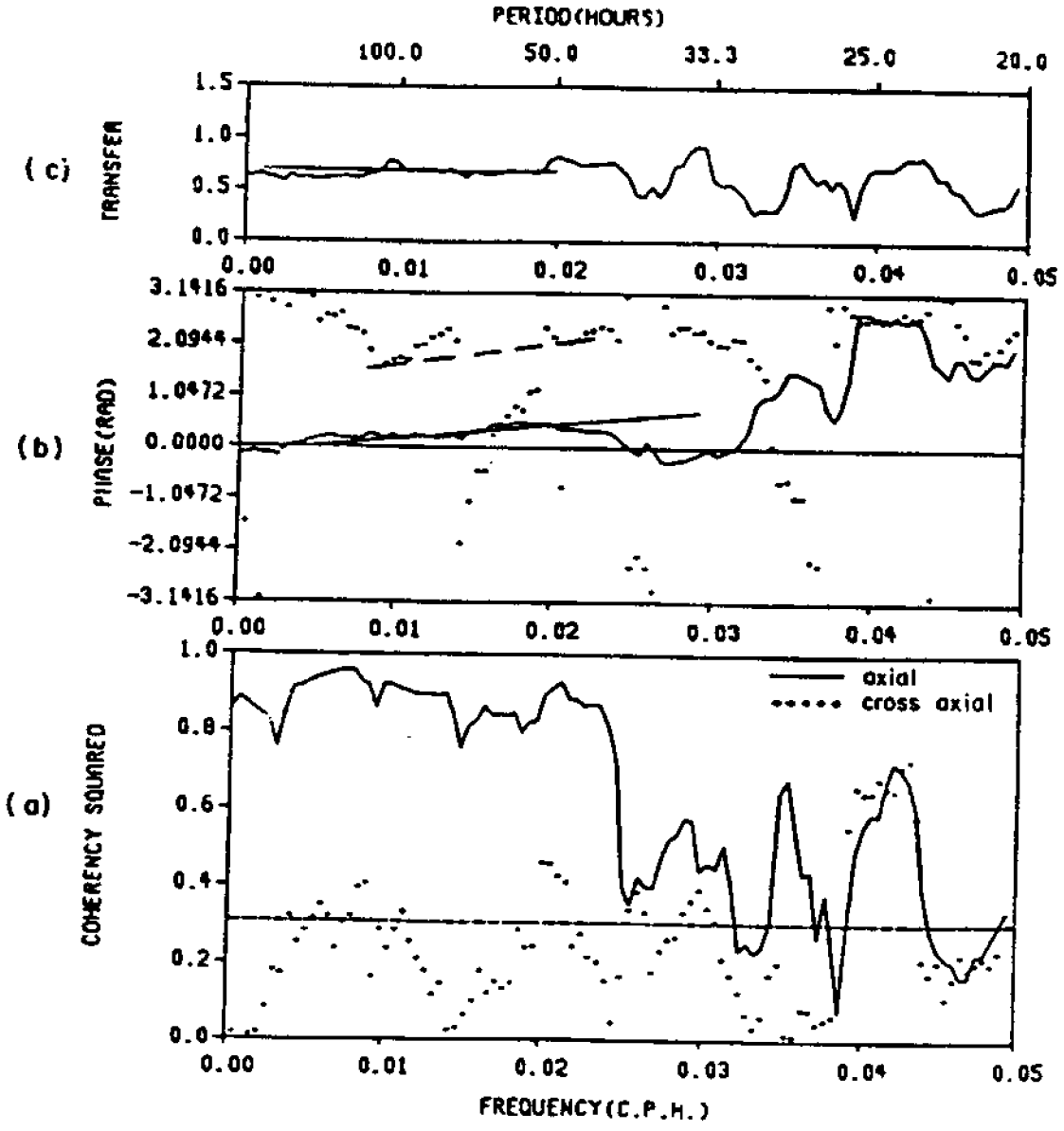

Figure 47. (a) Coherency squared, (b) cross-phase and (c) transfer function amplitudes between axial and cross-axial wind stress components and Bomb Tower minus Brant Island sea level differences during the North Carolina State University 1978 summer study.

1.0 m/sec of longitudinal wind speed.

The relationship between sea level slope between Bomb Tower and Brant Island and axial windstress component τ_y for the summer 1978 period the slope per unit dyne/cm^2 of wind stress is 0.26 cm/km/(dyne/cm^2). This result compares identically to that obtained for the year-long period and shows incredible consistency.

7. The Winter (18 December, 1978 - 26 February, 1979) Experiment

The summertime 1978 experiment was rerun during the 1978/1979 winter period to provide seasonal comparison. Kinematical wind descriptors for the period 18 December, 1978 - 26 February, 1979 are shown in Figure 48. The KED of the axial and lateral components of the wind stress vector are shown in Figure 49. The two figures indicate that the wintertime windfield is quite different from its summertime counterpart. During the winter the windfield is elliptically and clockwise polarized. Both the maximum and minimum coherencies are relatively high for atmospheric windfield motions with periods greater than 2.45 days. However the ellipse of particle motion is only stable for atmospheric motions of 5.2 to 13.8 days. The principal axis orientation of these stable elliplical motions is between 30 and 35° east of north, or slightly skewed relative to the topographic axis of Pamlico Sound. Kinetic energy densities of the axial and cross-axial wind field components show peaks at periods of 4.2, 4.9 - 6.9 and 16.7 days with the cross-axial component also having a peak at 1 day; a peak absent from the axial component.

Potential energy density of sea level fluctuations at Avon, Englehard, Hatteras Inlet and Manteo Harbor are shown in Fig. 50. As was found for the summer period, the semi-diurnal tidal signal is prominent in the Hatteras Inlet water level record, but is not significant in the sound proper. The PED's of sea level in the sound show spectral peaks at periods within the band of 2 days to 2 weeks with more prominent peaks occurring at 3 and 4 days. Within the 2 to 14 day synoptic scale meteorological band, the spectrum is red and then whitens for motions with periods greater than 3 weeks. The winter time PED spectra indicate an overall energy level which is of the order of 20 to 50 percent higher than its summertime counterpart. This is simply a manifestation of the fact that the wintertime windfield is more energetic than the summertime windfield, as is evident from a comparison of Figures 44 and 50.

Coherency between wintertime winds and sea level in and around Pamlico Sound is shown in Figure 51. Stations Minnesott Beach and Brant and Cedar Islands are in the southern basin while Manteo Harbor, Englehard and Avon are in the northern basin. Hatteras Inlet provides a coastal inlet comparison. Brant Island and Manteo Harbor correlate well with both the axial and cross-axial wind components at periods greater than 2 days. Meanwhile, Avon, a barrier island locale, correlates well with the cross-axial component, τ_x, for periods of 2.7 to 4 days and 5.2 to 15 days with very low C^2 between η_A and τ_y, being marginally coherent at the singular periods of 3.3 days. Hatteras Inlet also shows marginal coherency between η_{HI} and τ_y at 3.3 days but excellent coherency with τ_x between 2 to 5.1 days and 15 to 30 days. Cedar Island and Minnesott Beach indicate a continuing affection for τ_y as η at both locales is highly coherent between 2 to 30 days. However, there is

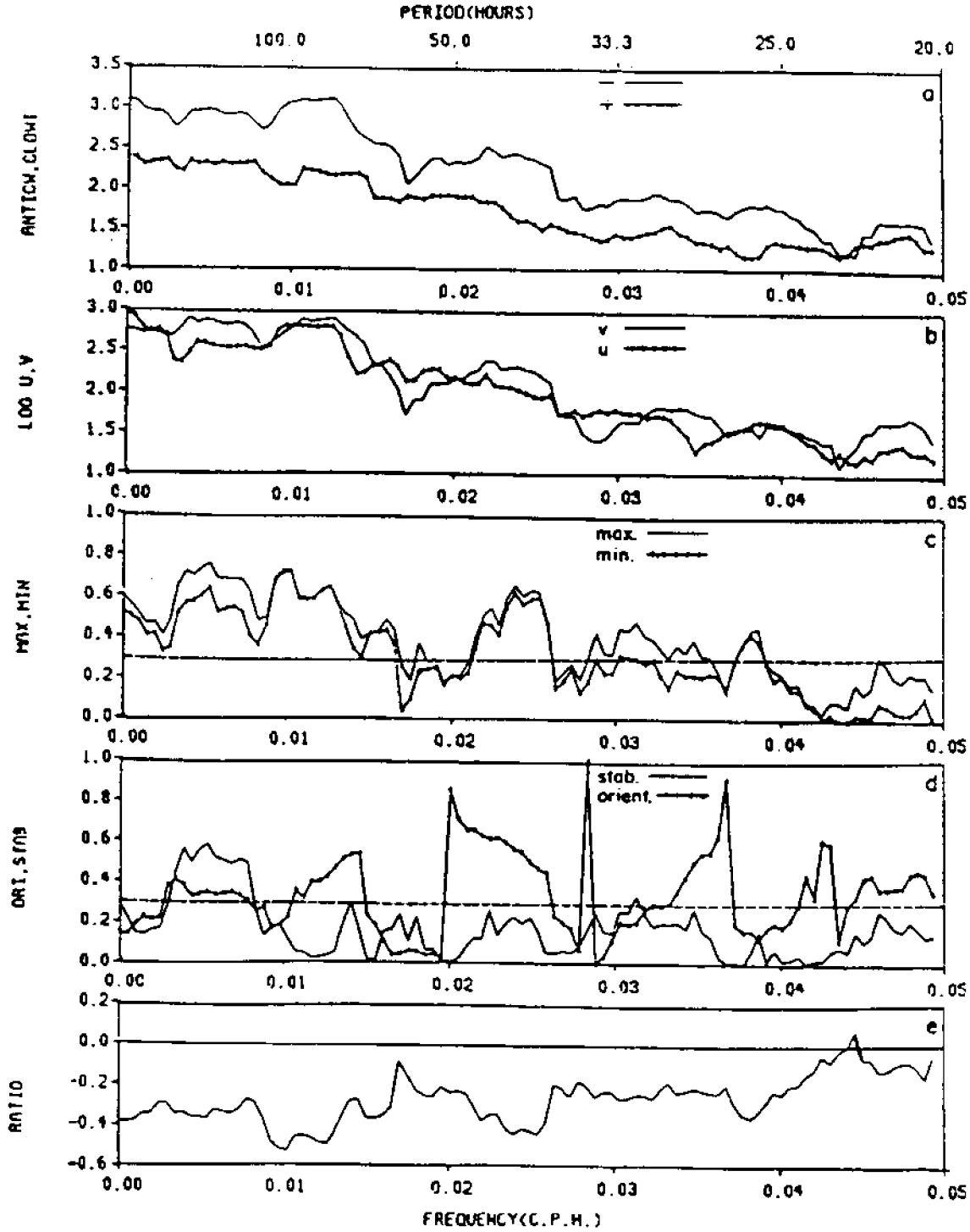

Figure 48. Hodograph, kinematic descriptors of averaged Hatteras and New Bern wind velocity vector components (+v, north; +u, east) during North Carolina State University 1978/79 winter study.

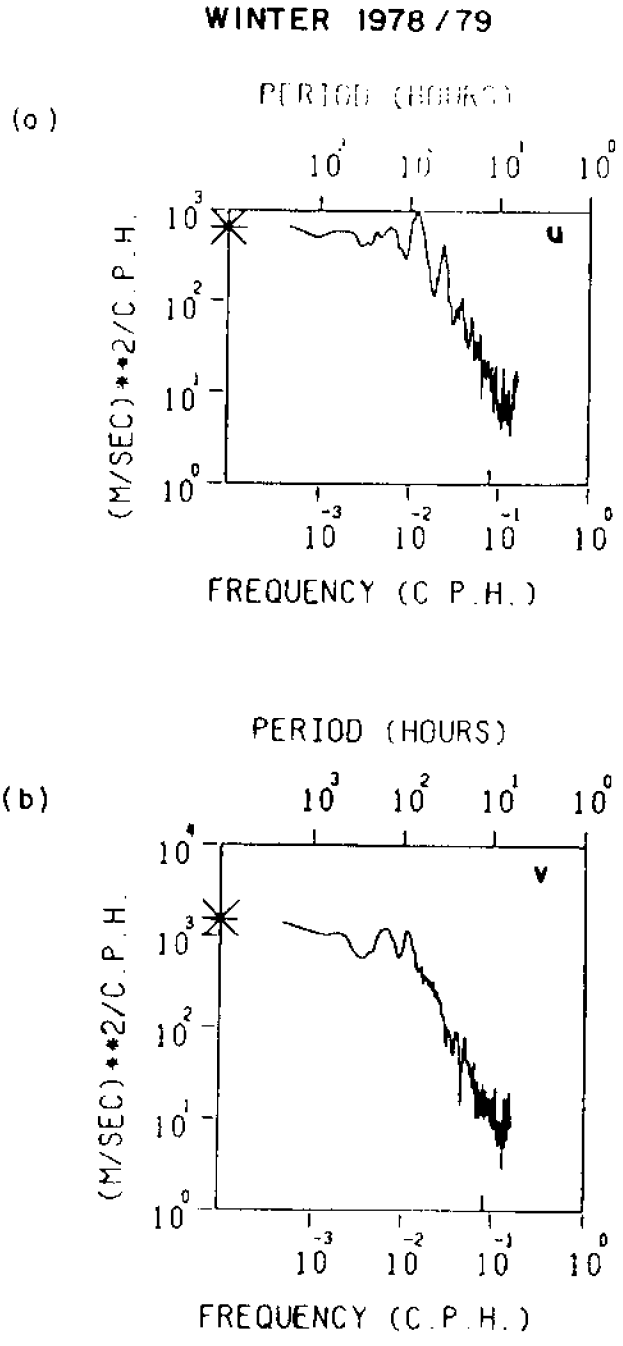

Figure 49. Kinetic energy densities of cross-axial, (a) U(NW-SE) and axial, (b) V(NE-SW) wind stress vector components during the North Carolina State University 1978/79 winter study over Pamlico Sound.

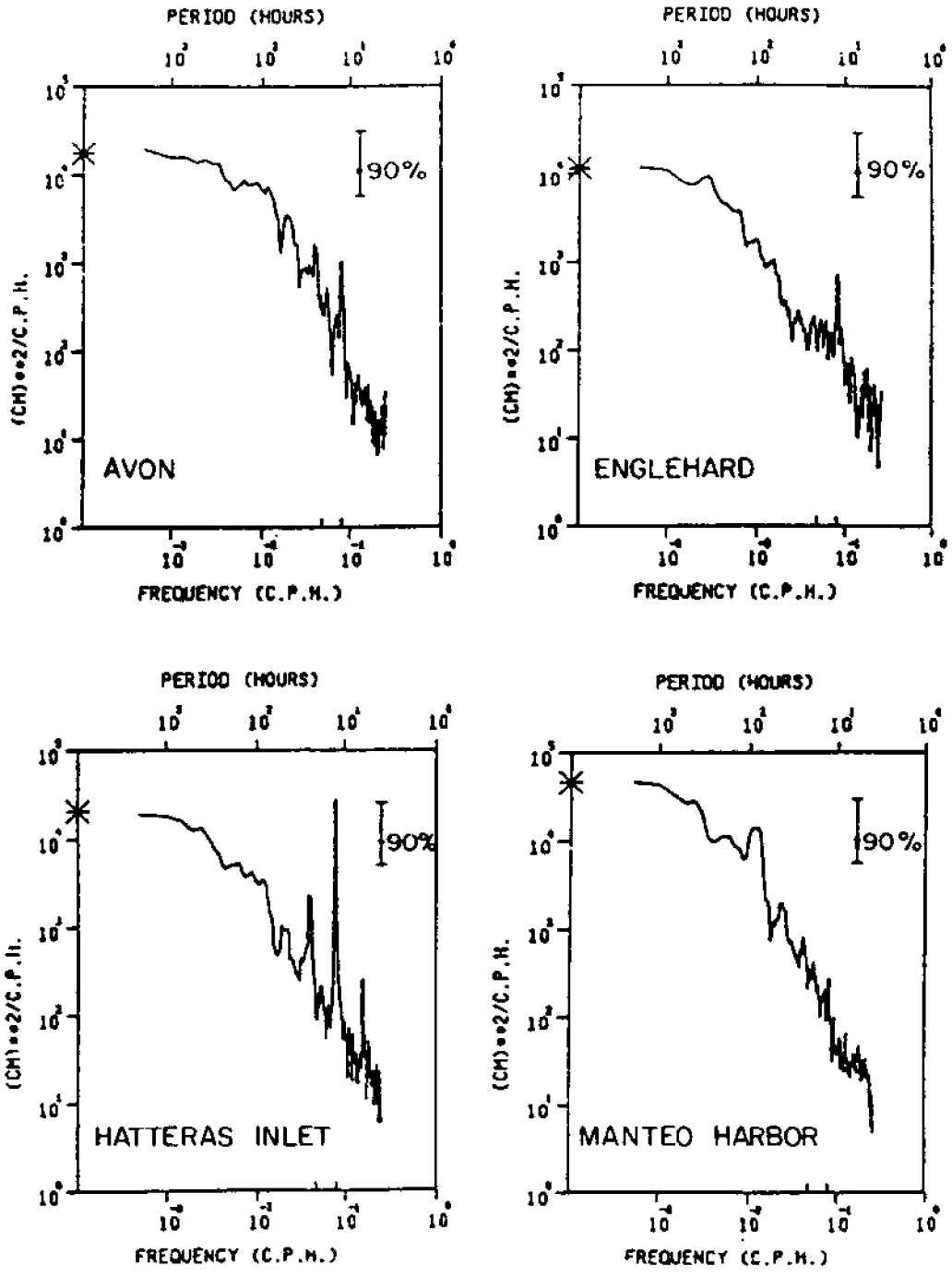

Figure 50. Potential energy density spectra of sea level during the North Carolina State University 1978/79 winter study.

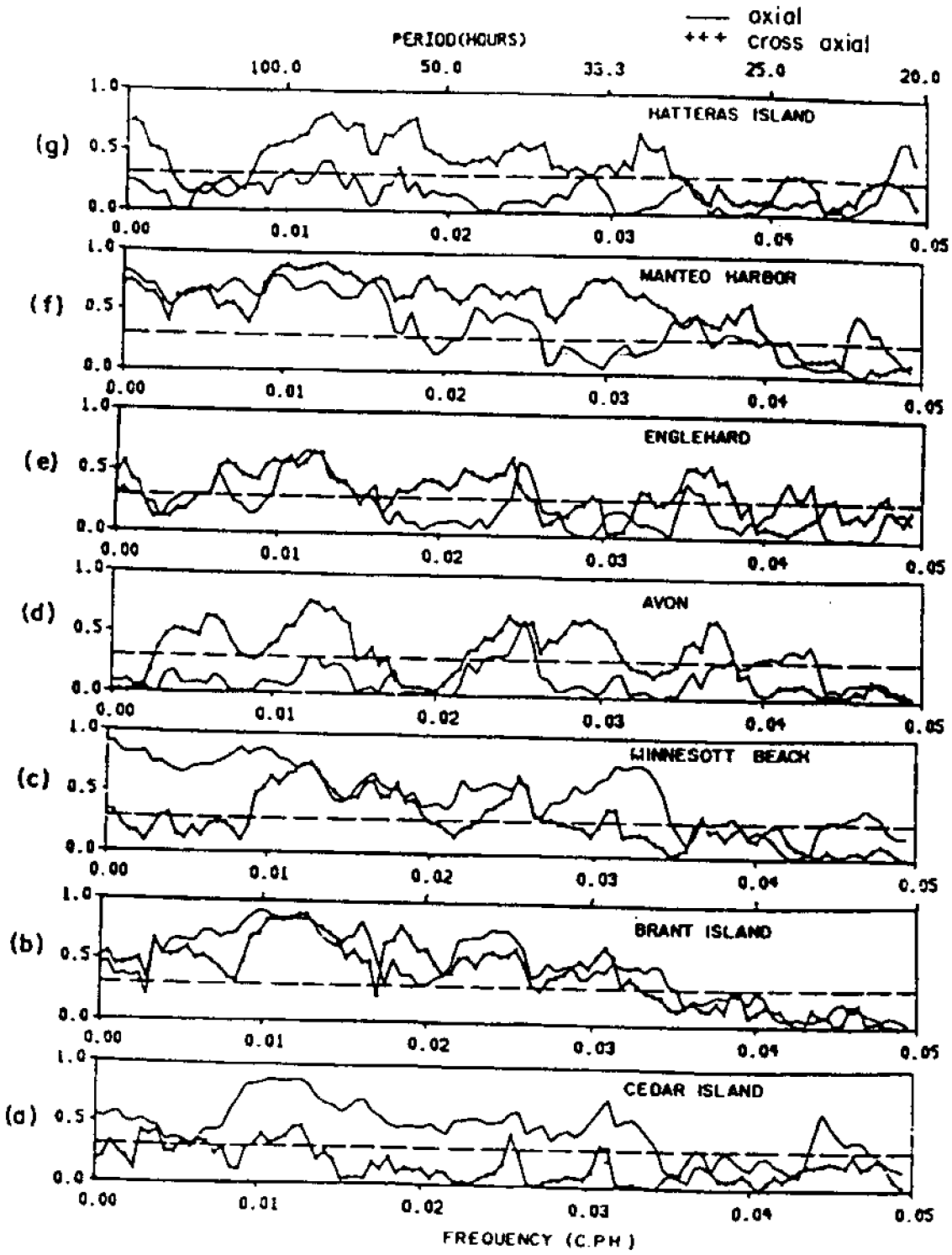

Figure 51. Squared coherencies between sea level and axial and cross-axial wind stress components during North Carolina State University 1978/79 winter study.

also good coherency between η_{MB} and τ^x and η_{CI} and τ^x between 2 to 4.5 and 11 days at Minnesott Beach and between 3.1 to 5.5, 7.1 and 10.5 to 14.7 days at Cedar Island, a very different result than is shown during the summertime.

A summary of the northern versus the central versus the southern sea level coherency with wind throughout the Pamlico Sound system during the summer, 1978 and winter, 1978 to 1979 periods is presented in Table 5. Also shown are the C^2 relationships between η and τ^x, τ^y at an open ocean coastal station.

Table 5 indicates that during the summer, the along-axis wind component, τ^y, i.e. the northeast-southwest wind, essentially controls the sea level fluctuations in the Pamlico Sound system. The summertime fluctuations have periods dominated by 2- to 30-day fluctuations. In the cross-axial direction the τ^x wind component is able to drive a weak response in sea level at periods of 2 to 10 days. The reason for this is that the wind motion is organized axially and the coherent response of sea level is to the organized, rectilinear motion of the windfield which happens to be aligned with the axis of the sound.

During the winter, the southern basin and the northern end of the northern basin both display a high coherency with the axial component of the wind over periods of 2 to 30 days. However the northern basin itself and the soundside of the barrier islands, including the inlets, respond to the axial wind very weakly and only at periods of 3 to 4 days. Alternatively, both the northern and southern basins and the central region, including the soundside of the barrier islands and the inlets, show a sea level response which is energetically tuned to the cross-axial wind component. At the northernmost periphery of the north basin, the η reponse occurs between 2 and 11 days and then again at periods of 3 weeks and longer. On the mainland side of the west wall, η responds to τ^x at 3-to 7-day periods and for periods greater than 4 weeks. On the soundside of the barrier islands, the response of η to τ^x occurs within 2 days to 2 weeks, and in the inlets the response is 2 to 5 days and greater than 2 weeks. In the southern basin η and τ^x correlate well from 2 to 11 days and greater than 3 weeks. Albeit, in the southernmost reaches of the south basin the good correlation between η and τ^x occurs at 3 to 6 days and 10 to 15 days.

The reason that η responds to both τ^x and τ^y during the winter is that τ^x and τ^y are organized jointly during this time of year. The wind field is elliptically polarized, i.e. the wind field particle motion moves about an ellipse which is oriented north-south and east-west on its major and minor axes. Moreover, the wind ellipse is stable. Why the various η's relate to τ^x and or τ^y as they do is not known at this time. Any study of transport pathways into and across Pamlico Sound will have to deal with this issue since η, η_x and η_y are coupled to the direct response of the flow field to the wind field. Additionally the surface elevation slopes set up interior and bottom currents which affect coupled transport pathways having different periods of existence.

In Figure 52, the squared coherency and phase relations between τ^x and τ^y and sea level slopes (differences) for the winter 1978-79 (December - February) period are shown. Here the sea level difference time series between Avon and Brant Island are cross correlated with the τ^x and τ^y wind components. The sea level differential, $\Delta\eta_{ABI} = \eta_A - \eta_{BI}$, follows τ^y by some 6 hr, 6 min, which is about twice the summer set up time. In the cross-axial direction we find that there is $\Delta\eta_{ABI}$ vs τx phase lag of 22.5 hours.

TABLE 5. High coherency between sea level and wind stress components as a function of fluctuation period

1978-1979 Winter	Minnesott Beach	Washington	Cedar Island	Brant Island	Ocracoke	Hatteras Inlet	Avon	Bomb Tower	Englehard	Stumpy Point	Manteo Harbor
(τ^x)	2-4.5 11		3.1-5.5 7.1 10.5-14.7			2-5.1 15.7-30	2.7-4.0 5.2-15		2.9-6.9 27+		2-11 20-30
(τ^y)	2-30		2-7 7.2-30			marginal at 3.3	marginal at 3.3		2.9-4.0		2-11 20-30
1978 Summer											
(τ^x)	marginal 4.9 10	none	marginal 3.6-10	marginal 3.6-10	marginal 6.9-10	very marginal 6.9-10	marginal ^{2} 4.6-6.7		marginal	marginal 5.5 11	2.2 4.5-6
(τ^y)	2-30	2.2-2.5 4.4 10.5-30	2-30	2-30	2.7-30	2.4-30	2-30	2-13.8		2.4-6.9	2-2.6 2.9-4 4.7-30

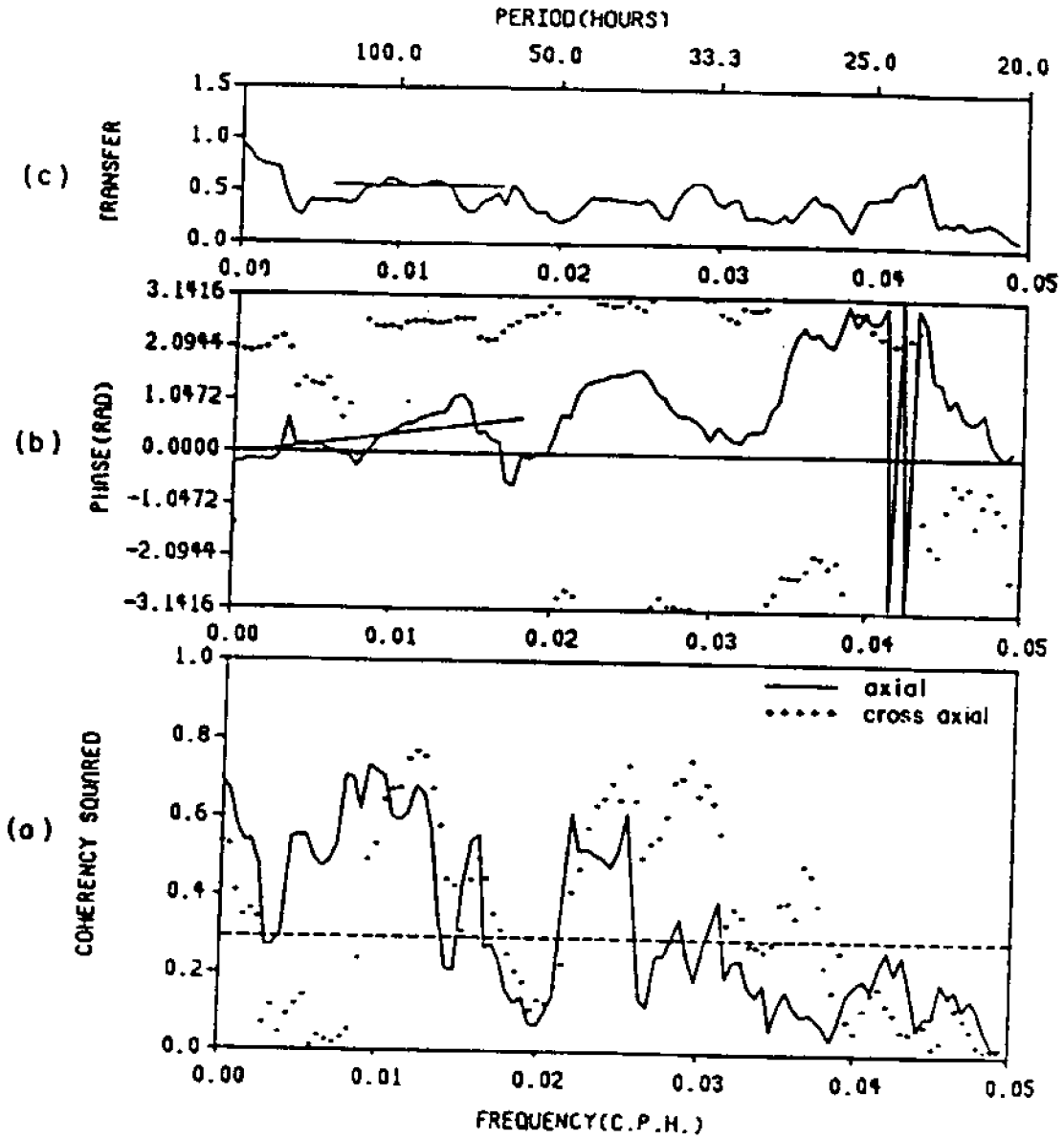

Figure 52. (a) Coherency squared, (b) cross-phase and (c) transfer function amplitudes between axial cross-axial wind stress components and the Avon minus Brant Island sea level differences during the North Caroina State University 1978/79 winter study.

8. Percent of Sea Level Slope Due to Wind Stress

In Sections II-6 and 7, it was shown that η and $\Delta\eta$ both are correlated with τ^x and τ^y; however we have not proved that the relationships are cause and effect. We now estimate the portion of sea level slope variance accounted for by the wind stress by conducting a multiple coherence analysis. In Figure 53, three types of coherences for both the winter and summer data sets are presented. The partial coherence squared between the axial wind stress component and the sea level slope during the summer, 1978 and winter, 1978 to 1979 sampling periods is shown by curves I, in Figures 53 a,b, respectively. Curves II, in Figures 53 a,b indicate the partial coherencies squared between sea level slope and the cross-axial wind component τ^x. Curves III, show the multiple coherencies squared between the scalevel slope and the total wind stress. While the partial coherencies yield the percentage, or fraction normalized to one, of the sea level slope variance caused by either of the wind stress components separately, the multiple coherence includes the causal effect on sea level slope of both wind stress components.

From Figure 53a, curves I and II, we see that at the diurnal period there is strong coherency between sea level slope and both τ^x and τ^y. However, for periods longer than a day, the axial wind stress component accounts for almost all of the subinertial frequency sea level slope fluctuations, reaching a value of 95 percent at the 5.6-day period. The cross-axial wind component is well below the 90 percent significance, or null hypothesis, level. Since only axial water surface slopes were computed in section 7, we conclude that not only does η not respond well to τ^x during the summer, but axial slopes are set up by axial winds. In general, τ^y accounts for 80 to 95 percent of the axial sea level slope variances, for periods greater than 1.7 days.

The winter data set provides very different results in that both τ^x and τ^y account for surface slope variance. In this case, based on the discussion in section I-8, both axial and cross-axial water level slopes were correlated with the τ^x and τ^y wind components, as well as their sum. Here η responds to both τ^x and τ^y, and $\frac{\Delta\eta}{\Delta x}$ is found to respond to τ^x while $\frac{\Delta\eta}{\Delta y}$ is found to respond to τ^y. Moreover, τ^x is found to be always as significant and sometimes more significant than τ^y in affecting surface slope. For periods greater than 2.6 days, $\tau^x + \tau^y$ account for 75 to 95 percent of the surface slope variance. Missing at this time of year is the causal effect of the sea breeze in setting up sea level slope. At subdiurnal frequencies, where the important meteorological action occurs (cf. Figure 46), the water surface slope is setting up in the direction that the wind stress acts.

9. Numerical Model Formulation

In this section we describe the assumptions of the numerical model used to predict both sea level and circulation in Pamlico Sound. From the sea level, current, temperature, salinity and atmospheric wind data presented in previous sections, it is evident that subinertial frequency parameter components comprise the substantial fraction of the energy spectrum. Moreover, these parameter constituents are dominated by highly time-dependent fluctuations of periods 10 hours to 10 days, so we take our model to be time dependent.

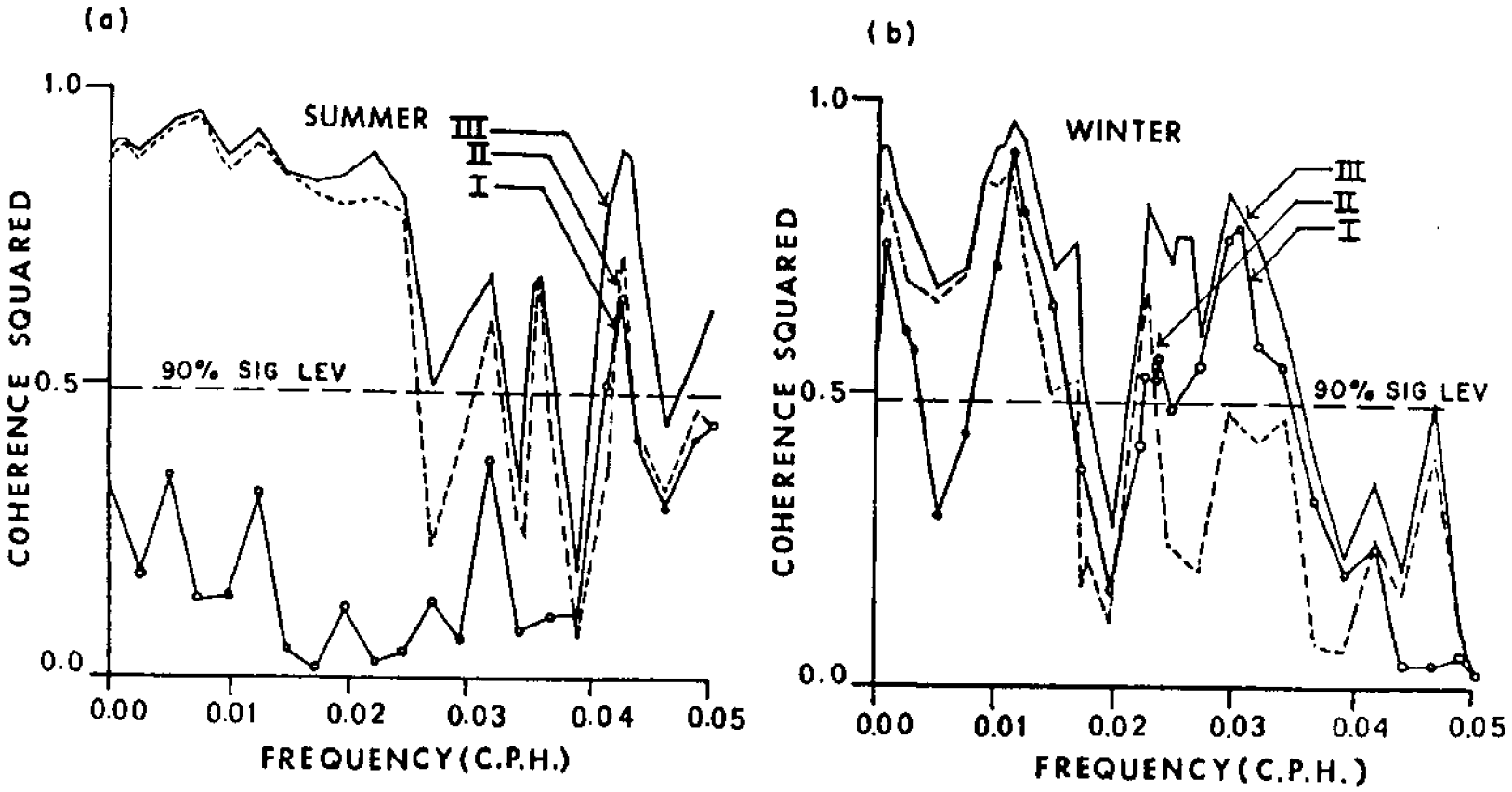

Figure 53. Multiple coherence squated between:
(I) Cross-axial wind stress component and sea level slope;
(II) Axial wind stress component and sea level slope;
(III) Between total wind stress vector and sea level slope during North Carolina State University 1978 summer and 1978/79 winter studies.

Next, both the wind field and the density field are taken to be uniform. Spatial gradients in the synoptic scale wind field can be small over distances the size of Pamlico Sound (Weisberg and Pietrafesa, 1983), so we assume the wind to be variable in time only. However, as we showed previously in Figure 27, coastal winds are typically larger than mainland winds so this assumption has obvious deficiencies. In fact, in Sections II-2,4,5,6,7 and 8, the CH and NB wind data were averaged with each other in the spectral analyses. Since the sound is everywhere shallow (mean depth of ~4.5 m) relative to wind-induced mixed layer thicknesses (Kraus, 1972) and because the ratio of the baroclinic to barotropic pressure gradient is small, a homogeneous model is acceptible. This pressure ratio can be written as $\Delta\rho H/\rho_o\eta$, where $\Delta\rho$ is the scale of density fluctuations, H is the mean depth, ρ_o is the mean density and η is the scale of sealevel fluctuations. For Pamlico Sound this ratio is of order 0.05 ($<<$ unity).

The model is taken to be linear as the ratio of sealevel fluctuations to mean depth is also of order 0.05.

Finally, the model is three-dimensional as opposed to vertically integrated. In the latter case the bottom stress is structured to oppose the mean motion throughout the water column. In reality, the bottom stress opposes the near-bottom motion, which is frequently in opposition or certainly at variance with the mean or vertically integrated motion. Hence, the bottom stress is incorrectly specified for wind-driven cases in vertically integrated models. The implications of this incorrect specification are numerous, so a more generic approach will be taken, as presented in Table 6. A comparison of the sea level elevations caused by a general wind stress are shown to be underpredicted by 33 percent in a vertically integrated model versus that predicted by a three-dimensional model (a 3DM). The obvious implication is that water level highs and lows around the coastline of the sound will be 33 percent higher and lower than what a vertically integrated model (a VIM) would predict. The actual current field will also be more energetic than that predicted by a VIM. An actual test case will be presented in the Results section which will compare the actual sea level change which was observed during the passage of Hurricane Donna (1960) versus those changes predicted by both a VIM (Amein and Airan, 1976) versus our 3DM.

At this juncture, model inadequacies or deficiencies worthy of further mention include our prior assumptions of spatial homogeneity of the wind field and neglect of nonlinear effects. Residents of the area and frequent visitors to Pamlico Sound know that small scale meteorological events can dominate the weather on any given day, and the wind stress field across the sound can vary considerably (cf. Figure 27). However, there is insufficient data to construct a two-dimensional spatially varying wind field. We thus adopt a spatially uniform wind. The ramifications of this are that since the sound responds to the actual wind field, model simulations will only be accurate during periods when the wind is, in reality, uniform.

Both linear and nonlinear effects in the momentum or circulation field can be invoked via variable topography. However, the bathymetry of the sound will be treated as monotonically varying as depicted in Figures 54 and 55. While it is appreciated that localized funneling and redirection of currents can occur due to small-scale nuances in the topography, the model bottom will be assumed to change with long wave- length undulations. A comparison of the model versus the actual topography can be made by comparing Figures 1, 2 and 3

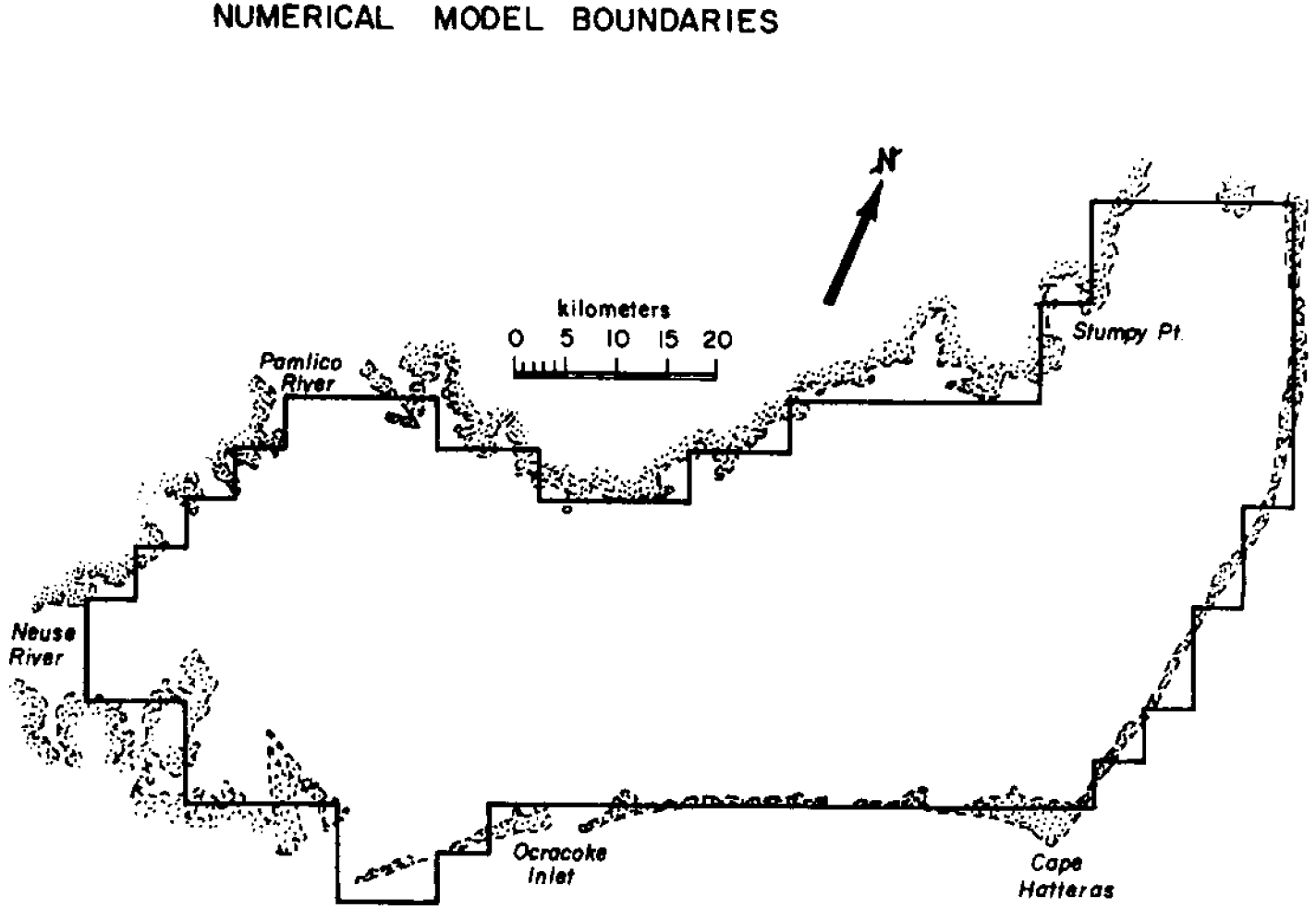

Figure 54. See text for figure discussion.

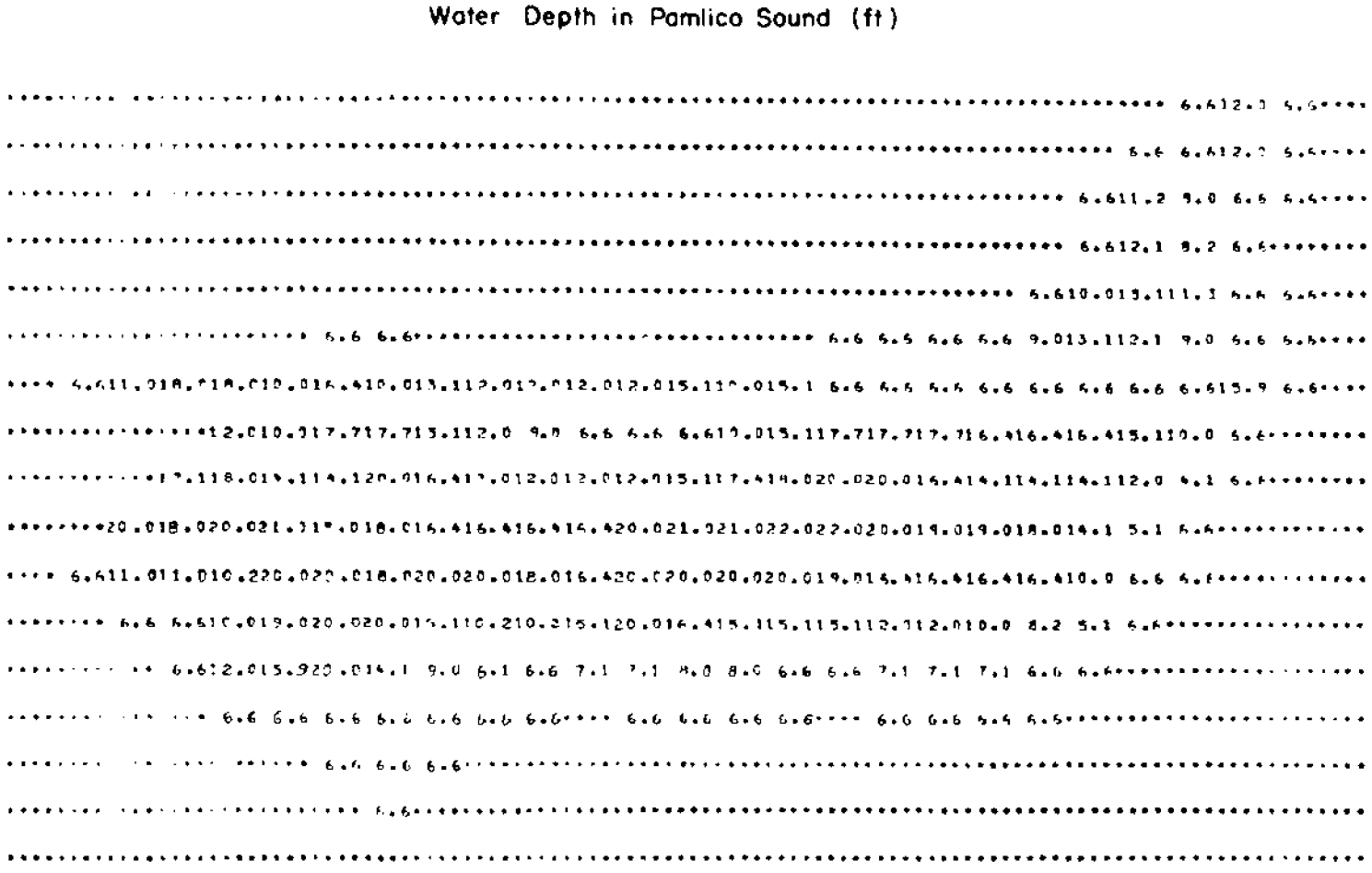

Figure 55. See text for figure discussion.

TABLE 6 Comparison, in steady state, or vertically integrated (VIM) and three dimensional (3DM) models

COMPARISON, IN STEADY STATE, OR VERTICALLY INTEGRATED (V.1) AND 3-D MODELS.

EQUATIONS: $0 = -gH\nabla\zeta + \underset{\sim}{\tau}_w - \underset{\sim}{\tau}_B$

$$\nabla \cdot \underset{\sim}{M} = 0$$

V.1. $\underset{\sim}{\tau}_B = K\underset{\sim}{M}$

3-D $\underset{\sim}{\tau}_B = 3A\underset{\sim}{M}/H^2 - \underset{\sim}{\tau}_w/2$

FOR CONSTANT DEPTH, $\underset{\sim}{M} = 0$

THEREFORE: $\nabla\zeta_{V.1} = \underset{\sim}{\tau}_w/gH$

HENCE: V.1. MODEL UNDERPREDICTS ζ BY 33% COMPARED TO 3-D MODEL

to 54 and 55.

Turbulent eddy momentum stresses are modeled using a spatially and temporally uniform eddy viscosity coefficient. For a homogeneous model, this assumption is adequate.

The Coriolis acceleration terms are retained in the model. However, as the Ekman number for Pamlico Sound is of order unity, the Coriolis effect will have only a slight influence on causing veering in the current field.

The equations which govern the flow in the sound in a right-handed Cartesian coordinate frame, with +x cross-Sound towards the coast, +y along-Sound toward the northeast, and z positive up, all rotating at $f_o/2$, are:

$$\frac{\partial \underset{\sim}{v}'}{\partial t'} + f_o \underset{\sim}{e}_z \times \underset{\sim}{v}' = -g\nabla'\eta' + A \frac{\partial^2 \underset{\sim}{v}'}{\partial z'^2} \tag{1}$$

and $$\frac{\partial M'x}{\partial x'} + \frac{\partial M'y}{\partial y'} + \frac{\partial \eta'}{\partial t'} = 0, \tag{2}$$

with $$M'x = \int_{-h'}^{\eta} u'dz' \quad , \quad M'y, = \int_{-h'}^{\eta} , v'dz' \ . \tag{3}$$

Here $\underset{\sim}{v}'$ is the horizontal velocity vector, η' the free surface elevation, h' the local depth, f_o the Coriolis parameter, A the constant eddy viscosity coefficient and M'x, M'y the volume flux vector components in the x and y, horizontal, directions, respectively.

The boundary conditions which drive the model are as follows:

$$\text{at the surface, } z = 0, \quad A \frac{\partial \underset{\sim}{v}'}{\partial z'} = \underset{\sim}{\tau}' s/\rho \tag{4}$$

where τ'_s is the effective surface wind stress, and at the bottom,

$$z' = -h' \text{ either} \quad (a) \ \underset{\sim}{v}' = 0$$

$$\text{or} \qquad (b) \ A \frac{\partial \underset{\sim}{v}'}{\partial z} \alpha \ \underset{\sim}{v}'b \tag{5}$$

where α is a bottom drag coefficient (cm/sec) and $\underset{\sim}{v}'b$ is the 'bottom' velocity vector (within several centimeters of the actual physical bottom). Additionally, at the lateral boundaries, $\underset{\sim}{M}' \cdot \underset{\sim}{n} = 0$, where $\underset{\sim}{n}$ is a horizontal vector normal to the boundaries; except at the inlets and river junctions where a normal flux proportional to $|\eta'|$ 1/2 is taken. The model equations, inputs and outputs are summarized in Table 7.

To more clearly demonstrate the physics, we nondimensionalize both the dependent and independent variables. Let $(x,y) = (x',y')/L$, $\sigma = z/h'(x,y)$, $h = h'/h_r$, $t = t'(h_r^2/A)$, $(u,v) = (u',v')/h_r\tau_t/\rho_o A)$, $\eta = \eta'/(\tau_r L/gh_r)$, $\tau = \tau'/\tau_r$, $c = A^2L^2/dh_r^5 = T_w^2/T_D^2$ and $E = fo\ hr^2/A$. Here L is a horizontal length scale for the basin, h_r a reference depth, and τ_r a reference wind stress. The parameter c is the square of the ratio of the time of propagation of a surface gravity wave across the basin, T_w, to a turbulent diffusion time scale, T_D. The dimensionless equations are then:

$$\frac{\partial \underset{\sim}{\chi}}{\partial t} + E\, \underset{\sim}{e}_z \times \underset{\sim}{\chi} = -\nabla\eta + \frac{1}{h^2}\,\frac{\partial^2 \underset{\sim}{\chi}}{\partial z^2} \tag{6}$$

$$\frac{\partial m_x}{\partial x} + \frac{\partial m_y}{\partial y} + c\,\frac{\partial \eta}{\partial t} = 0\ , \quad \underset{\sim}{m} = h \int_{-1}^{0} \underset{\sim}{\chi}\, d\sigma, \tag{7}$$

$$\frac{\partial \underset{\sim}{\chi}}{\partial z}\Big|_{\sigma=0} = \underset{\sim}{\tau}\ , \quad \underset{\sim}{\chi}\Big|_{\sigma=-1} = 0 \quad \text{or} \quad A\,\frac{\partial \underset{\sim}{\chi}}{\partial z}\Big| = C_D \underset{\sim}{\chi}\Big| \tag{8}$$

and $\underset{\sim}{m} \cdot \underset{\sim}{n} = 0$ (9)

around the periphery. The method of solution of this system is now described.

We are given $\underset{\sim}{\tau}(x,y,z = 0,t)$. A horizontal rectangular grid with points spaced Δ_H apart in the horizontal and $\Delta\sigma$ apart in the vertical is set up with

TABLE 7 3DM Numerical model

INPUT: WIND STRESS AS A FUNCTION OF TIME, AND RIVER RUNOFF.

MODEL EQUATIONS:

$$\frac{\partial \underset{\sim}{v}}{\partial t} - f_o \underset{\sim}{K} \underset{\sim}{v} = -g \nabla \zeta + A_v \underset{\sim}{v}_{zz}$$

$$\nabla \cdot \underset{\sim}{M} = 0$$

$$\underset{\sim}{M} \cdot \underset{\sim}{n} = 0 \text{ (AT COAST)}$$

$$= R \text{ (AT RIVERS)}$$

$$= C\sqrt{\zeta} \text{ (AT INLETS)}$$

OUTPUT: $\underset{\sim}{v}$, $\underset{\sim}{M}$, ζ CALCULATED EVERY THREE MINUTES. SURFACE ELEVATION, ζ, PRINTED EVERY THIRTY MINUTES.

$$\underset{\sim}{v}(x,y,\sigma,t) = \underset{\sim}{v}(i\Delta_H,\ j\Delta_H,\ \frac{N+1-k}{k}\Delta\ ,n\Delta t) \tag{10}$$

$$= \underset{\sim}{v}_{i,j,k}$$

and

$$\eta(x,y,t) = \eta(i\Delta_H,\ j\Delta_H,\ n\Delta\tau) = \eta^n_{i,j} \tag{11}$$

Note that when k = 1 and $\sigma = -1$, we take $\underset{\sim}{v}^n_{i,j,1} = 0$ to satisfy the boundary condition at $\sigma = -1$. When k = N+1, $\sigma = 0$. The boundary condition at the top is given by $\underset{\sim}{v}^n_{i,j,N+2} - \underset{\sim}{v}^n_{i,j,N} = 2\Delta\sigma\ \underset{\sim}{\tau}$. Let us be given $\underset{\sim}{v}$ and η at $t = n\Delta t$. To find v^{n+1} and η^{n+1}, we first write the horizontal momentum equation in implicit finite difference form, i.e.

$$\frac{u^{n+1}_{i\cdot j\cdot} - u^n_{i\cdot j\cdot k}}{\Delta t} - \varepsilon v^n_{i,j,k} = \frac{1}{2\Delta_H}(\eta^n_{i+1,j} - \eta^n_{i-1,j}) \tag{12}$$

$$+ \frac{1}{h^2\Delta\sigma^2}(u^{n+1}_{i,j,k+1} + u^{n+1}_{i,j,k-1} - 2u^{n+1}_{i,j,k})$$

For k = 2,...,N+1

$$\frac{v^{n+1}_{i,j,k} - v^n_{i,j,k}}{\Delta t} + \varepsilon u^n_{i,j,k} \tag{13}$$

$$= \frac{1}{l\Delta_H}(\eta^n_{i,j+1} - \eta^n_{i,j-1}) + \frac{1}{\eta^2\Delta^2_\sigma}(v^{n+1}_{i,j,k+1} + v^{n+1}_{i,j,k-1} - 2\ v^{n+1}_{i,j,k})$$

with $$\underset{\sim}{v}^{n+1}_{i,j,1} = 0 \tag{14}$$

$$\underset{\sim}{v}^{n+1}_{i,j,N+2} = \underset{\sim}{v}^{n+1}_{i,j,N} + 2\ \Delta_\sigma \underset{\sim}{\tau}^n$$

These algebraic equations may be solved for $\underset{\sim}{v}^{n+1}$ by Gaussian elimination. We can then compute $\underset{\sim}{M}^{n+1}$ and finally, using

$$\eta_{ij}^{n+1} = \eta_{ij}^{n} - \Delta t\left(\frac{\nabla\cdot M^{n+1}}{c}\right) , \qquad (15)$$

we can find the sea surface elevation at the new time step.

We note that $\underset{\sim}{v}^{n+1} = {}_1\underset{\sim}{v}^{n+1} + {}_2\underset{\sim}{v}^{n+1}$, where ${}_1\underset{\sim}{v}^{n+1}$ depends on v^n and τ^n and ${}_2\underset{\sim}{v}^{n+1}$ depends on $\nabla\eta^n$. At lateral boundaries, where $\underset{\sim}{M}\cdot\underset{\sim}{n} = 0$, the term $\underset{\sim}{n}\cdot\nabla\eta$ is taken to satisfy this condition. For example, at points on the boundary where the boundary is parallel to the y-axis (the southwest to northeast-lying, major axis of Pamlico Sound), the x-momentum equation is first solved with the surface slope term suppressed to obtain ${}_1\underset{\sim}{v}^{n+1}$. Then we obtain

$$\frac{2\tilde{U}_{2i,j,k}^{n+1}}{\Delta t} = \frac{1}{h^2\Delta^2\sigma}\left(2\tilde{U}_{2i,j,k+1}^{n+1} + {}_2\tilde{U}_{1i,j,k-1}^{n+1} - 2{}_2\tilde{U}_{1i,j,k-1} - {}_2\tilde{U}_{2i,j,k+1}\right) + 1$$

and let 2un+1 = c2un+1. Thus Mn+1 = 1Mn+1 + C2Mn+1, and for Mn+1 = 0, we choose C = -Mx1/2mx.

At the coast, to determine a value of η^{n+1}, we need $\nabla\cdot\underset{\sim}{M}^{n+1}$, and this is not totally known. For example, if the boundary is parallel to the y-axis at I,J with water at $x > I\Delta_H$, we need a value for $\frac{\partial M_x^{n+1}}{\partial x}$ I,J. To obtain this we write,

$$M_x(x,y_J)^{n+1} = \alpha(x-x_I) + B(x-x_I)^2$$

as, $Mx(x_I,y_I) = 0$. Then (18)

$$Mx_{I+1,J} = a\Delta H + B\,\Delta_H^2$$

$$Mx_{I+2,J} = \alpha(2\Delta_H) + 4(B\,\Delta_H)^2$$

and

$$\alpha = \frac{\partial M_x}{\partial x}\,I,J = (4Mx_{I+1,J} - Mx_{I+2,J})^{n+1}/2\Delta_H. \qquad (19)$$

The values for $Mx_{I+1,J}$, $Mx_{I+2,J}$, the interior points, are known and we know α, or equivalently, since

$$\frac{\partial M_x}{\partial x} = \frac{Mx_{I+1,J} - Mx_{I-1,J}}{2\Delta H} , \tag{20}$$

then

$$Mx_{I-1,J} = Mx_{I+2,J} - 3\, Mx_{I+1,J} . \tag{21}$$

So, in summary, the model equations are solved numerically by first replacing z' with $\sigma = z'/h'$. The resulting equations are nondimensionalized and then written in finite difference form. Central differences are used for spatial derivations and forward differences for the temporal derivations.

In the horizontal momentum equations, the Coriolis and pressure gradient terms are evaluated at the present time step, the frictional terms at the next time step and the temporal derivative contains the next as well as the present time step values, i.e. the equations are in implicit form. The new velocites at N+1 levels in the vertical are then obtained by Guassian elimination at each horizontal grid point. Updated values of M' are obtained by vertically integrating the updated velocities. The updated values of M' are used in the vertically integrated continuity equations to update the sea level, and the entire process begins anew. All dependent variables are initialized to zero. At the coast, the normal gradient of sea level is adjusted to ensure that the normal volume flux vanishes.

The dynamics of the present model are characterized by two dimensionless parameters. The Ekman number is of order unity for the sound. Numerical, experimental model-runs were made with and without the Coriolis terms to test the importance of these terms. The results indicate that sea level is relatively unaffected by these terms although the velocity field does show a small but noticeable effect. A second parameter, $C = (L/\sqrt{\lambda ghr})^2/(hr^2/A)^2$, is a measure of importance of the free surface effect and is the square of the ratio of gravity wave propagation time to vertical diffusion time. This parameter is of order one but does depend on the value of A, which we choose to be proportional to the square root of the magnitude of the average wind stress during any event.

The wind stress will be calculated using an assumed wind velocity (measured at 10 m above the surface in the real world) via the bulk aerodynamic formula

$$\tau = \rho_a C_D\, W|w| \tag{22}$$

where ρ_a is the air density and C_D is a drag coefficient assumed to be $2.6(10^{-3})$ in this study. Bunker (1976) provides a complete list of preferred C_D's.

10. Numerical Model Output

Numerical model results are now presented in a format which ultimately yields a conceptual picture of currents and water elevations throughout the sound. From the actual topographic map (Figure 3), numerical model boundaries (Figure 54) and numerical model bottom bathymetry (Figure 55) were created. Numerical model water velocity vector components are denoted by u, the

southeast ($u > 0$) and northwest ($u < 0$), and v, the northeast ($v > 0$) and southwest ($v < 0$) flow field designators. These are plotted out throughout the model sound (Figure 55) as per the examples presented in Figures 56a and b. The water level height, or sea level, numerical model results are also plotted out in the "model" sound as shown in Figure 57. From this depiction one can either connect equal elevation points to create constant surface height lines, as shown in Figures 58 and 59, or surface topography maps, as depicted in Figure 60. The water level topography depiction in Figures 58 and 59 is two-dimensional, while that in Figure 60 is three-dimensional.

For conceptual neatness we choose to represent the current fields by creating a velocity vector, $\bar{v}$, at a specified horizontal point in x and y (say x_o, y_o) for specified vertical elevations, say the surface of the water and at one meter above the bottom, so $\bar{v}_s = \bar{v}(x_o, y_o,$ z = surface) and $\bar{v}_b = \bar{v}(x_o, y_o,$ z = 1 meter above H at x_o, y_o).

Likewise, we choose the 2-D representation of water level topography (Figure 59) over the 3-D surface elevation map (Figure 60) because in the latter case, depressions or valleys in the surface may be hidden behind hills or mounds in the surface depending on the orientation of the model sound. The 2-D representation in Figure 59 is chosen over that shown in Figure 58 for reason of visual preference.

A time step of six minutes, which is well within the CFL criteria (Carnahan et al, 1969) is used in the computation. Each model run used 42 seconds of computer time on the Triangle Universities Computational Center (TUCC) computer.

An initial question concerns the rapidity with which the sound can "spin up" or fully respond to a wind which suddenly turns on at time zero and remains constant in both time and space, i.e. the wind is assumed to be a "causal function." Figures 61-63 indicate that within 5 to 7 hours of the onset of steady 3.38 dyne/cm^2 or 10m/sec winds either down axis from the northeast or cross axis from the southeast, that the circulation response in the sound is essentially established. All model test cases indicate that Pamlico Sound "spins up," i.e., reaches a quasi-steady state condition, in a period of less than 10 hours after the onset of nonhurricane-force, persistent, steady winds. Recent studies of the coastal meteorology in this region (Weisberg and Pietrafesa, 1983) indicate that while there are monthly to seasonal mean winds which generally repeat from year to year, the major portion of the wind variability occurs over time scales of 2 days to 2 weeks. Thus, while the sound is capable of responding to the wind in less than a half day, in general the dominant winds in this region blow sufficiently long for the sound's response to become fully established.

The next numerical experiment which we conduct is the comprehensive study referred to earlier.

We now compare actual field data to numerical model results. In Case III-1, our numerical model of Pamlico sound is subjected to actual hurricane forcing. We then compare the model results to both actual tide gage data collected during the passage of the hurricane and also to the results derived from the vertically averaged model of Amein and Airan (1976). In cases III-2

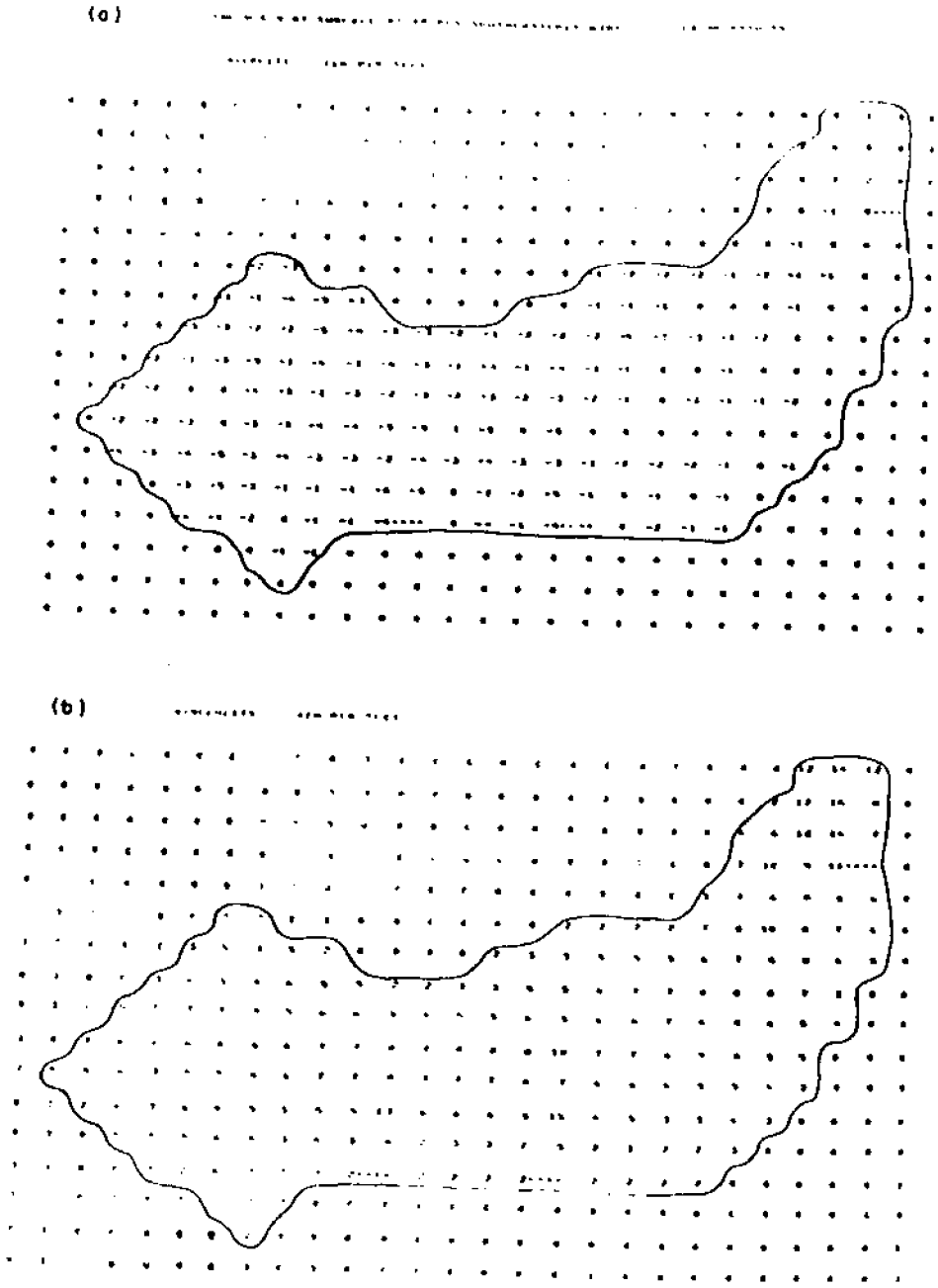

Figure 56. Numerical model results including:
a. Cross-sound component of surface current vector in cm/sec.
b. Along-sound axis component of surface current vector in cm/sec.

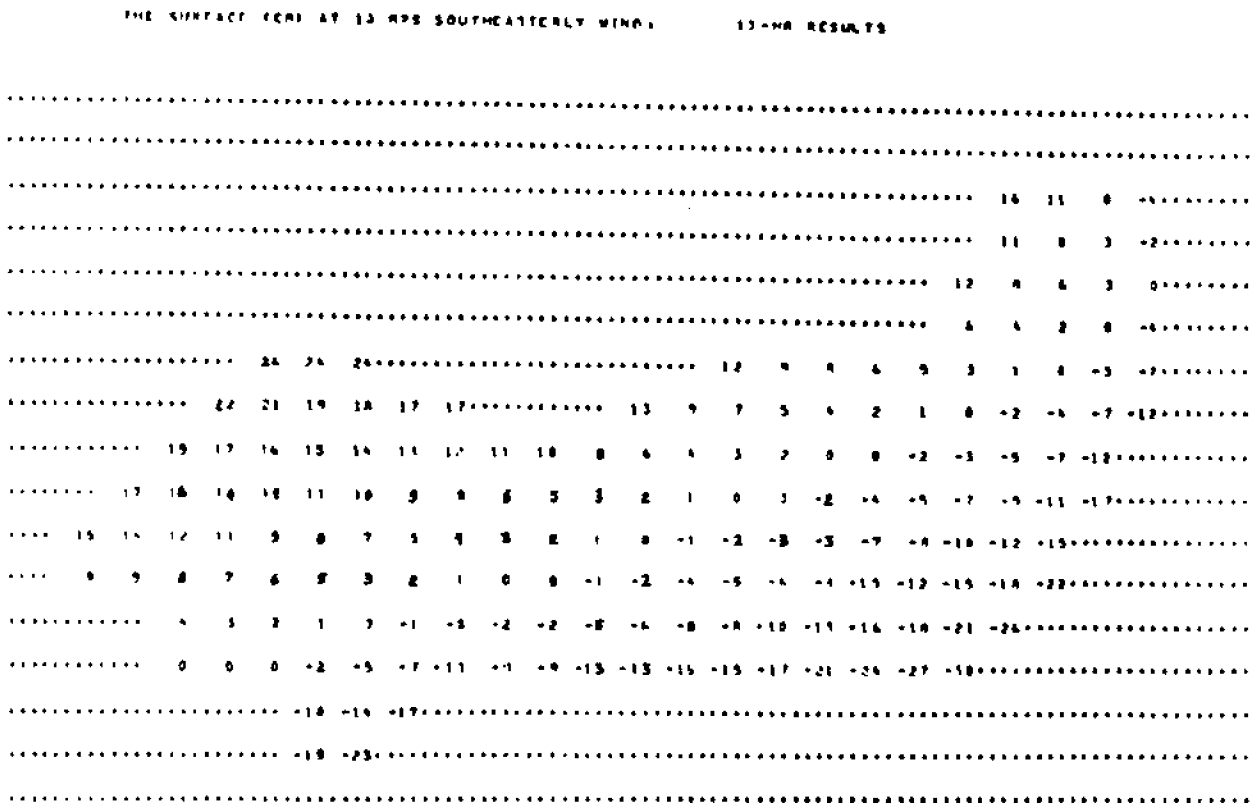

Figure 57. Numerical model results of seasurface elevation in Pamlico Sound 10 hours after the onset of a steady southeasterly (Northwestward) 10 m/sec wind. Heights are presented in centimeters above zero mean (+) and below zero mean (-).

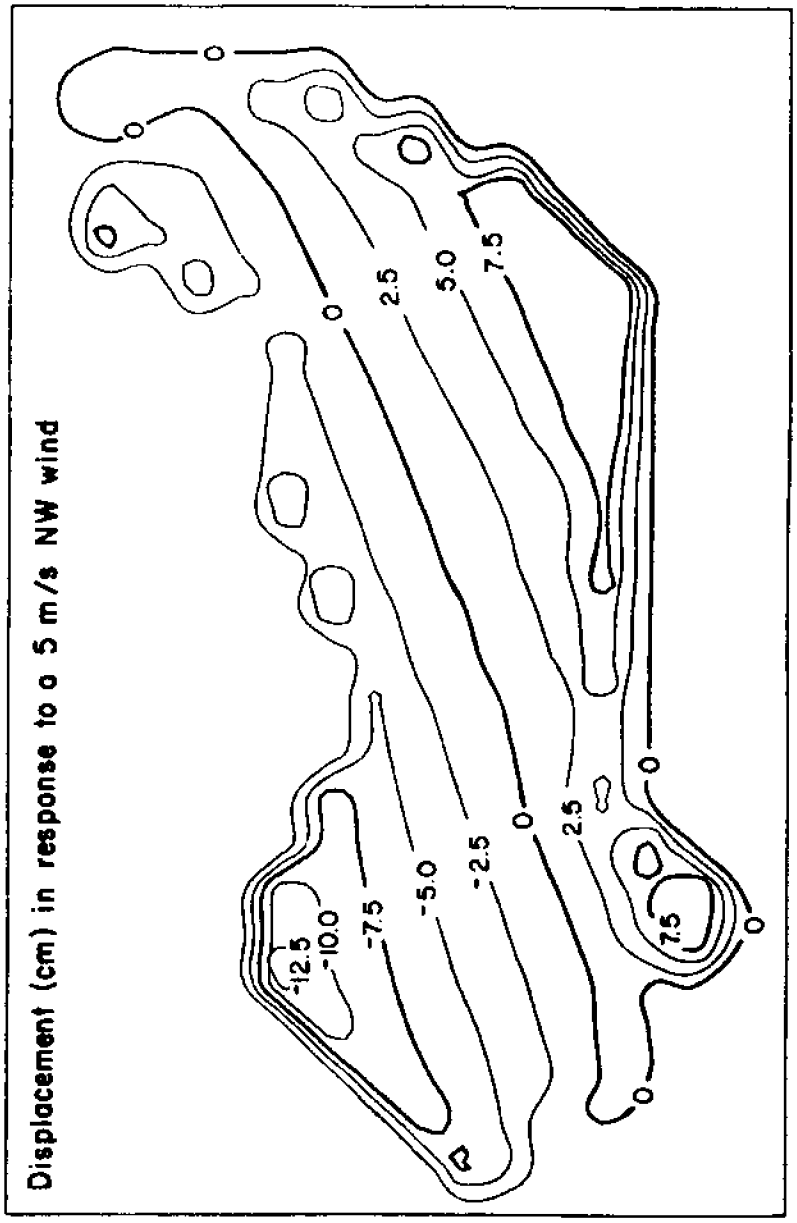

Figure 58. See text for figure discussion.

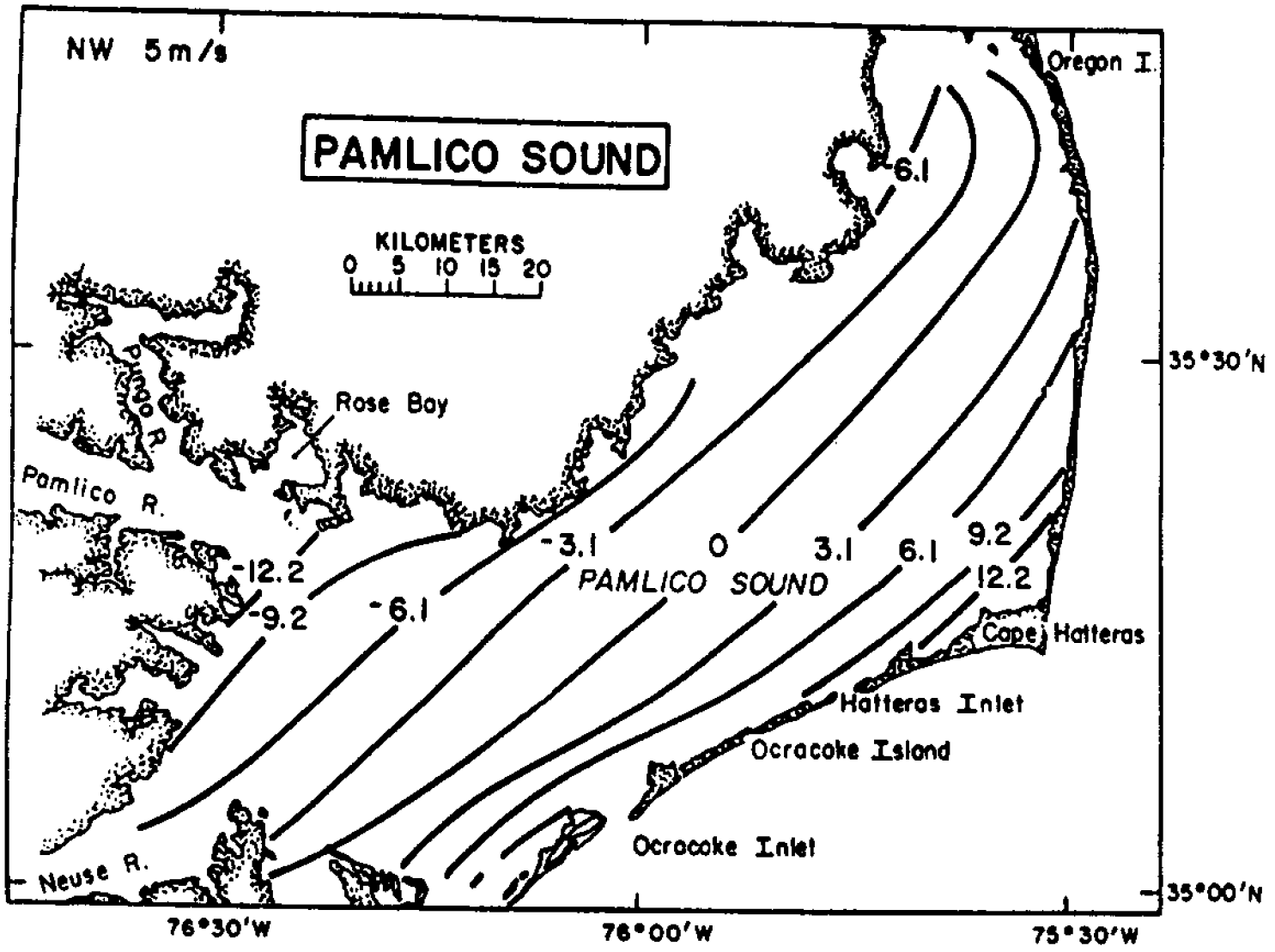

Figure 59. Model sea level distribution in sponse to a southeastward wind.

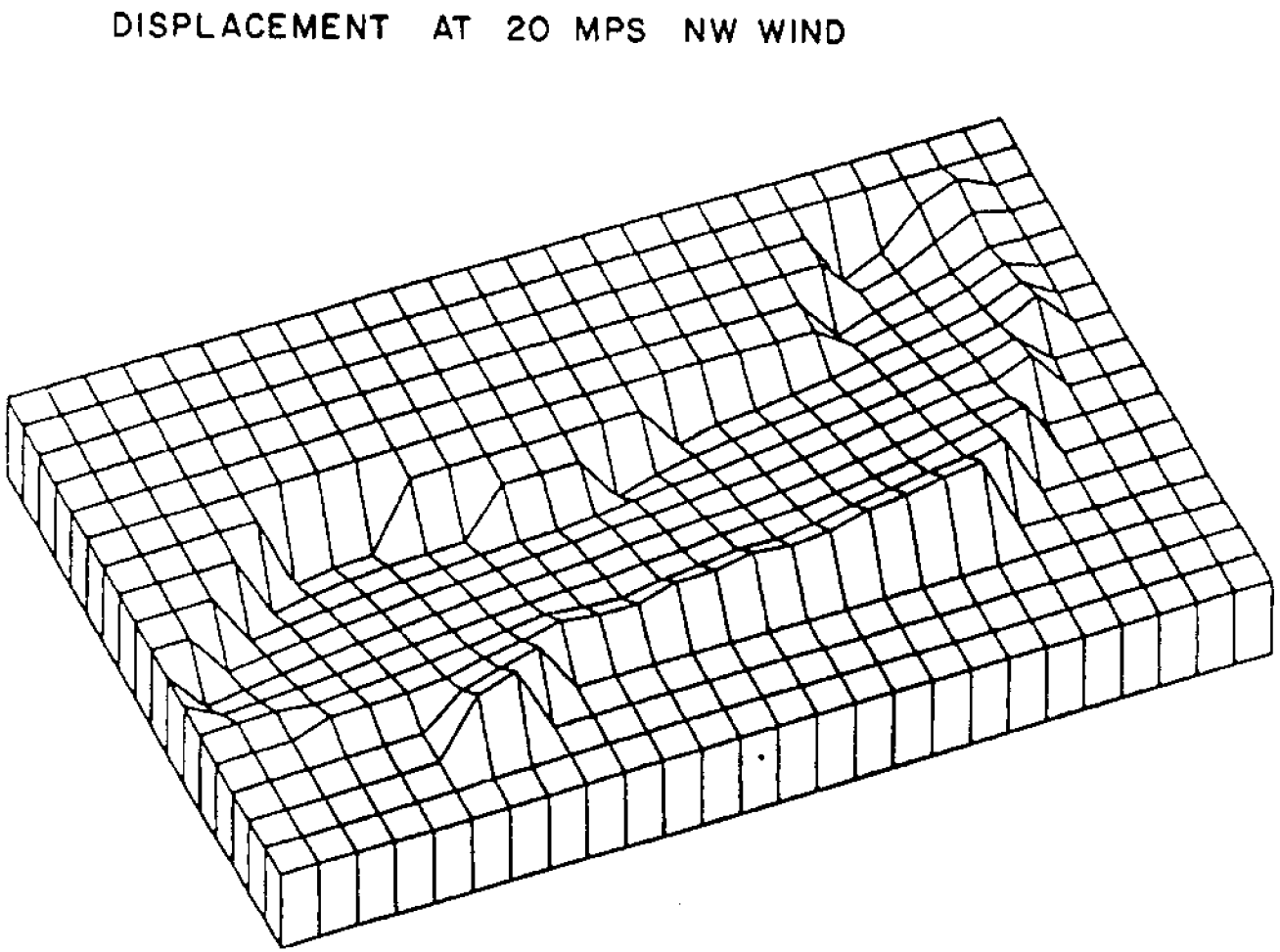

Figure 60. Model m/s sea level distribution in response to a 20 m/s wind.

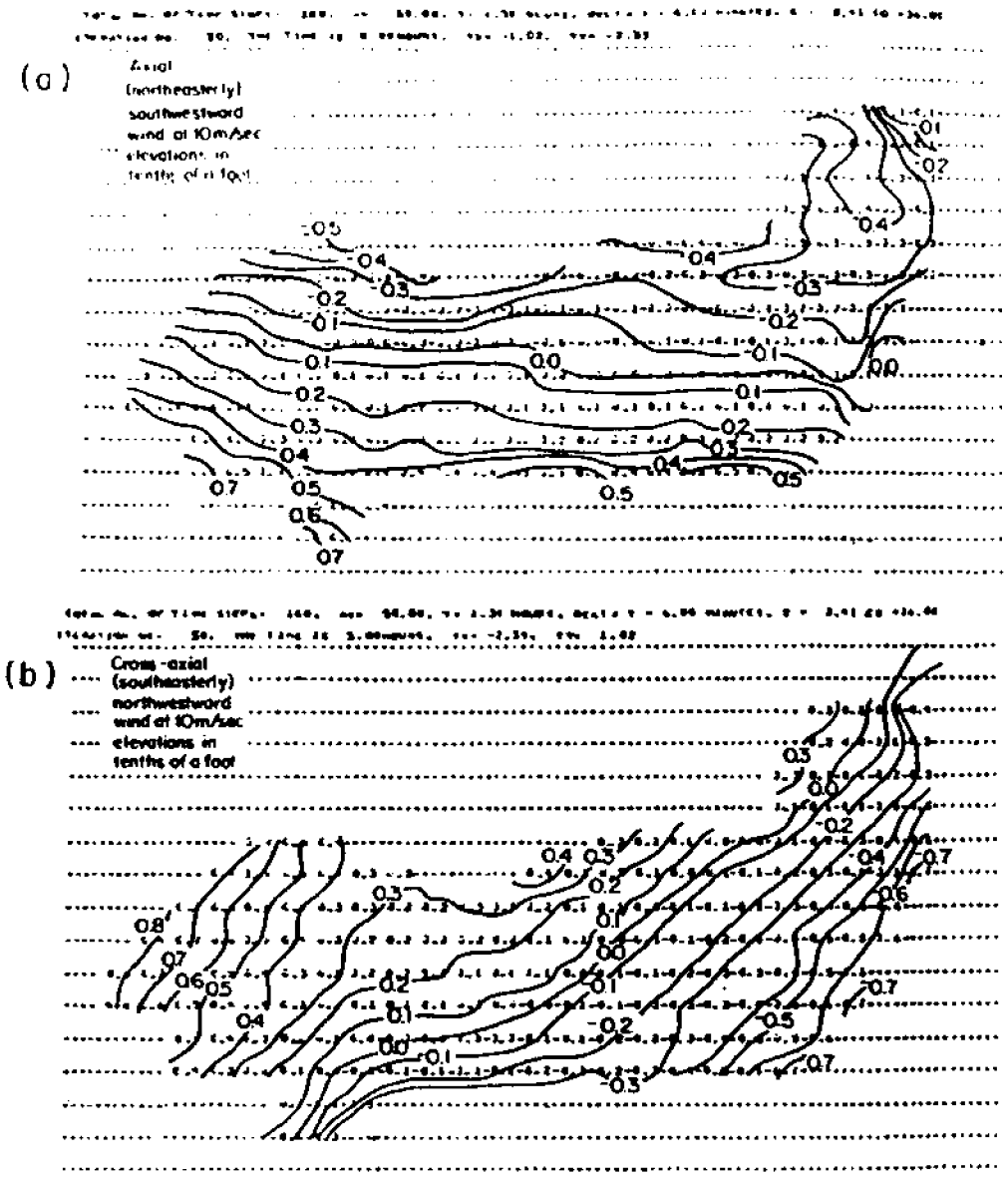

Figure 61. Model results of:
a. Axial (northeasterly) southwestward wind at 10 m/sec elevations in tenths of a foot.
b. Cross-axial (southeasterly) northwestward wind at 10 m/sec elevations in tenths of a foot.

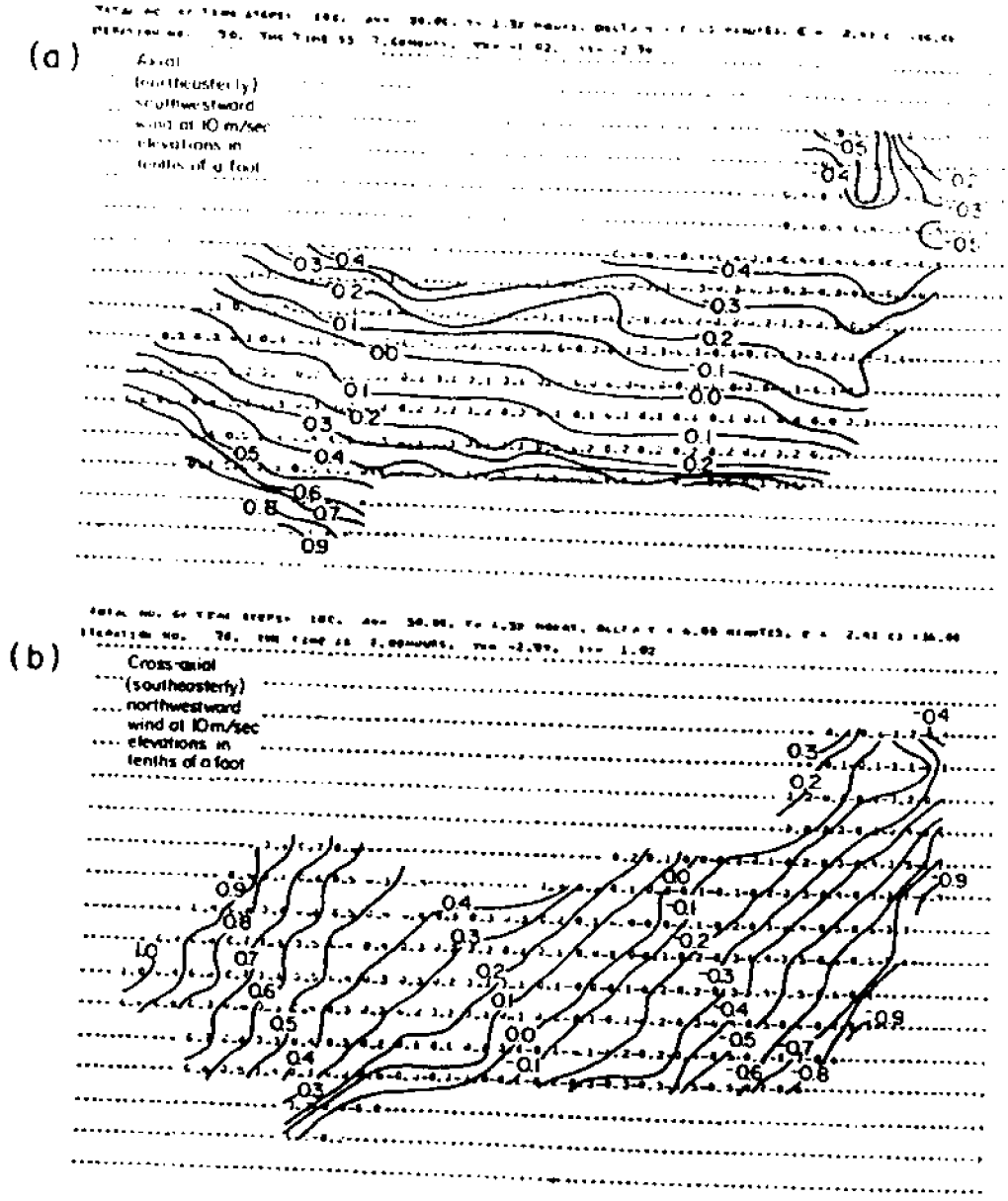

Figure 62. Model results of:
a. Axial (northeasterly) southwestward wind at 10 m/sec elevations in tenths of a foot.
b. Cross-axial (southeasterly) northwestward wind at 10 m/sec elevations in tenths of a foot.

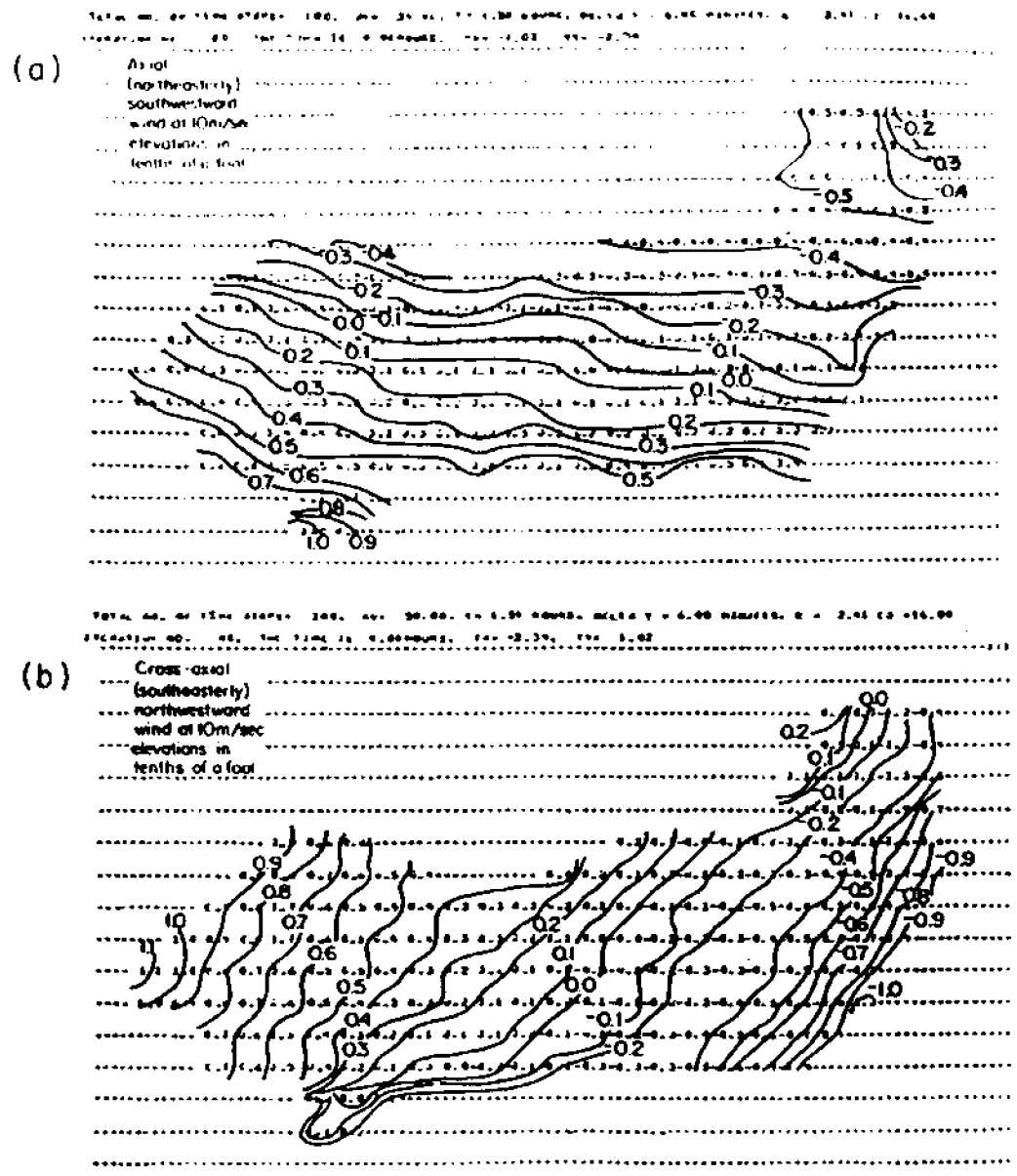

Figure 63. Model results of:
a. Axial (northeasterly) southwestward wind at 10 m/sec elevations in tenths of a foot.
b. Cross-axial (southeasterly) northwestward wind of 10 m/sec elevations in tenths of a foot.

and 3 we compare north and south basin data to 3D$\bar{M}$ results under similar wind forced conditions. Unfortunately, there are few $\bar{v}$ data sets which exist for inter-comparisons.

Section III. Results and Discussion

1. Sea level 3DM and VIM Model Predictions vs. Tide Gage Data During the Passage of Hurricane Donna: 11-12 September, 1960.

In the sections preceeding, it was demonstrated both in field observations and from numerical modeling results that larger wind stress creates larger sea level as well as sea level gradient fluctuations, or departures from the mean. Consequently, the largest water level fluctuations in Pamlico Sound should occur during the passage of hurricane which contain the highest sustained wind speed and stresses. Times of hurricane passage present periods of highest currents and waves, greatest land inundation and highest concentration of fluid flow energy which affects periods of maximum erosion. Figure 64 provides a selected summary of hurricane tracks over and about Pamlico Sound. While the frequency of occurrence of hurricane forcing in the vicinity of the sound is relatively low, the prospects of any tropical cyclone being damaging around the sound's periphery is very high, as indicated in Figure 64. To assess the potential for flooding from any individual tropical cyclone we now consider the response of sound waters to a specific hurricane.

During the period 23 August - 14 September, 1960, the tropical cyclone Donna wended its way northwest between Cuba and the Bahamas, turned north passing over the Florida Everglades and Daytona Beach, Fla., and then continued northeasterly passing over Pamlico Sound 11 to 13 September before it ventured out to the Mid-Atlantic Bight. Using actual National Weather Service winds collected during the passage of Donna, the wind stress time series between the period for 1700 hrs EDT on 11 September to 0900 hrs EDT, 12 September was constructed using the drag law $\vec{\tau} = \rho_a C_o \vec{W}|\vec{W}|$, as shown in Figure 65. In this depiction of the windstress vector, a stick directed upwards is a wind blowing towards the north while a stick directed to the right (along the time axis) is a wind blowing towards the east. The wind stress vector was about 5 dynes/cm^2 directed NW at 1700 hrs EDT on 11 September, increased in magnitude to 13 dynes/cm^2 some 7 hours later (at midnight) rotated clockwise, NNW, with a magnitude of 22 dynes/cm^2 in an additional 3 hour period (0300 hrs, 12 Sept) and then rotated clockwise to be directed eastward at 0500 hrs. The scenario of 3DM numerical model during water level response during the passage of Donna is depicted in Figures 66-68 for hours 1,5,10,12,13 and 14 after the onset of the hurricane. For visual comparison of model results to actual observations, Figures 69 a,b provide the U.S. Army Corps of Engineers (ACE, 1961) depiction of water level throughout the sound at 0200 and 0500 hours on 12 September (compare Figure 67a to 69a and Figure 68b to 69b).

The comparisons between 3DM model generated sea level elevation contours and the Army Corps contoured maps are excellent. Given the deficiencies of the 3DM results and the discrepancies which must exist in the ACE surface contour plot, the agreement is remarkable. Both the 3DM and the ACE contour plots indicate the incredibly fast response of sound waters to the mechanical forcing of Donna's wind field. Between 0200 and 0500 hours on 12 September, the windfield varies from being 20.5 dyne/cm^2 towards the north-northwest to bring 20 dynes/cm towards the east. At 0200 hrs observation and theory both indicate a rise of 4 ft of water at the mouth of the Pamlico River and a drop of 4 ft from mean behind (on the soundside of Hatteras Island). Within 3

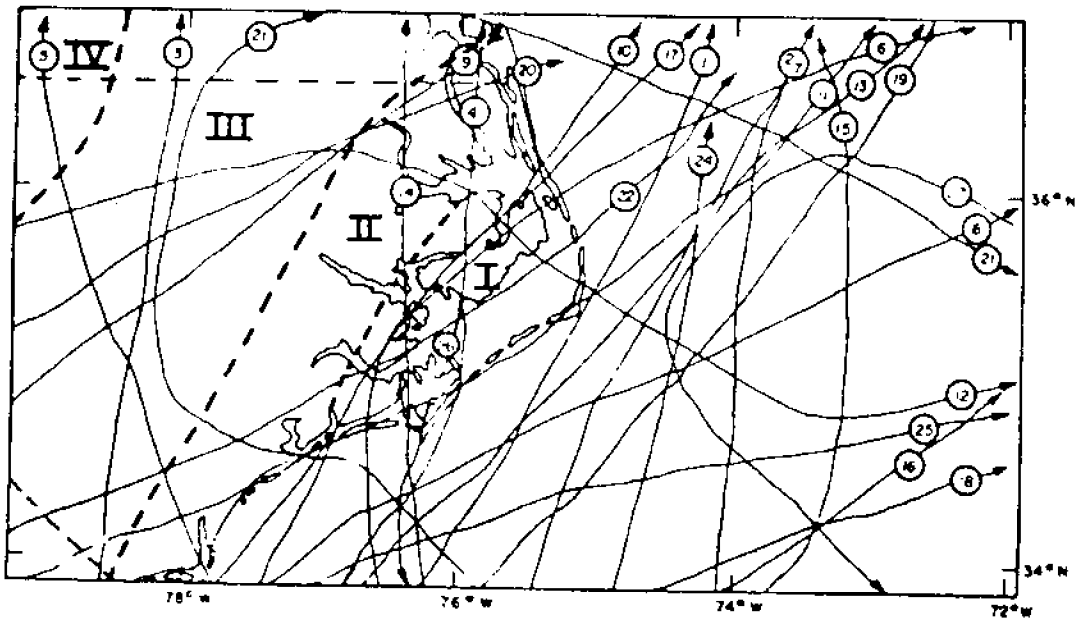

Tropical Cyclones

1.	Carol	08/25 - 09/01/54
2.	Edna	09/02 - 09/15/54
3.	Hazel	10/05 - 10/18/54
4.	Connie	08/03 - 08/15/55
5.	Diane	08/07 - 08/21/55
6.	Ione	09/10 - 09/24/55
7.	Daisy	08/24 - 08/31/58
8.	Helene	09/21 - 10/04/58
9.	Cindy	07/05 - 07/12/59
10.	Donna	08/29 - 09/14/60
11.	Alma	08/26 - 09/02/62
12.	Cleo	08/20 - 09/05/64
13.	Dora	08/28 - 09/16/64
14.	Isbell	10/08 - 10/17/64
15.	Alma	06/04 - 06/14/66
16.	Doria	09/08 - 09/21/67
17.	Abby	06/01 - 06/13/68
18.	Dolly	08/10 - 08/17/68
19.	Gerda	09/06 - 09/10/69
20.	Alma	05/17 - 05/27/70
21.	Ginger	09/06 - 10/05/71
22.	Agnes	06/14 - 06/23/72
23.	Dawn	09/05 - 09/14/72
24.	Belle	08/06 - 08/10/76
25.	Clara	09/05 - 09/12/77
26.	Bob	07/09 - 07/16/79

Numbers of Damaging Tropical Cyclones, 1901 - 1955

I.	21+	III.	11 - 15
II.	16 - 20	IV.	6 - 10

Figure 64. Selected tropical cyclones between 1954-1979 impacting the Pamlico Sound area. Arrows indicate direction of propogation of hurricane eye.

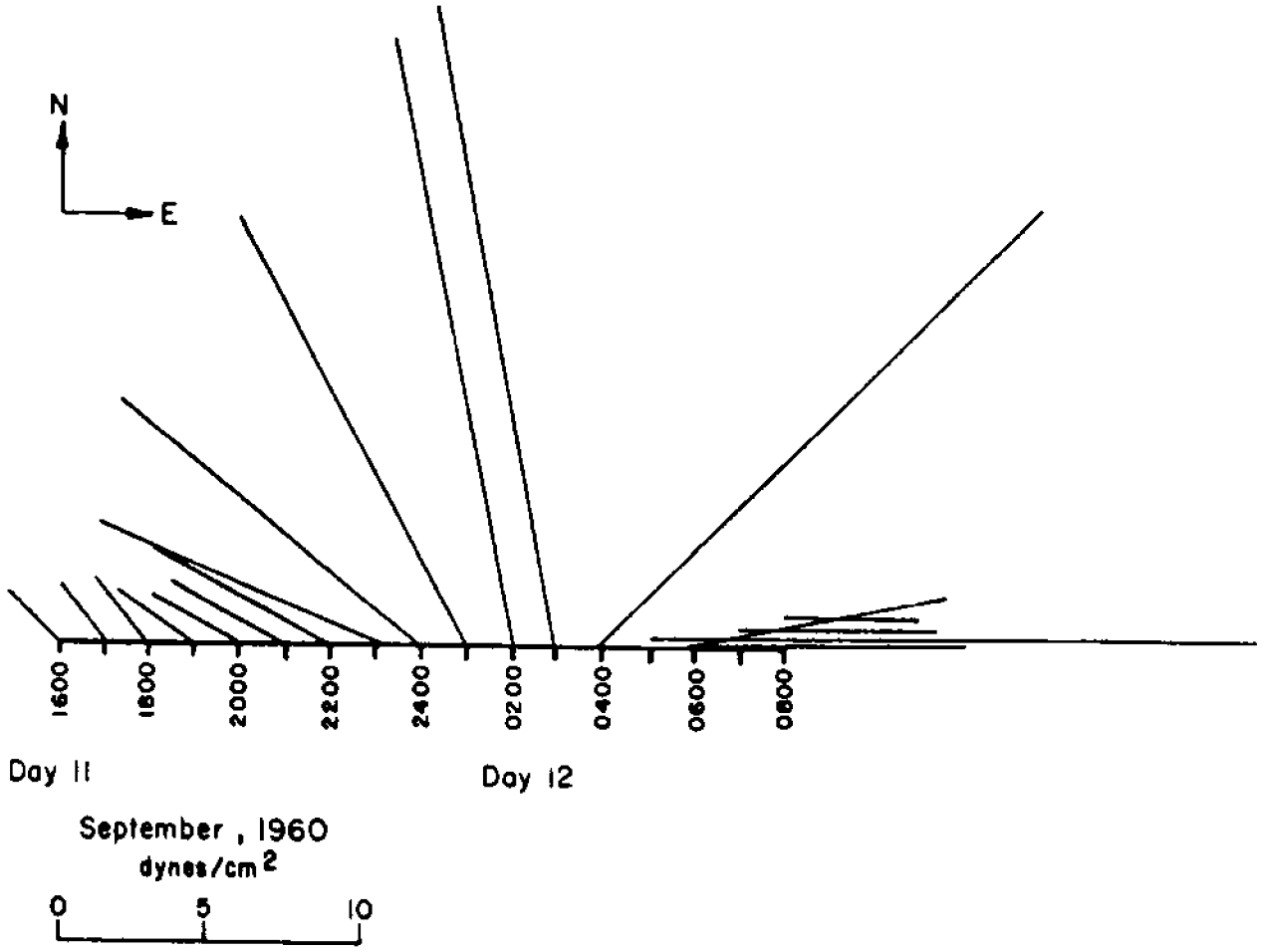

Figure 65. Wind stress vectors measured at Cape Hatteras and Cherry Point (and averaged) during passage of Hurricane Donna.

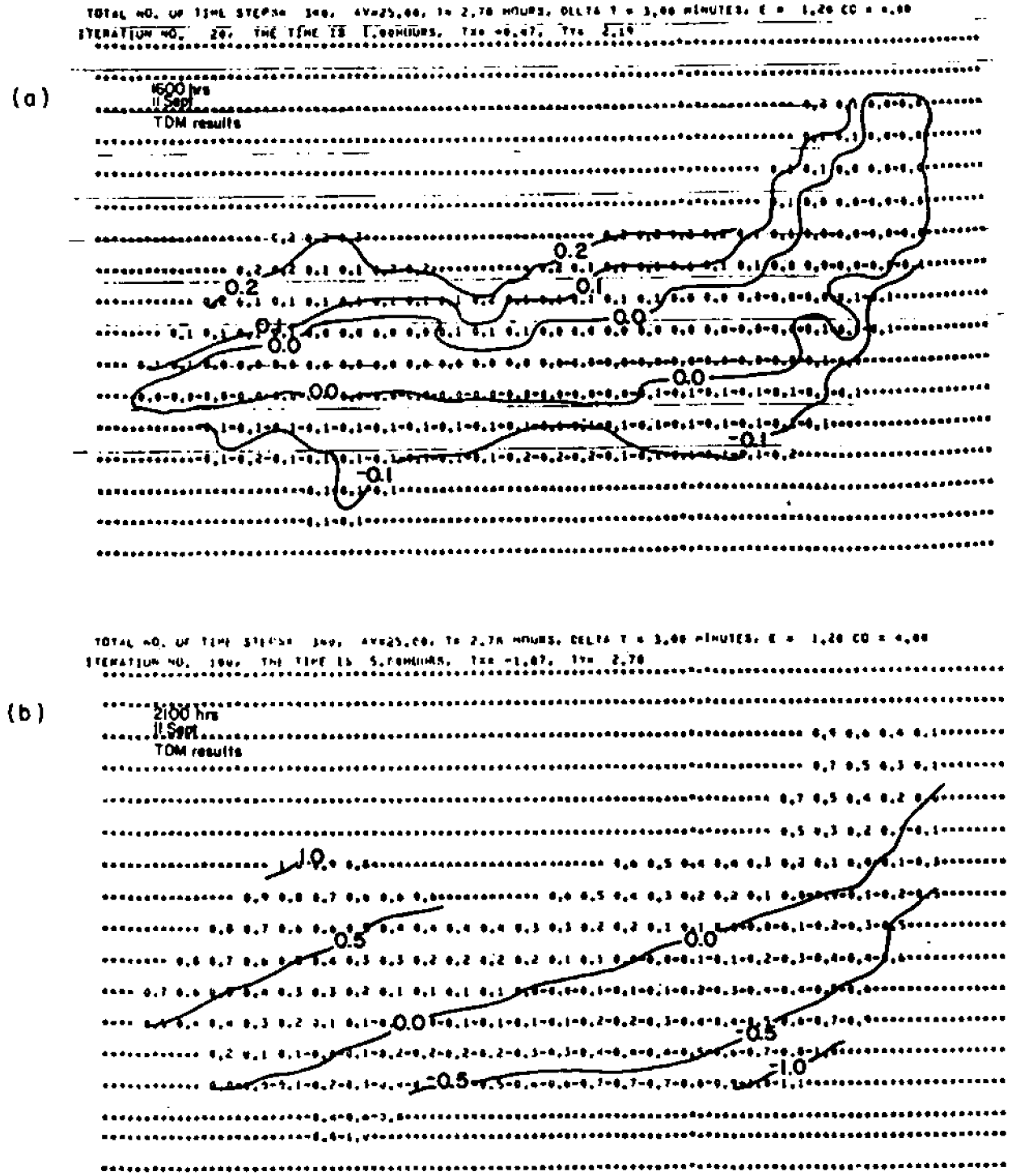

Figure 66. Three-dimensional model predictions of sea level topography in Pamlico Sound at
a. 1600 hours, 11 September 1960, prior to onset of Hurricane Donna
b. 2100 hours (Donna has arrived). (Heights in feet with + above and - below zero mean.)

(a)

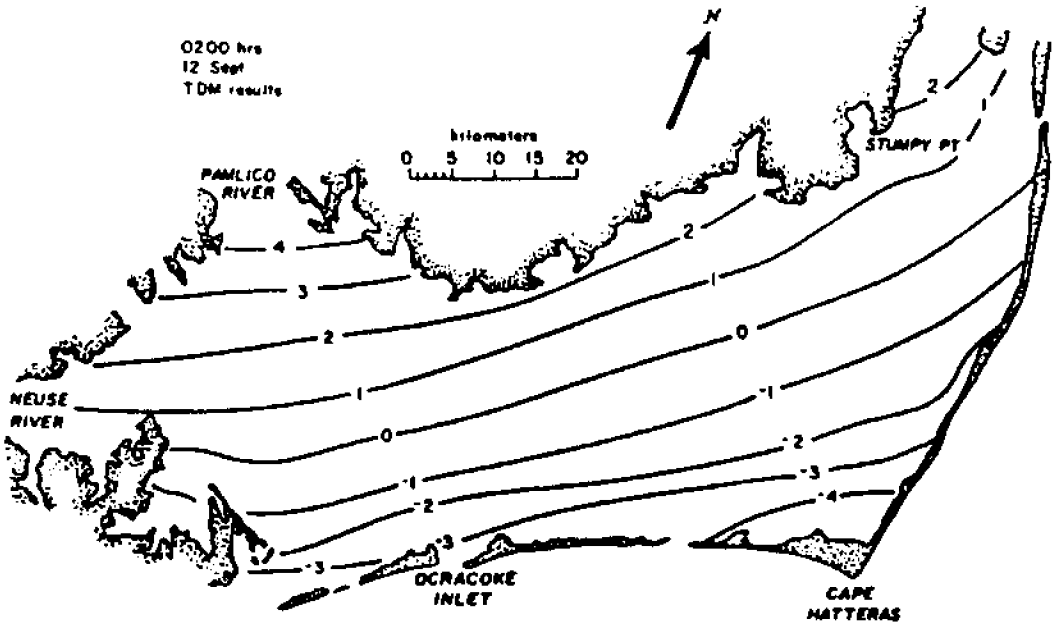

(b)

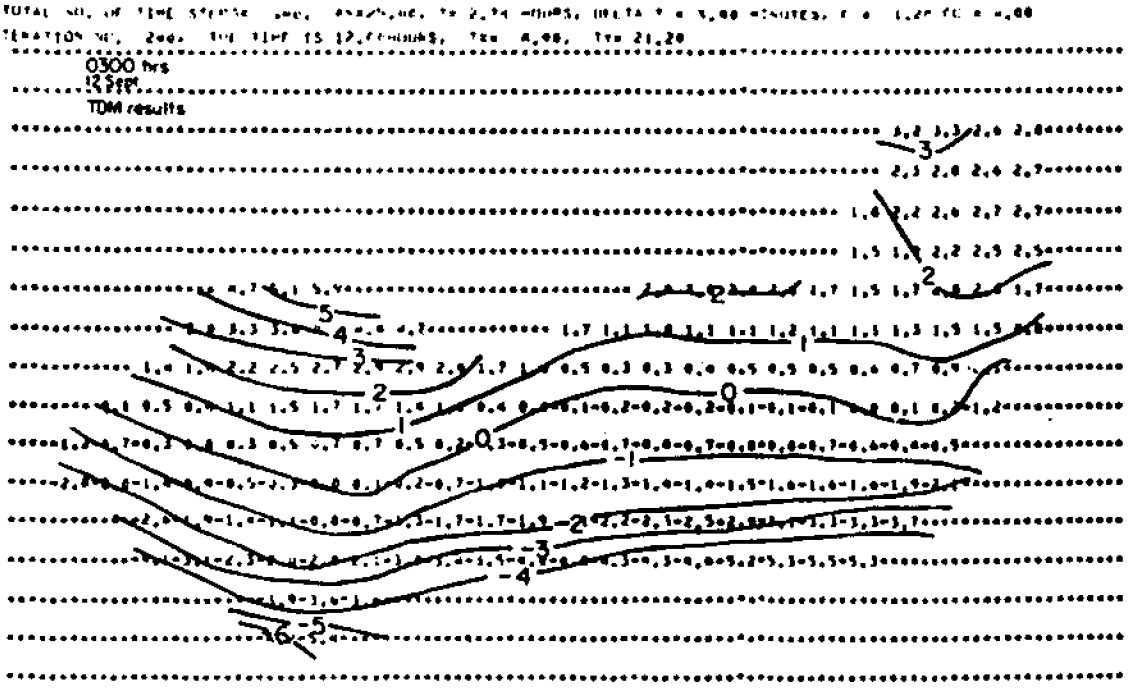

Figure 67. Three-dimensional model predictions of sea level topography in Pamlico Sound at:
a. 0200 hours, 12 September 1960
b. 0300 hours (Donna has arrived). (Heights in feet with + above and - below zero mean.)

(a)

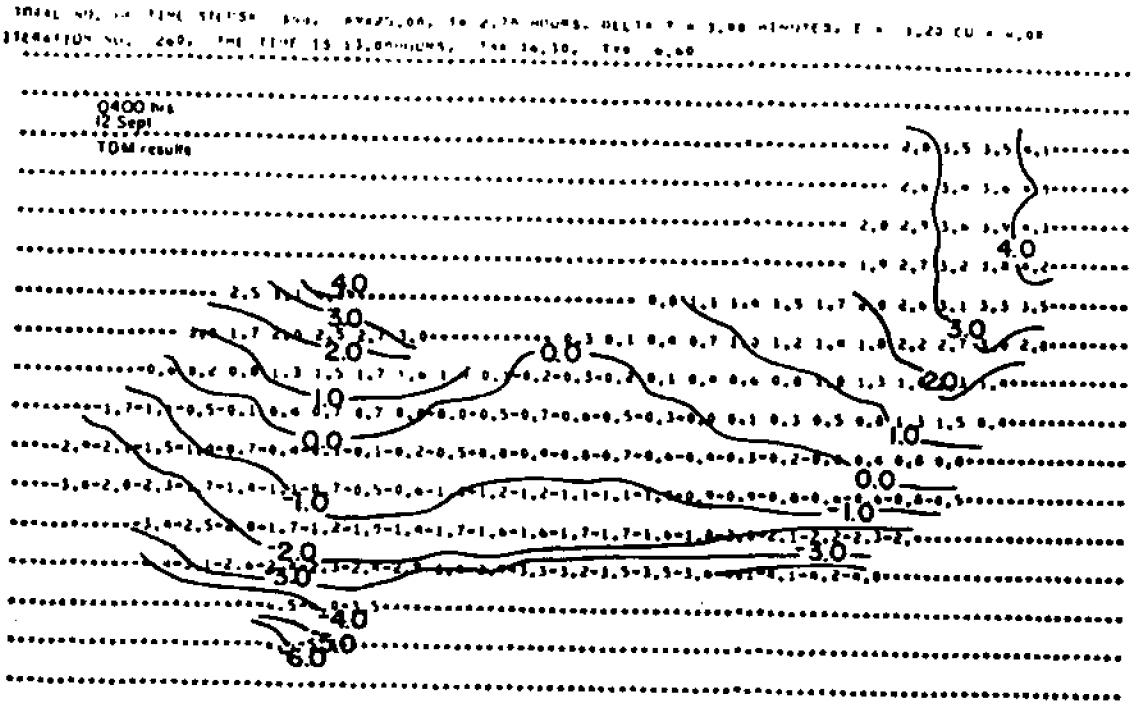

(b)

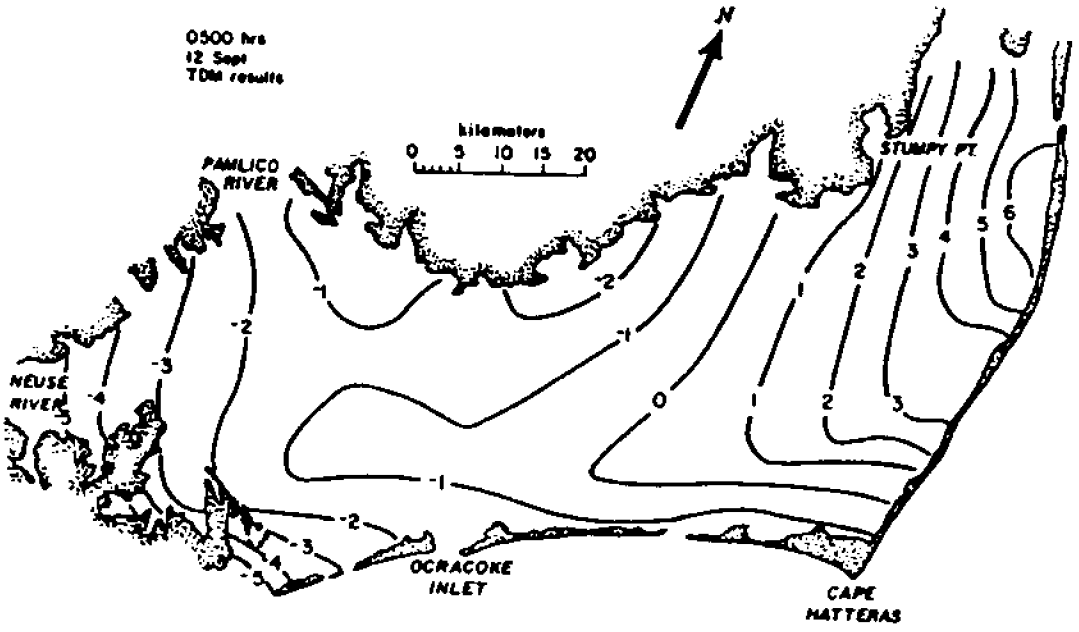

Figure 68. Three-dimensional model predictions of sea level topography in Pamlico Sound at:
a. 0400 hours, 12 September 1960
b. 0500 hours (Donna has arrived). (Heights in feet with + above and - below zero mean.)

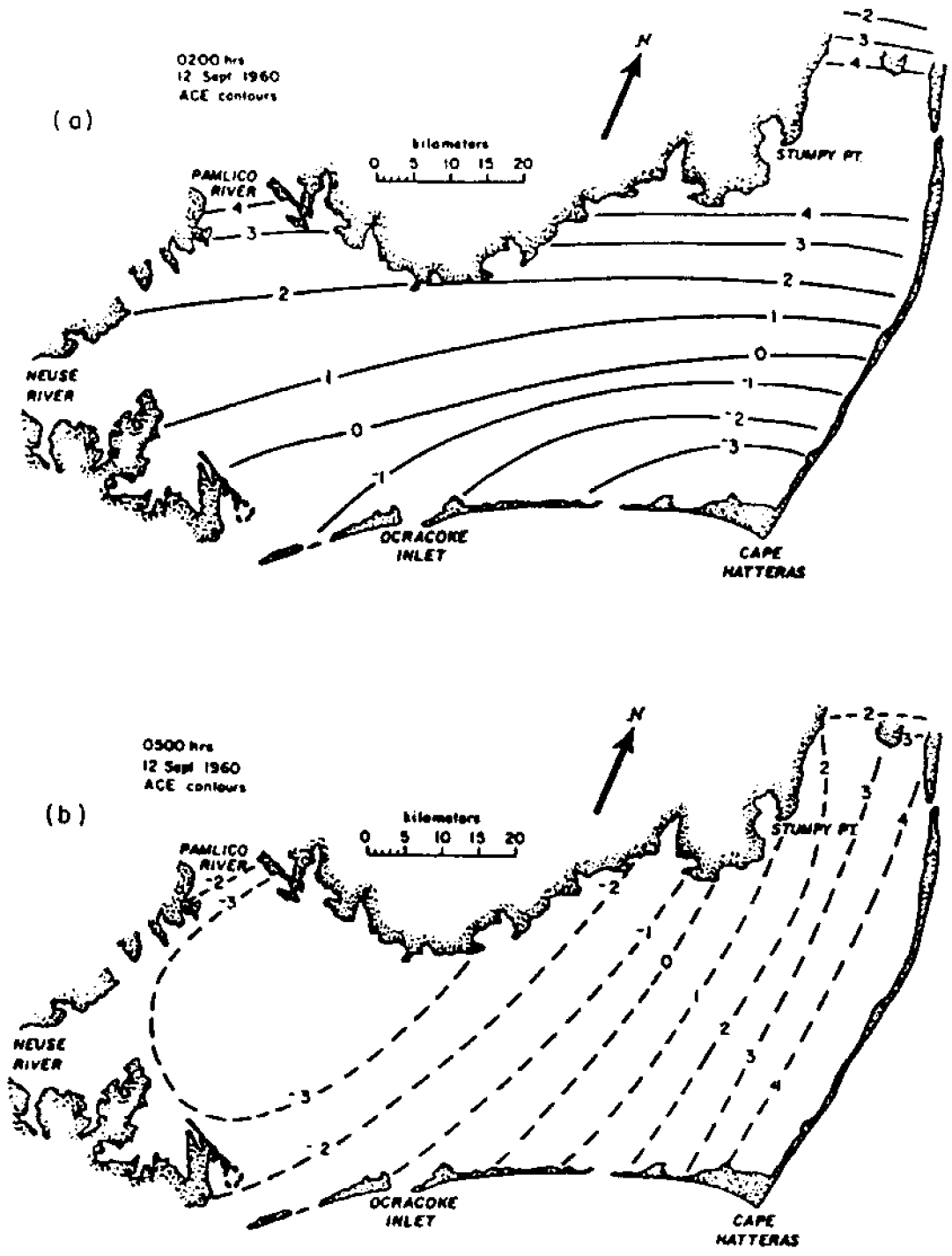

Figure 69. Army Corps of Engineers reconstructed three-dimensional predictions of sea level in Pamlico Sound at:
a. 0200 hours, 12 September 1960
b. 0500 hours (Donna has arrived).

hours, theory and observation show Hatteras Island's backside to be 1 to 6 ft above zero mean while the mouth of the Pamlico River is now 2 ft below zero mean. The mouth of the Pamlico River realized a 6 ft change in water height while the soundside of Hatteras Island experienced water height fluctuations of between 5 to 7 ft, as a function of Hatteras Island locale, all within a period of 3 hours.

The currents associated with such extreme slopes could be estimated as $u \sim \frac{gh^2}{A}\frac{\Delta\eta}{\Delta x}$, which in the case of the surface topography exhibited in Figure 67a at 0200 hrs on 12 September, 1960, would drive currents the order of 200 - 240 cm/sec or 3.9 - 4.7 knots. Superposing this current on a gravity wave field would create enormous bottom shear stress resulting in major erosion.

In the development of our three-dimensional, time-dependent (3DM) numerical model, a discussion of the serious deficiencies of a vertically integrated model (VIM) of the sound (as for example, that of Amein and Airan, 1976) was presented. As an indication of the deficiency of the VIM approach, we compare the surface elevations on the inshore side of Oregon Inlet as predicted by the VIM of Amein and Airan (1976) to that of our 3DM to the actual tide gage observations obtained from the National Ocean Survey (NOS), The period of intercomparison was the period of passage of Hurricane Donna, i.e. 1600 hrs on 11 September through 0800 hrs on 12 September, 1960. It is clear that the 3DM did not spin sea level at Oregon Inlet up as quickly as nature did, missing by some 26 hours. However, the 3DM model results, using two different eddy viscosity coefficients of values 25 and 50 cm^2/sec, brackets the actual rise and fall of sea level. So while the 3DM was late in its prediction of response time, it clearly was correct in its prediction of the total elevation achieved at Oregon Inlet.

Alternatively, the prediction made by the VIM is not only delayed in time, but grossly underestimates the surface elevation excursion actually observed. Table 3 indicated that the VIM would underpredict sea level fluctuations by 33 percent relative to the 3DM, however the underpredition ranges from 33 to 67 percent; a very serious deficiency of the VIM.

Note that while the results of the 3DM effort are very revealing in terms of their physics, improvements to the 3DM could greatly improve the model verity, applicability and utility. Improvements of the three-dimensional model include the following series of modifications. First, a temporally and spatially varying bottom stress boundary condition, such as bottom condition, 5b, as contrasted with the no-slip condition, 5a, should be introduced. Second, the wind field should be specified by actual observations. Third, the horizontal resolution would be greatly improved by decreasing the horizontal grid spacing, which in the present model is set at 5 km in both the x and y directions. The vertical resolution of $\Delta\sigma = 0.1$ is deemed adequate. Fourth, the effects of sea level variation in the coastal ocean due to both tidal and wind driven forcing should be incorporated. It should be noted that Albemarle, Croatan, Roanoke and Core sounds all connect with Pamlico Sound in the present model.

The effect of the variable bottom and periphery on the u and η fields is

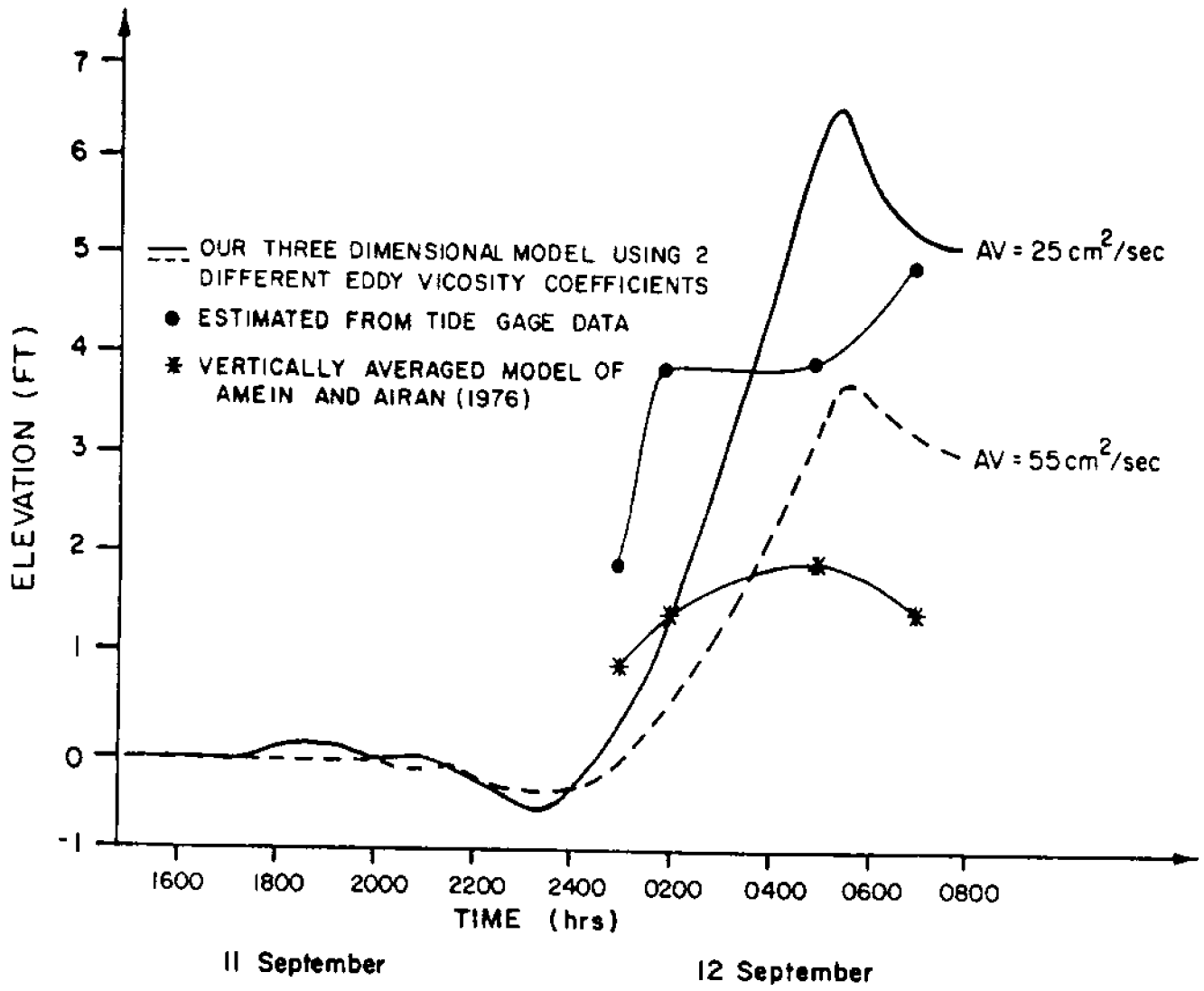

Figure 70. Measured and predicted sea level time series at the Oregon Inlet tide gage during the passage of Hurricane Donna.

incorporated into the model, but the horizontal grid spacing is too coarse to feel the effects that features such as Bluff Shoals (for example) may provide. There is a need for the biologists to understand the potential impact of the shoals on the transport pathways local to the shoals (Pietrafesa et al., 1986). Therefore a grid scale of 1 km is desirable. Additionally, the effects of not only time varying but also spatially varying winds need to be evaluated to understand both the near-and far-field effects of small scale meteorological events, such as squalls, on the integrated physics of the sound. Pietrafesa et al (1986) showed that the physics of the sound seems to strongly influence the spatial and temporal variability of juvenile fish found in the mainland fish nurseries via the occasional creation of transport pathways favorable for migration. Additionally, physical affects derived variously from both semi-and diurnal North Atlantic tides and their associated currents, which jet into and out of the sound via Ocracoke, Hatteras and Oregon Inlets, need to be assessed. Pietrafesa and Janowitz (1986) showed that these inlet currents have both tidal and subtidal frequency components of flow, and that the latter dynamics are strongly coupled to physical processes occurring in adjacent continental shelf waters. Other important factors which should be considered in model improvements are an interrogation of the sea breeze, and fluctuations in the discharge from or flow into rivers and bays located around the sound.

As is clear from the above, several improvements in the model derive from adjusting the model coding. However, the bulk of model improvements will occur only with the availability of better input data. These data can only be obtained via the conduct of a major field program.

2. Flow Field 3DM Model Predictions vs. Current Meter Data in the North Basin

There are virtually no current meter data in the northern basin of Pamlico Sound. However, a study of flow through Oregon Inlet, was conducted in February, 1974 by Singer and Knowles (1975). This study, while brief, will serve to evaluate currents in the northern basin. The study area is depicted in Figure 71 and current wind data for the period 15-22 February are presented in Figure 72. Before discussing the physics of these data we need to first consider the physics on the seaward side of the barrier islands.

On the coastal, seaward side of the barrier islands, the basic wind-driven dynamics have been described in section I-8 following the works of Chao and Pietrafesa (1979) and Janowitz and Pietrafesa (1980). An example of coastal sea level at Cape Hatteras, an open coastal station, responding to local winds is shown in Figure 73. In effect, northward to northeastward winds cause sea level to drop at the coast in concert with a surface Ekman transport offshore and vice-versa for winds which are southward to southwestward; i.e. sea level rises at the coast. The response occurs within a period of 8-10 hours. This response has been shown by Pietrafesa et al (1980) to occur from Cape Hatteras to Charleston, and occurs at Oregon Inlet as well, with southward or northward winds being important for coastal convergence or divergence, respectively.

Clearly shown is the relationship that when the winds are northward, the subtidal frequency flow is out of the inlet (an "ebb') and when the winds are southward, the flow is into the sound (a "flood"). Note that currents from

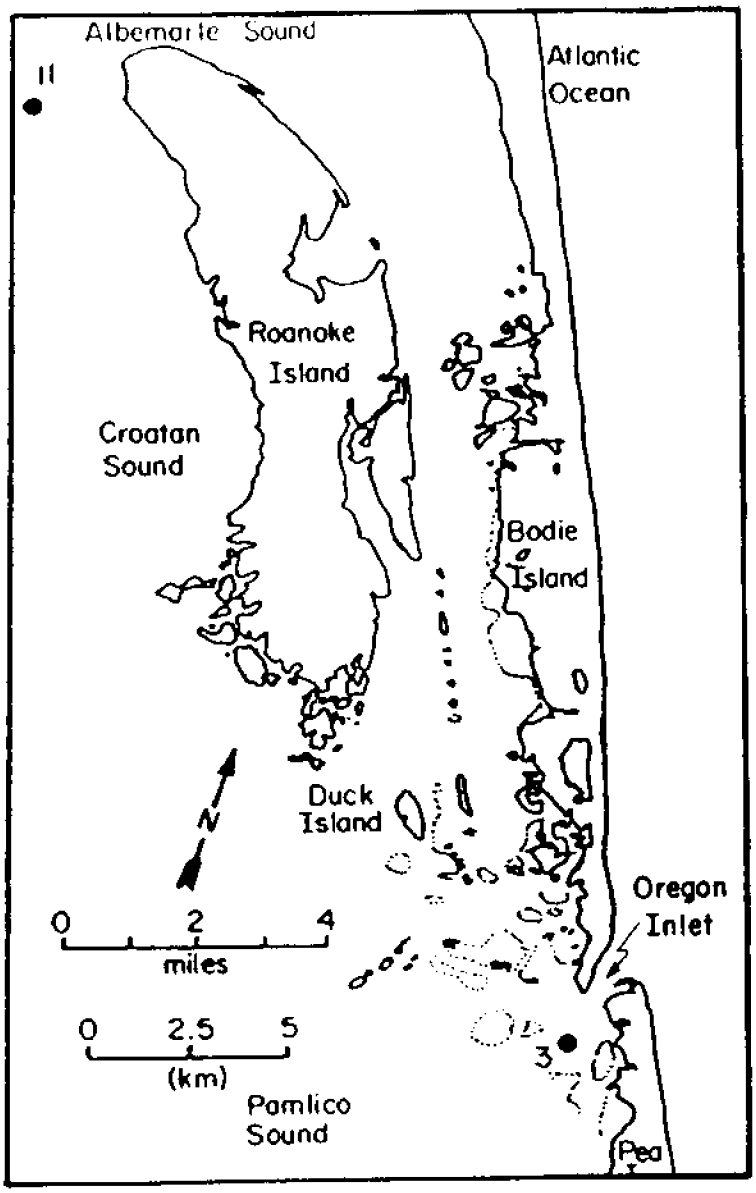

Figure 71. Location of station 11, in north Pamlico Sound, and station 3, on the sound side of Oregon Inlet, during a study of currents recorded by bottom mounted current meters during period 1/3-3/3, 1974. Field study conducted by Singer and Knowles (1975).

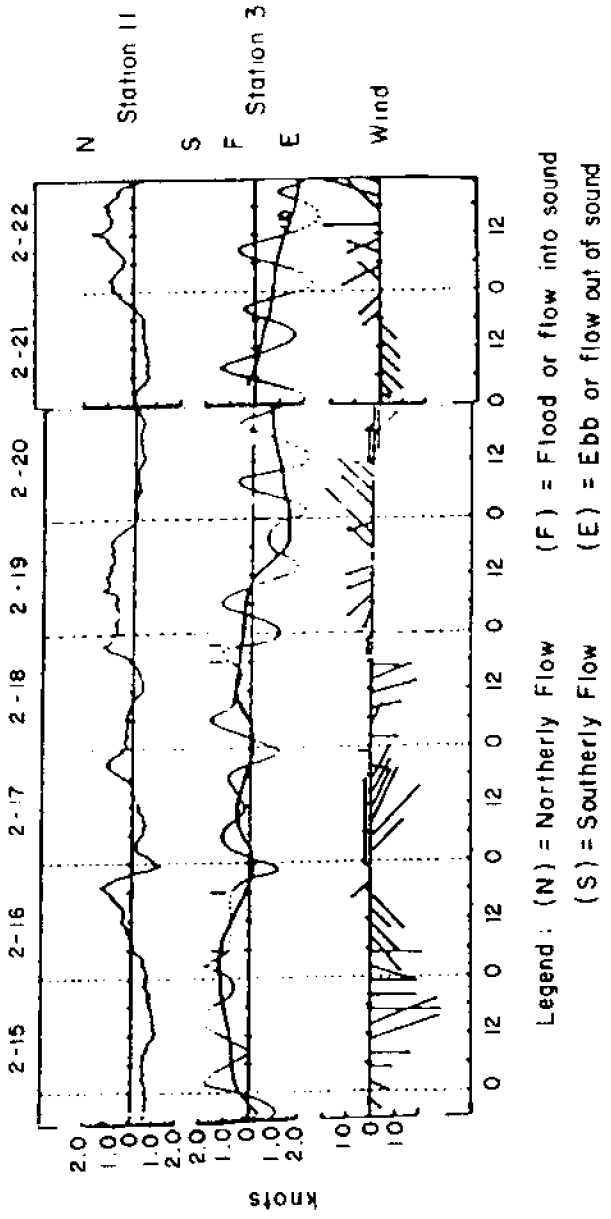

Figure 72. Currents and winds at stations 3 and 11 near Oregon Inlet as shown in figure 71. Station 3 shows both a tidal signal as well as subdiurnal frequency currents.

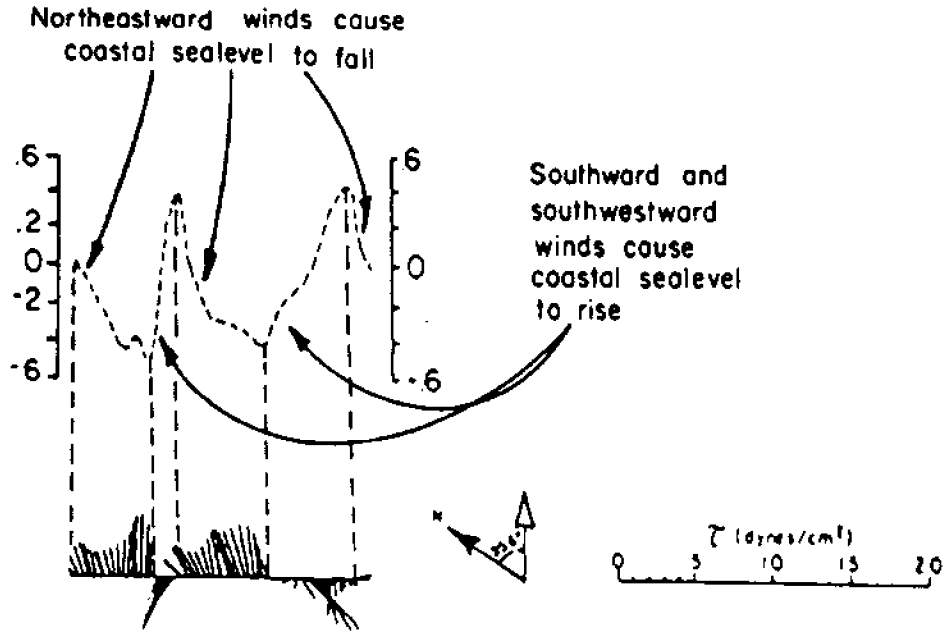

Figure 73. Example of sea level response to alongshore winds on the seaward side of the barrier islands.

station 11 offer a point verification of the 3DM numerical model results presented in Figures 74 and 75. We see from Figure 72 that when winds persist to the north, the inlet drains or "ebbs" even on flood tides, as shown by station 3a currents, while within the sound at Station 11, the flow is to the north. The opposite scenario also holds true; when winds are southward, the inlet floods and flows within the sound are to the south, at Station 11. Monthly mean winds for the North Carolina coast have been described in Section I-7 and II-2. The October through February period contains northerlies (and southerlies) which, via the Janowitz and Pietrafesa (1980) or Pietrafesa et al (1980) rationale (refer to Figure 73) would pile water up against (or away from) the seaward side of the islands, and by our 3DM Pamlico Sound model results would drive the water away from (towards) Oregon Inlet (cf Figures 74 and 75 for model results). In the northern basin, currents at Station 11 are to the north with northward winds and to the south with southward winds in nominal agreement with the model results.

So in summary, we conclude that synoptic scale wind events dominate the coastal marine climatology in the Pamlico Sound region and these winds create drops or rises in sea level which occur within 8 to 10 hours on either side of the barrier islands and related inlets. These sealevel adjustments on either side of the inlet can cause a rise on the ocean side and a fall on the sound side such that an axial inlet pressure gradient is created. This pressure gradient force can drive a flooding current of several knots. The opposite case is that a northward wind will pile water up against the back side of the barrier islands while the coastal ocean will act like the plug was just pulled. Both scenarios are depicted in Figure 76. Without further data, we can only conclude that circulation through the barrier island inlets are forced directly by the M2 tide, and non-locally on both sides, by winds via sea level gradients which affect the creation of pressure gradient forces, or heads, through the inlets. Moreover, the 3DM model results and data indicate that flows in the north basin may be in sync with the inlet dynamics.

3. Flow Field and Sea Level 3DM Model Predictions vs. Data in the South Basin

As is the case for the northern basin of Pamlico Sound, there is a paucity of $\bar{v}$ and η data in the southern basin. However, a study of the S variability in and around the Rose Bay nursery (cf Figure 5) in the southern and western side of the sound (Pietrafesa et al, 1986) do provide some testimony concerning the character of both the flow and the sea level fields. In Figure 77, currents and water elevation data are shown in concert with prevailing wind velocity vector components.

From Figure 77 we see that alongsound-axis winds directed towards the southwest cause water to run into the mouth of Rose Bay while sea level is rising there. Alternatively, northeastward winds cause water to run out of the mouth of Rose Bay in concert with falling sea level. Figures 78 and 79 provide the 3DM predictions of currents and sea level under like wind conditions. Water column response of both currents and water height occurs within several hours of the onset of the winds, in both observations and model output. Currents are in the range of $\pm$20 cm/sec and sea level adjustment is within $\pm$20 cm for winds 5-10 m/sec from both model and observations.

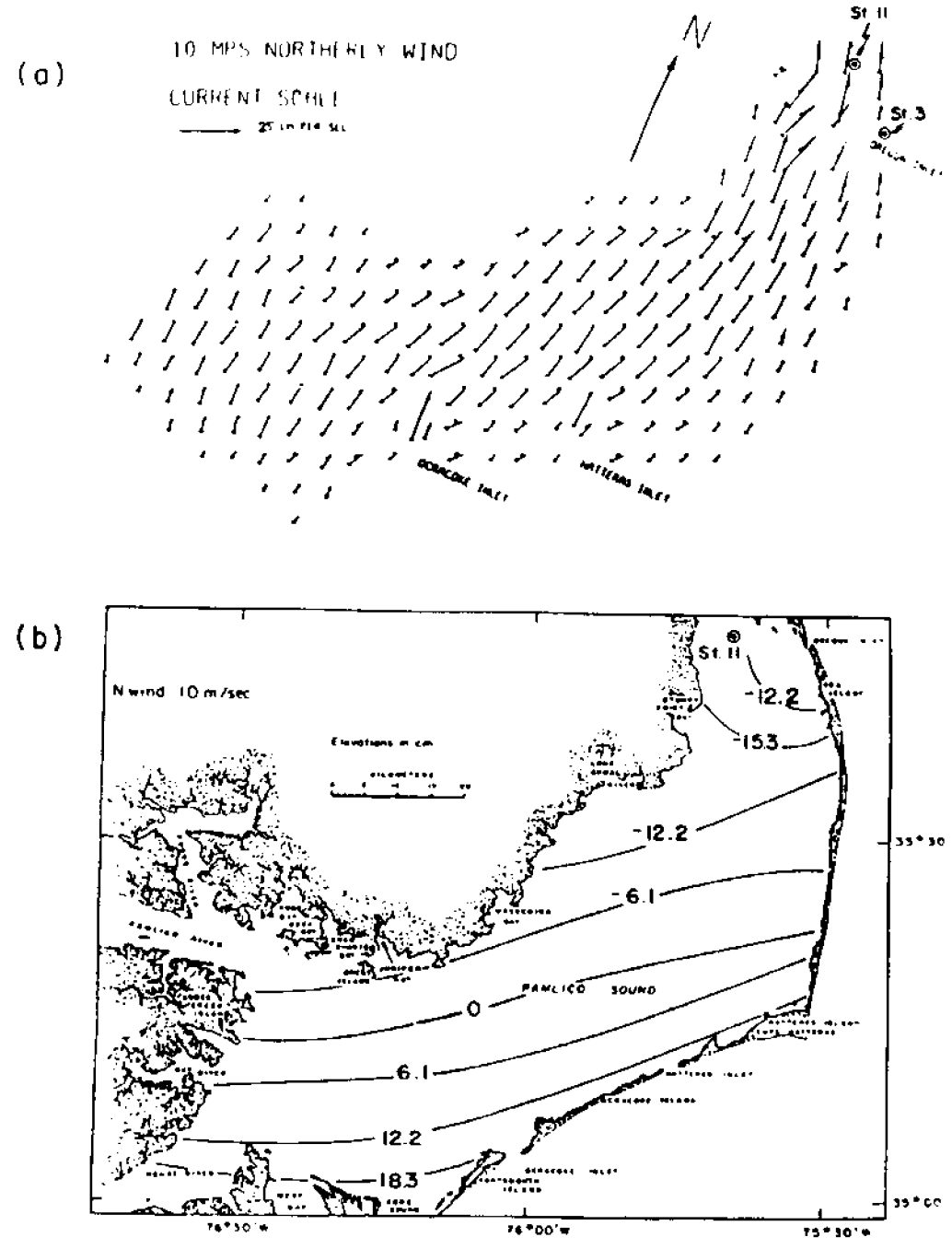

Figure 74. a. Surface (long arrow) and near-bottom (short arrow) model current-vector velocities throughout Pamlico Sound in response to a 10 m/s northerly (southward) wind. Bottom velocities are computed 1 meter above the bottom.
b. Model sea level distribution in Pamlico Sound in response to a 10 m/s southward wind.

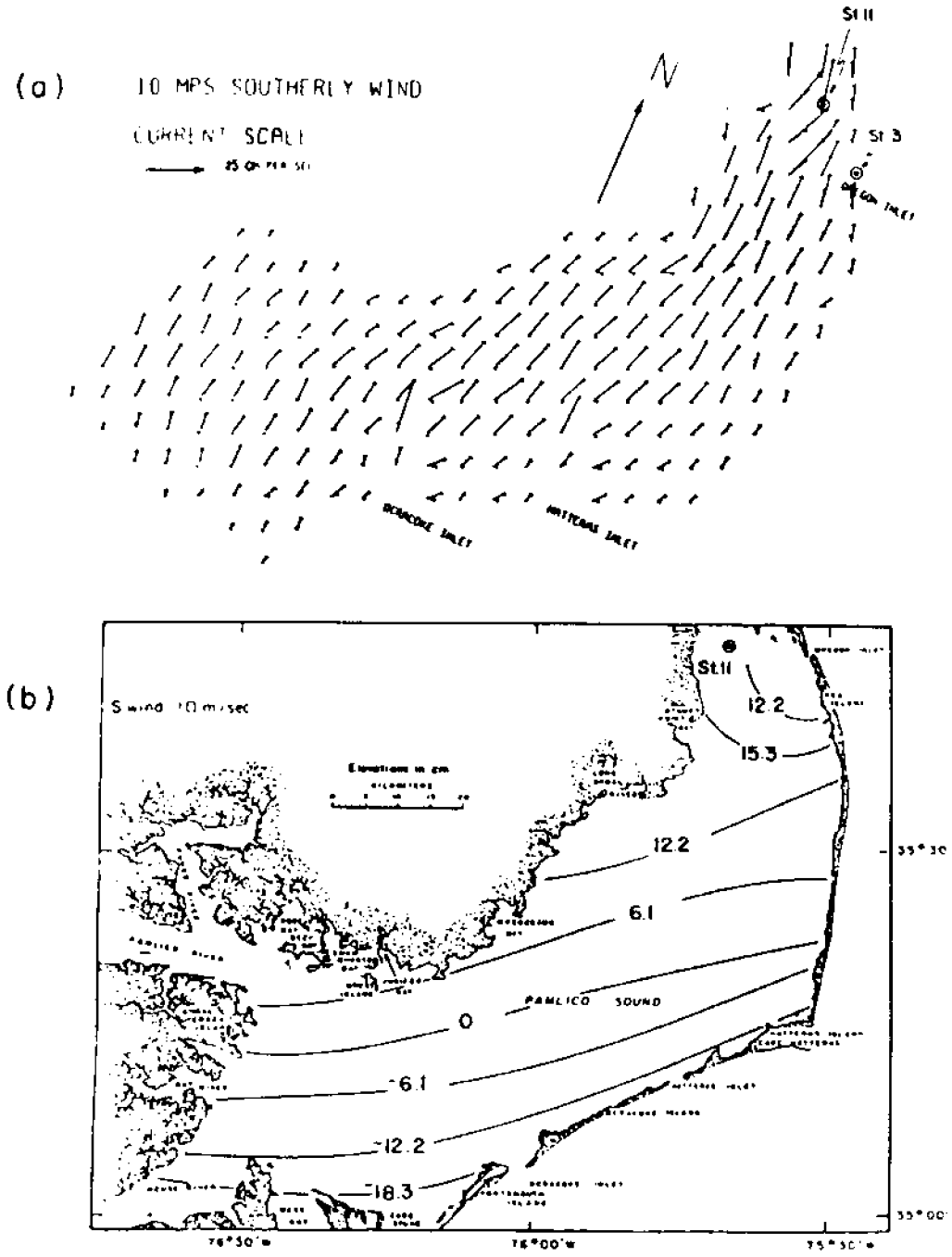

Figure 75. a. Surface (long arrow) and near-bottom (short-arrow) model current-vector velocities throughout Pamlico Sound in response to a 10 m/s southerly (northward) wind. Bottom velocities are computer 1 meter above the bottom.
b. Model sea level distribution in Pamlico Sound in response to a 10 m/s northward wind.

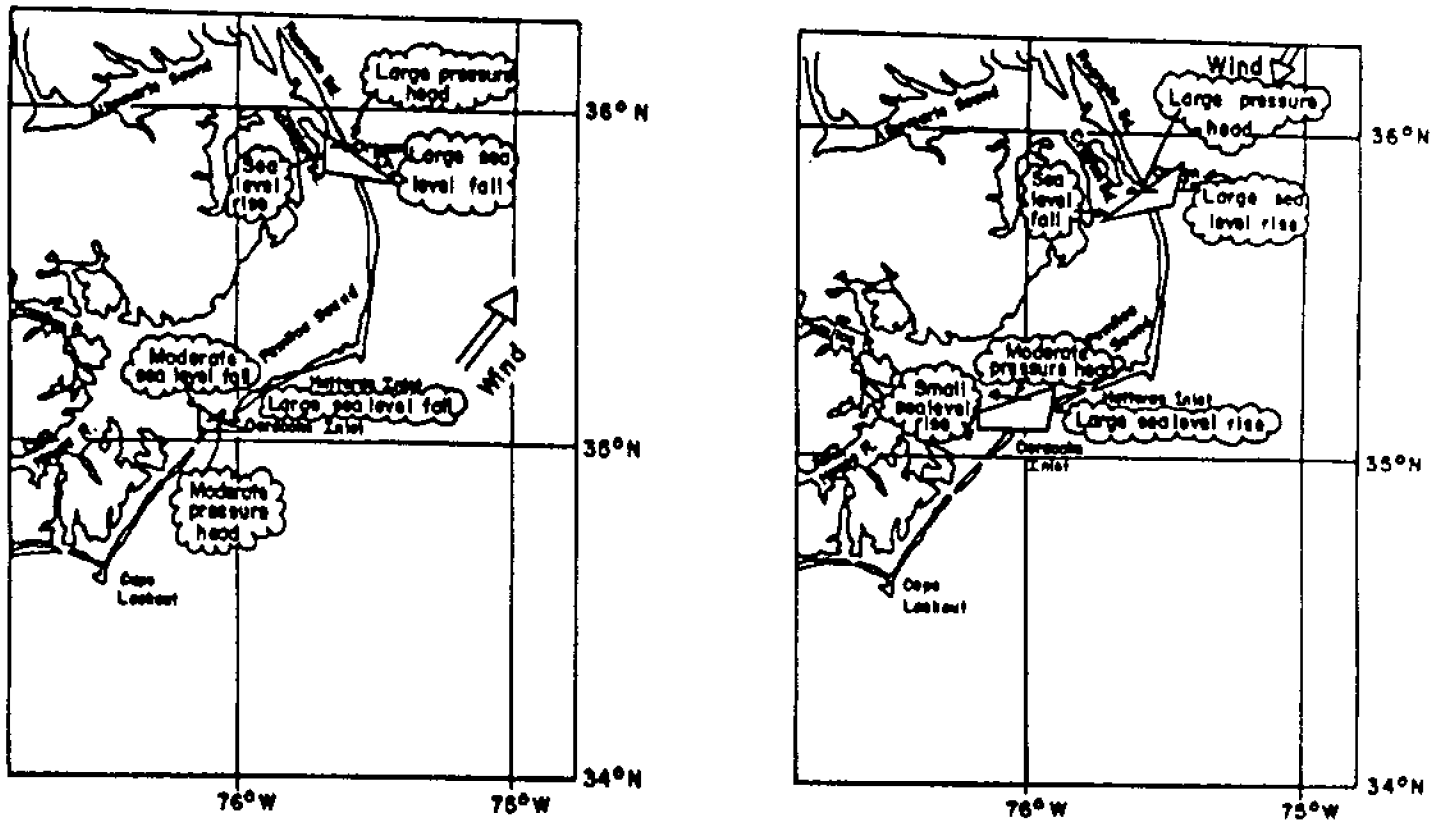

Figure 78. a. Surface (Long arrow) and near-bottom (short-arrow) model current-vector velocities throughout Pamlico Sound in response to a 10 m/s northeasterly (southwestward) wind. Bottom velocities are computed 1 meter above the bottom. b. Model sea level distribution in Pamlico Sound in response to a 10 m/s southwestward wind.

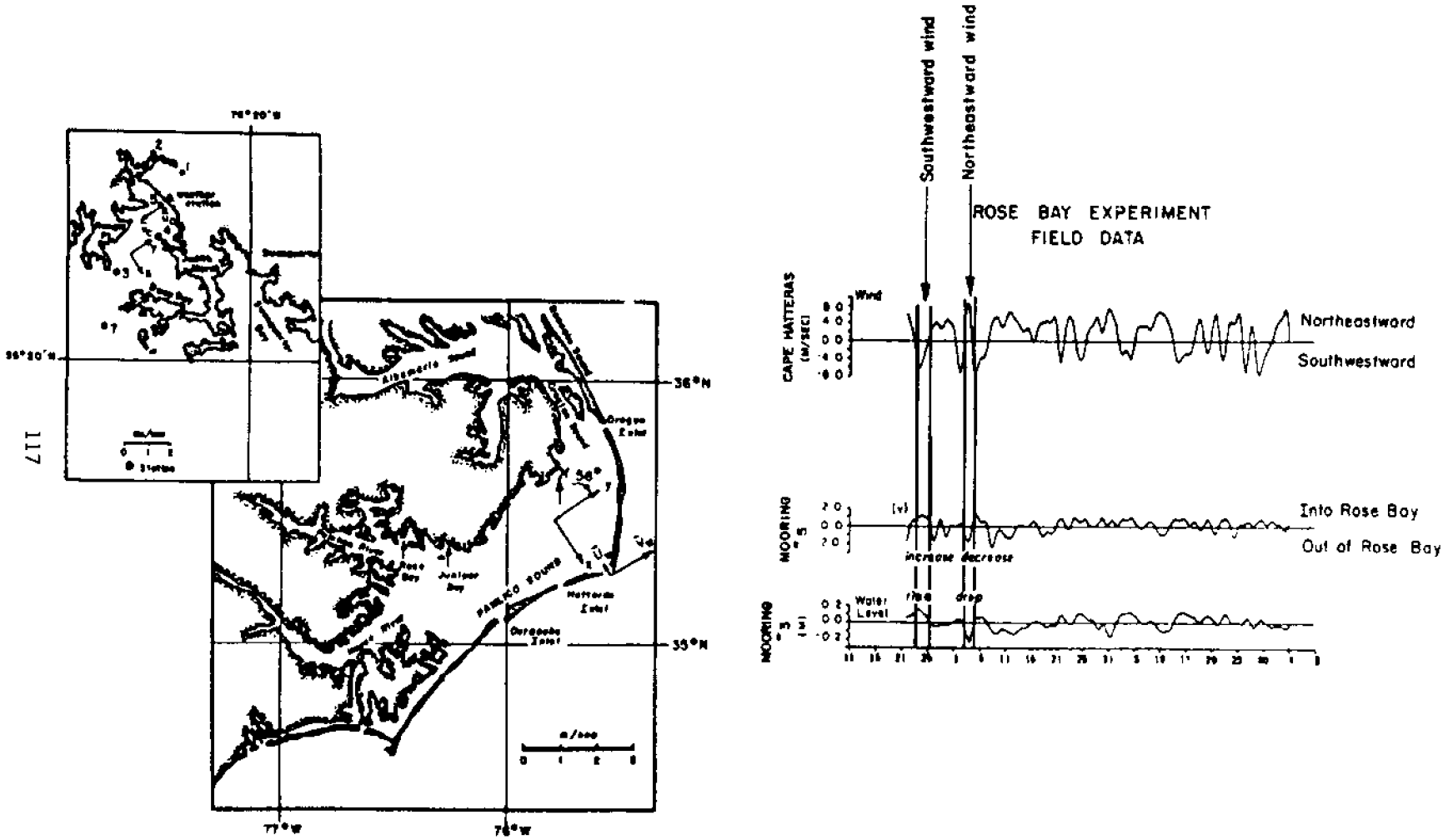

Figure 77. Winds, currents and sea level at the mouth of Rose Bay in the south basin.

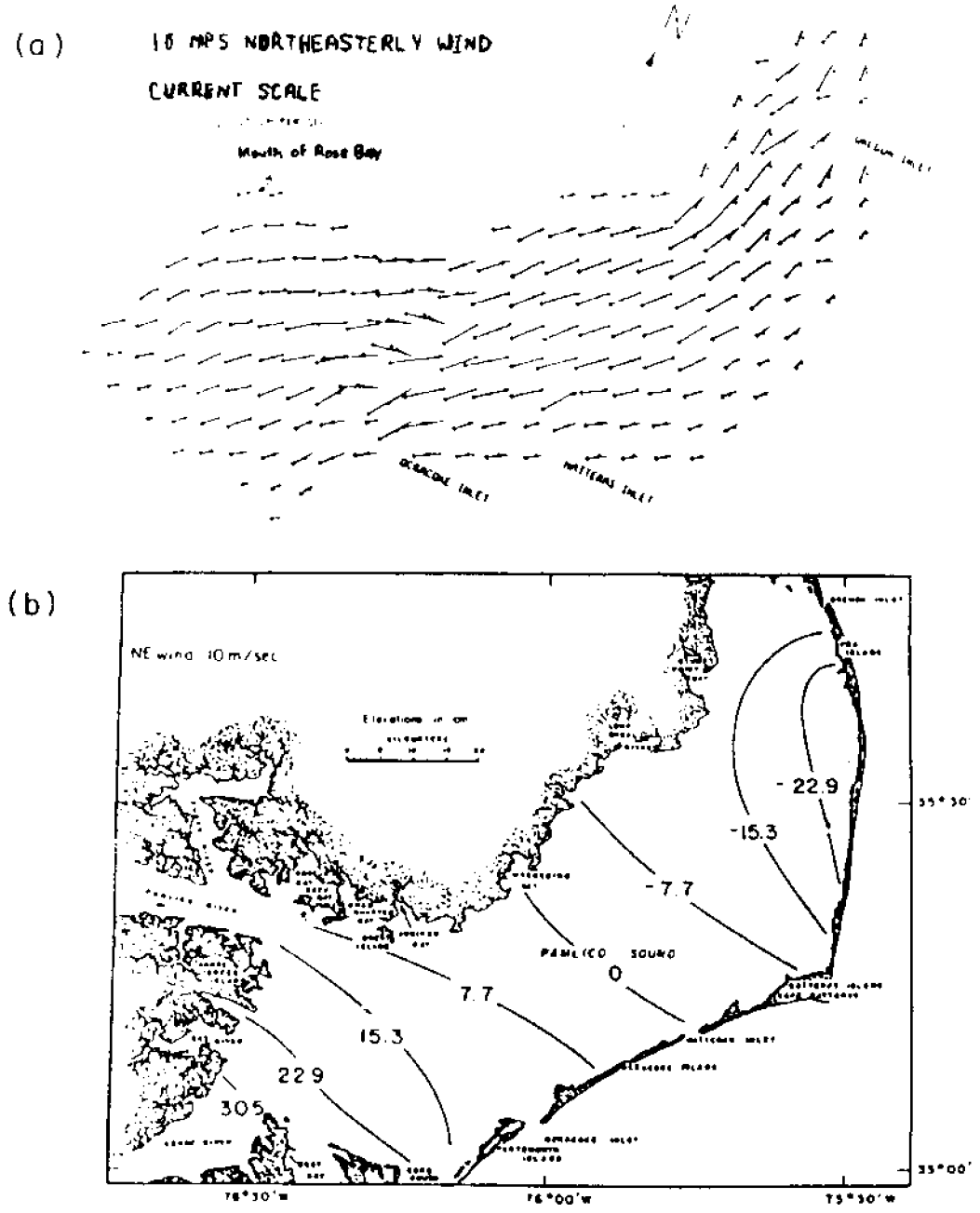

Figure 78. a. Surface (long arrow) and near-bottom (short arrow) model current-vector velocities throughout Pamlico Sound in response to a 10 m s^{-1} northeasterly (southwestward) wind. Bottom velocities are computed 1 meter above the bottom.

b. Model sea level distribution in Pamlico Sound in response to a 10 m s^{-1} southwestward wind.

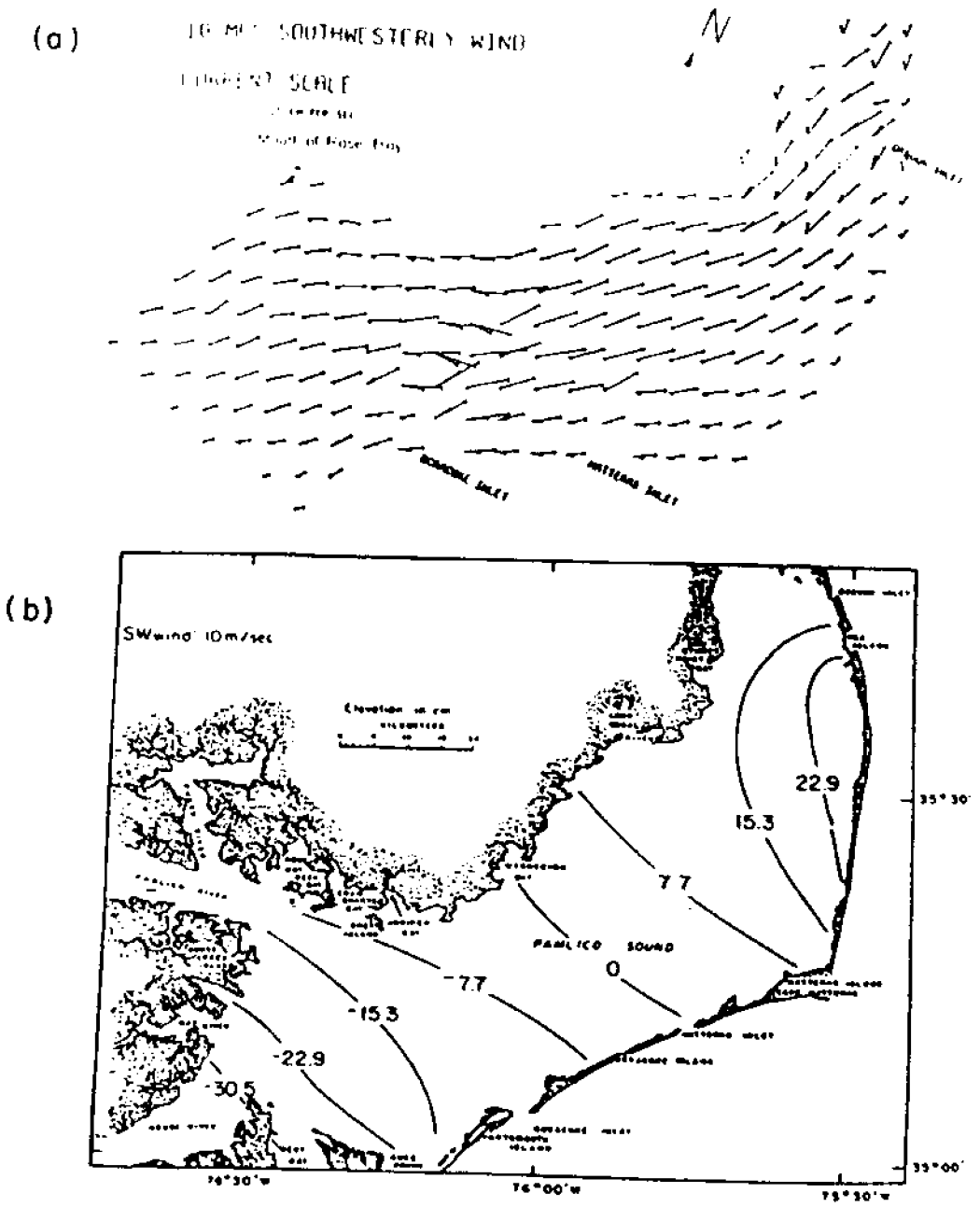

Figure 79. a. Surface (long arrow) and near-bottom (short arrow) model current-vector velocities throughout Pamlico Sound in response to a 10 m s^{-1} southwesterly (northeastward) wind. Bottom velocities are computed 1 meter above the bottom.

b. Model sea level distribution in Pamlico Sound in response to a 10 m s^{-1} northeastward wind.

In Part II of this report series, Pietrafesa et al demonstrate that Rose Bay responds to the mechanical forcing of the wind in a "non-local" way. In summary: if the wind field affecting Pamlico Sound circulation is such that water is being driven away from (towards) the region of the sound local to Rose Bay, then Rose Bay will drain (fill) with speeds almost equal to the speeds of the flow in the sound proper, accompanied by a drop (rise) in sea level which is nearly equal to the fluctuation of water height in the sound proper. This scenario is a summary of the comparison of $\bar{v}$ and η data collected from Stations 3,4,5,6 and 7 (refer to Figure 5 for station locations) and their relationships to atmospheric forcing and buoyancy influence and drainage.

IV. Conclusions and Recommendations

We will list the major conclusions and ancillary recommendations.

The thermohaline structure of sound waters is more variable both spatially and temporally than is commonly believed. Therefore, continuous time series at fixed locations of both T and S need to be collected. Also T-S towed surveys should be be conducted to establish the existence of T-S fronts.

The inlets couple the sound and coastal waters. Tidal influence is greatest in and on either side of the inlets and speak to the need for a study in and on either side of the inlets. The synoptic scale physical activity through the inlets is not well known and needs to be established.

The wind field is the principal forcing function of the physical dynamics of Pamlico Sound spatially variable on time scales of hours to days and must be measured sufficiently spatially to establish its characterization as a forcing function in order to fully appreciate the response of sound waters.

Sea level sets up within 10 hours of the onset of a causal wind. Sealevel gradients ensue. Telescoping grids of water level recorders need to be established as a function of locale to more fully understand the response of η, η_x, and η_y to $\bar{\tau}$.

Monthly to seasonal to annual fluctuations in sea level relate directly to the rise and fall of North Atlantic (Ocean) central water and to the seasonality of the wind field as it affects the rise and fall of sea level on the coastal side of the barrier islands. Flooding and erosion of the mainland and barrier islands adjoining the sound are affected by monthly mean water levels. Several years of sea level data from the periphery of the sound and the coastal ocean need to be analyzed and compared to locales and periods of high erosion to establish a predictive capability. A study of the circulation of the sound is a must in this regard.

During the late spring and early fall, wind motion aligned with the axis of Pamlico Sound appears to be more highly coherently organized relative to cross-axial wind motion, i.e. the wind field tends to be rectilinear. Consequently, sea level fluctuations are coupled to axial winds. A coordinated study of sea level response to cross-axial winds is needed.

During the late spring to early fall, sea level slope appears to be predominately aligned with the principal axis of Pamlico Sound and to be strongly coupled to the axial wind component. However, insufficient tide gage data exist to thoroughly assess the cross-sound sea level slopes. Since sea level slopes drive bottom currents in the reverse direction of the slope, it is important to more thoroughly investigate this problem.

During the late fall to early spring, wind field motion is elliptically polarized, i.e. organized motion occurs in both the direction of the main axis of the sound as well as across the sound in a coupled fashion. Sea level and sea level slopes appear to set up in an organized fashion to whichever wind component is present.

Sea level slopes in the direction of the principal axis of the sound appear to set up at 02.-0.26 cm/km per dyne/cm^2 of wind stress in the direction of the wind within 10 hours while cross-sound sea level slopes take a full day to set up. Since sea level set-up inundates property and since sea level slopes drive bottom currents, these preliminary results need to be further investigated.

Atmospheric pressure fluctuations do not affect sea level nor current fluctuations except under hurricane conditions.

There is a degradation of the coherency between wind and sea level in the vicinity of the juncture of Roanoke, Croatan, Albemarle and Pamlico Sounds and Oregon Inlet. This degradation may be due to freshwater and coastal water fluxes. This water exchange problem may be an indicator of an Albemarle-Pamlico Sound and coastal ocean coupling of which we presently know nothing. The problem needs to be addressed.

Pamlico Sound can be topographically decomposed into northern and southern basins, separated by Bluff Shoals. Sea level fluctuations in Pamlico Sound may decouple somewhat into a north basin set and a south basin set. The circulation associated with this decoupling or coupling is totally unknown.

A three-dimensional, time-dependent model of circulation and sea level reveals that sound waters respond fully to winds within 10 hours of the onset of forcing in good agreement with data. Model bottom currents, driven by sea level slope pressure gradients, are shown to veer by as much as 180° from mechanically driven surface currents. The 3DM model is a great aid in establishing a predictive capability for the physics of Pamlico Sound. However the 3DM model needs improvements, including:

the imposition of a variable bottom-stress condition; the incorporation of spatial variability in the wind field (which requires a commensurate field program to yield the variability of the windfield); greater topographic resolution by reducing model grid size, particularly near shoals; inlet conditions need to be reassessed, particularly via the inclusion of actual inlet data; a nonhomogeneous, T,S field should be imcorporated in both diagnostic and prognostic modes; the tides, particularly the semi-diurnal mode, need to be incorporated into the model; and riverine, connective sound and drainage inputs need to be better established via a field program.

Vertically integrated models are shown to either underestimate or miss much of the basic physics of the sound and therefore should never be used.

The horizontal and vertical structure as well as the temporal variability of the circulation field is essentially unknown save for a few, singular observations and for the 3DM predictive output. The study reported on in section II and III of this report have introduced a new level of understanding for the physics of Pamlico Sound. However, this study simply established the foundation for a more complete study of the entire sound system. How $\bar{v}$ couples to $\bar{\tau}$, η, η_x, η_y, T-S, to the coastal ocean via the inlets, to the feeder rivers, bays and sounds, to bottom topography, particularly near shoals, and to atmospheric buoyancy flux, can only be speculated upon at this time. A thorough study of the circulation must be conducted.

The gravity wave field which exists within Pamlico Sound proper and through the inlets and tributary rivers is totally unknown. This field is omnipresent and may contribute significantly to sediment transport, i.e. erosional processes and to flooding under high wind conditions.

V. Acknowledgements

The principal support for the Pamlico Sound study was from the North Carolina Sea Grant College Program, Office of Sea Grant, National Oceanographic and Atmospheric Administration, U.S. Department of Commerce, under Grant No. NA81AA-D-0002, the N.C. Department of Administration and the Water Resources Research Institute. Support for the complementary coastal ocean study was provided by the U.S. Department of Energy under Contract No. DOE-AS09-EY00902 and Grant No. DE-FG09-85-ER60376. The U.S. Army Corps of Engineers, Wilmington, N.C. is acknowledged for providing their tide gage data at no cost.

Ms. Brenda Batts is thanked for her heroic effort in processing and reprocessing the verbiage. Ms. LuAnn Salzillo is acknowledged for her tireless work with the figures and Ms. Monica Homan for her editorial assistance. Charles Gabriel and T.S. Wu provided support in data processing and model coding, and Paul Blankinship and Lawrence Ives assisted in the field effort along with a bevy of cheerful graduate students.

Dr. John Miller and his stable of technicians and students are also thanked for having aided and abetted this study.

References

Airan, D.S. 1974. Explicit modeling of circulation and water quality for two-dimensional unsteady flow. Ph.D. dissertation, North Carolina State University.

Amein, N. 1971. Circulation in Pamlico Sound. Report to the Board of Science and Technology, North Carolina State University.

Amein, N. and D.S. Airan. 1976. Mathematical modeling of circulation and hurricane surge in Pamlico Sound, North Carolina. UNC Sea Grant College Publication UNC-SG-76-12.

Carnahan, B., H.A. Luther and J.O. Wilkes. 1969. Applied Numerical Methods. John Wiley & Sons, Inc.

Chao, T-Y. 1981. The Response of the Pamlico Sound Sea Level to Atmospheric Forcing. North Carolina State University, Raleigh, NC. 122 pages.

Chao, T-Y. and L.J. Pietrafesa. 1980. The subtidal response of sea level to atmospheric forcing in the Carolina Capes. Journal of Physical Oceanography, Vol. 10, No. 8, pp. 1246-1255.

Chu, H.L. 1970. Numerical techniques for non-linear wave refraction and for propagation of long waves in a two-dimensional shallow water basin. Ph.D. dissertation, North Carolina State University.

Fofonoff, N.P. 1969. Spectral characteristics of internal waves in the ocean. Deep Sea Research, Supplement 16- 59-71.

Giese, G.L., H.B. Wilder and G.G. Parker, Jr. 1985. Hydrology of Major Estuaries and Sounds of North Carolina. U.S. Geological Survey Water-Supply Paper 2221.

Gilliam, J., J. Miller, L. Pietrafesa and W. Skaggs. 1985. Water Management and Estuarine Nurseries. UNC Sea Grant Working Paper 85-2.

Hammack, J.L. 1969. A mathematical investigation of freshwater flow through Pamlico Sound, North Carolina. M.S. thesis, North Carolina State University.

Jarrett, T.J. 1966. A study of the hydrology and hydraulics of Pamlico Sound and their relation to the concentration of substances in the sound. M.S. thesis, North Carolina State University.

Khorram, S., and H.M. Cheshire. 1985. "Remote Sensing of Water Quality in the Neuse River Estuary, North Carolina," Photogrammetric Engineering and Remote Sensing, Vol. 51, No. 3, pp. 329-341.

Lee, T.N. and C. Rooth. 1972. Exchange Processes in Shallow Estuaries. Offshore Technology Conference, Dallas, Texas, paper #OTC 1703, pp. II777-II783.

Marshall, N. 1951. Hydrography of North Carolina Marine Waters, pp. 1-76. In H.F. Taylor (ed.), Survey of Marine Fisheries of North Carolina. University of North Carolina, Chapel Hill, N.C.

Milne-Thompson, L.M. 1968. Theoretical Hydrodynamics. The Macmillan Co.

Moody, J.A., B. Butman, R.C. Beardsley, W.S. Brown, P. Daifuku, J.D. Irish, D.A. Mayer, H.O. Mofjeld, B. Petrie, S. Ramp, P. Smith and W.R. Wright. 1984. Atlas of Tidal Elevation and Current Observations of the Northeast American Continental Shelf and Slope. U.S. Geological Survey Bulletin 1611.

Pattulo, J., W. Mund, R. Revelle and E. Strong. 1955. The seasonal oscillation in sea level. Journal of Marine Research, 14(1), pp. 88-155.

Pietrafesa, L.J. 1983. Shelfbreak Circulation, Fronts and Physical Oceanography: East and West Coast Perspectives. Society of Economic Paleontologists and Mineralogists, Special Publication No. 33. pps. 233-250.

Pietrafesa, L.J., R. D'Amato, C. Gabriel and R.J. Sawyer, Jr. 1978. Continental margin atmospheric climatology and sea level. Sea Grant Publication No. UNC-SG-78-09, North Carolina State University, 189 pp.

Pietrafesa, L.J., G.S. Janowitz and R.H. Weisberg. 1977-1980. Physical Studies of Pamlico Sound, N.C. UNC Sea Grant proposal, Project No. R/ES-27.

Pietrafesa, L.J., J.O. Blanton, J.D. Wang, V. Kourafalou, T.N. Lee, and K.A. Bush. 1985. The Tidal Regime in the South Atlantic Bight, AGU Coastal and Estuarine Monography Series, Vol. 2, pps. 63-76.

Pietrafesa, L.J., G.S. Janowtiz, J.M. Miller, E.B. Noble, S.W. Ross and Sheryan P. Epperly. 1986. Abiotic Factors Influencing the Spatial and Temporal Variability of Juvenile Fish in Pamlico Sound, North Carolina. Estuarine Variability.

Pond, S. 1975. The Exchange of Momentum, Heat and Moisture at the Ocean-Atmospheric Interface. Numerical Models of Ocean Circulation, National Academy of Sciences. pps. 26-38.

Posner, G.S. 1959. Preliminary oceanographic studies of the psitive bar built estuaries of North Carolina, U.S.A., International Oceanography Congress AAAS, Washington, D.C.

Redfield, A.C. 1958. The influence of the continental shelf on the tides of the Atlantic coast of the U.S. Journal of Marine Research, 17:432-448.

Roelofs, E.W. and A.W. Bumpus. 1953. The hydrography of Pamlico Sound. Bulletin Marine Science Gulf and Caribbean, 3(3):181-205.

Schwartz, F.W. and Chestnut, A.F. 1972. Hydrographic atlas of North Carolina estuarine and sound waters. 1972: University of North Carolina Sea Grant publication 73-12, 132 pp.

Singer, J.J. and C.E. Knowles. 1975. Hydrology and circulation patterns in the vicinity of Oregon Inlet and Roanoke Island, North Carolina University of North Carolina Sea Grant publication 75-15, 171-pp.

Smallwood, C. and M. Amein. 1967. A mathematical model for the hydrology and hydraulics of pamlico Sound. Proceeding Symposium Hydrology. Coastal Waters N.C., Rep. No. 5, Water Resouces Research Institute of the The University of North Carolina, Raleigh, N.C.

U.S. Army Corps of Engineers. 1961. Report on the Tropical Hurricane of September (Donna): Wilmington, N.C.

Weisberg, K.H. and L.J. Pietrafesa. 1983. Kinematics and correlation of the surface wind field in the South Atlantic bight. Journal of Geophysical Research, 88 (C8) 4593-4610.

Welander, P. 1957. Wind Action on a Shallow Sea: Some Generalizations of Ekman's Theory. Tellus IX (1957).

Williams, A.B., G.S. Posner, W.J. Woods and E.E. Deubler, Jr. 1973. A Hydrographic Atlas of Larger North Carolina Sounds. UNC Sea Grant Publication 73-02.

Winslow, Fracis. 1889. Report on the sounds and estuaries of North Carolina with reference to oyster culture: U.S. Coast and Geodetic Survey Bulletin no. 10, p. 52-136.

Woods, W.J. 1967. Hydrographic studies in Pamlico Sound, in Proceedings of a symposium on hydrology of the coastal waters of North Carolina Water Resources Institute Report no. 5, p. 104-114.